EVALUATION OF A FLUIDIC TEMPERATURE SENSOR/AIR EJECTOR ASSEMBLY

J. E. Whicker

General Motors Corporation

Prepared for:

Air Force Aero Propulsion Laboratory

November 1974

UNCLASSIFIED

SECURITY CLASSIFICATION OF THIS PAGE *(When Data Entered)*

REPORT DOCUMENTATION PAGE		READ INSTRUCTIONS BEFORE COMPLETING FORM
1. REPORT NUMBER AFAPL-TR-74-58	2. GOVT ACCESSION NO.	3. RECIPIENT'S CATALOG NUMBER AD-A007 978
4. TITLE *(and Subtitle)* EVALUATION OF A FLUIDIC TEMPERATURE SENSOR/AIR EJECTOR ASSEMBLY		5. TYPE OF REPORT & PERIOD COVERED Final Report July 1973—April 1974
		6. PERFORMING ORG. REPORT NUMBER EDR 8137
7. AUTHOR(s) J. E. Whicker		8. CONTRACT OR GRANT NUMBER(s) F33657-73-C-0618
9. PERFORMING ORGANIZATION NAME AND ADDRESS Detroit Diesel Allison, Division of GM P. O. Box 894 Indianapolis, Indiana 46206		10. PROGRAM ELEMENT, PROJECT, TASK AREA & WORK UNIT NUMBERS Proj. 3066 Task 306603
11. CONTROLLING OFFICE NAME AND ADDRESS Air Force Aero Propulsion Laboratory (TBC) Wright-Patterson AFB, Ohio 45433		12. REPORT DATE November 1974
		13. NUMBER OF PAGES 122
14. MONITORING AGENCY NAME & ADDRESS*(if different from Controlling Office)*		15. SECURITY CLASS. *(of this report)* Unclassified
		15a. DECLASSIFICATION/DOWNGRADING SCHEDULE N/A

16. DISTRIBUTION STATEMENT *(of this Report)*

Approved for public release; distribution unlimited

17. DISTRIBUTION STATEMENT *(of the abstract entered in Block 20, if different from Report)*

18. SUPPLEMENTARY NOTES

19. KEY WORDS *(Continue on reverse side if necessary and identify by block number)*

1. Gas Temperature Measurement
2. Turbine Engine Controls
3. Fluidic Sensors

20. ABSTRACT *(Continue on reverse side if necessary and identify by block number)*

A fluidic, edgetone resonator sensor designed for gas temperature measurement at the compressor inlet of gas turbine engines was fabricated and evaluated on a burner rig at simulated engine conditions. Tested with the sensor was an air ejector used to lower the sensor back pressure to maintain proper sensor operation (choked flow at the discharge orifices)

DD FORM 1 JAN 73 1473 EDITION OF 1 NOV 65 IS OBSOLETE

UNCLASSIFIED

SECURITY CLASSIFICATION OF THIS PAGE *(When Data Entered)*

20. Abstract (cont)

over the entire range of engine flight conditions. Steady-state performance of the sensor/ejector combination when compared with test thermocouples was acceptable in terms of both accuracy and repeatability. Transient response performance, however, was somewhat less than desired. Subsequent heat transfer analyses revealed the problem areas and identified several likely improvements. Incorporating these improvements and analytically comparing the improved sensor response with that of an exposed junction thermocouple, as a temperature measurement input to a compressor geometry control loop, revealed minimum gains. The advantages over the thermocouple approach will only be apparent if a) a very rapid temperature measurement response is desired for compressor surge control, or b) a digital (or frequency) output sensor is needed for direct input to a digital computer controller.

NOTICE

When Government drawings, specifications, or other data are used for any purpose other than in connection with a definitely related Government procurement operation, the United States Government thereby incurs no responsibility nor any obligation whatsoever; and the fact that the Government may have formulated, furnished, or in any way supplied the said drawings, specifications, or other data, is not to be regarded by implication or otherwise as in any manner licensing the holder or any other person or corporation, or conveying any rights or permission to manufacture, use, or sell any patented invention that may in any way be related thereto.

This final report was submitted by Detroit Diesel Allison, Division of General Motors, under Contract F33657-73-C-0618. The effort was sponsored by the Air Force Aero-Propulsion Laboratory, Air Force Systems Command, Wright-Patterson AFB, Ohio, with Lester L. Small, AFAPL/TBC, as Project Engineer. J. E. Whicker of Allison was technically responsible for the work.

This report has been reviewed by the Information Office, (ASD/OIP), and is releasable to the National Technical Information Service (NTIS). At NTIS, it will be available to the general public, including foreign nations.

This technical report has been reviewed and is approved for publication.

Lester L. Small

LESTER L. SMALL, GS-12
Project Engineer

FOR THE COMMANDER

Charles E. Bentz

CHARLES E. BENTZ
Tech Area Manager, Controls

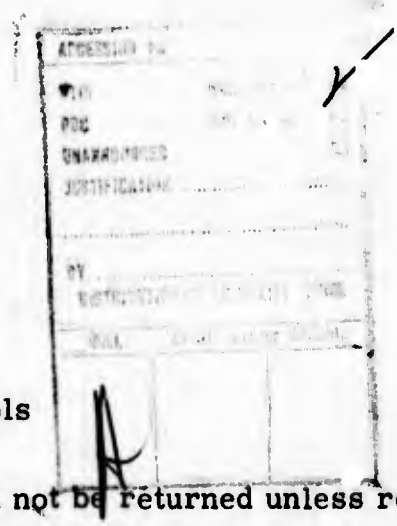

Copies of this report should not be returned unless return is required by security considerations, contractual obligations, or notice on a specific document.

TABLE OF CONTENTS

LIST OF ILLUSTRATIONS

LIST OF TABLES

I. INTRODUCTION

Detroit Diesel Allison (DDA) has been actively engaged in research and development programs concerned with gas temperature measurement. Years of thermocouple research and development have yielded a variety of operational air-cooled and nonair-cooled thermocouples for such application as power limiting and control of the T56 gas turbine engine. Not only has DDA been concerned with thermocouple development, but in 1966 began evaluating fluidic temperature sensors for incorporation in improved engine control systems. DDA's varied experience with temperature sensors for engine control purposes formed the basis of work conducted during this program.

The objectives of this program were to:

- Design a fluidic temperature sensor to measure the inlet air temperature to the HP compressor of a turbofan engine technology demonstrator (The measured inlet air temperature would be used for scheduling variable compressor vanes on the engine.)
- Fabricate two fluidic temperature sensors and air ejector assemblies suitable for mounting at the HP compressure inlet location of a TF41 test engine (The air ejector is needed to maintain proper sensor operation under low pressure threshold conditions at the inlet to the HP compressor.)
- Conduct rig testing to evaluate the performance of both sensors under steady-state and transient conditions in a simulated engine environment.

II. FLUIDIC TEMPERATURE SENSOR

OPERATION

A schematic of the fluidic temperature sensor/air ejector assembly is shown in Figure 1. The sensor measures the temperature of an airstream by diverting a small quantity of the airstream into its probe. The sampled air flows upward through the probe and enters a fluidic resonating cavity. This air entering the resonating cavity impinges on a splitter edge and produces an acoustical (edgetone) frequency which is transmitted in the resonating cavity at sonic velocity and, thus, is gas-temperature dependent. The resulting acoustical alternations become amplified by the resonator cavities to a level that can be detected by a piezoelectric pressure transducer. Stable operation of the sensor is achieved when the pressure drop across the two exit orifices is sufficient to cause choked flow. Once the exit orifices of the sensor become choked, the sensor output frequency is nearly insensitive to airstream pressure variations and changes only as a function of static gas stream temperature. Transient response of this fluidic sensor, as will be subsequently discussed, consists of two parts: a relatively fast reponse caused by gas "flushing" from the resonant cavities and a relatively slow response as a result of the thermal inertia of the sensor body.

The fluidic temperature sensor developed during this program was required to operate under airstream conditions ranging from a pressure of 18 to 75 psia at airstream temperatures up to 500°F. Since stable sensor operation requires a substantial (10-15 psia) driving pressure differential, an air ejector was integrated into the sensor to extend its operating pressure range. By use of the air ejector, a pressure lower than the ambient airstream pressure is produced downstream of the sensor discharge exit orifices, thus permitting them to remain choked at lower inlet pressure levels.

SENSOR GEOMETRY

Major considerations in the design of the temperature sensor were (1) to provide a sensor probe configuration of high structural integrity that could be

used on a TF41 turbofan engine for shakedown evaluation and on the Joint Technology Demonstrator Engine (JTDE) for subsequent evaluation, (2) integration of the fluidic edgetone resonator into the probe structure, and (3) the close coupling of the sensor transducer and air ejector to the mounting head.

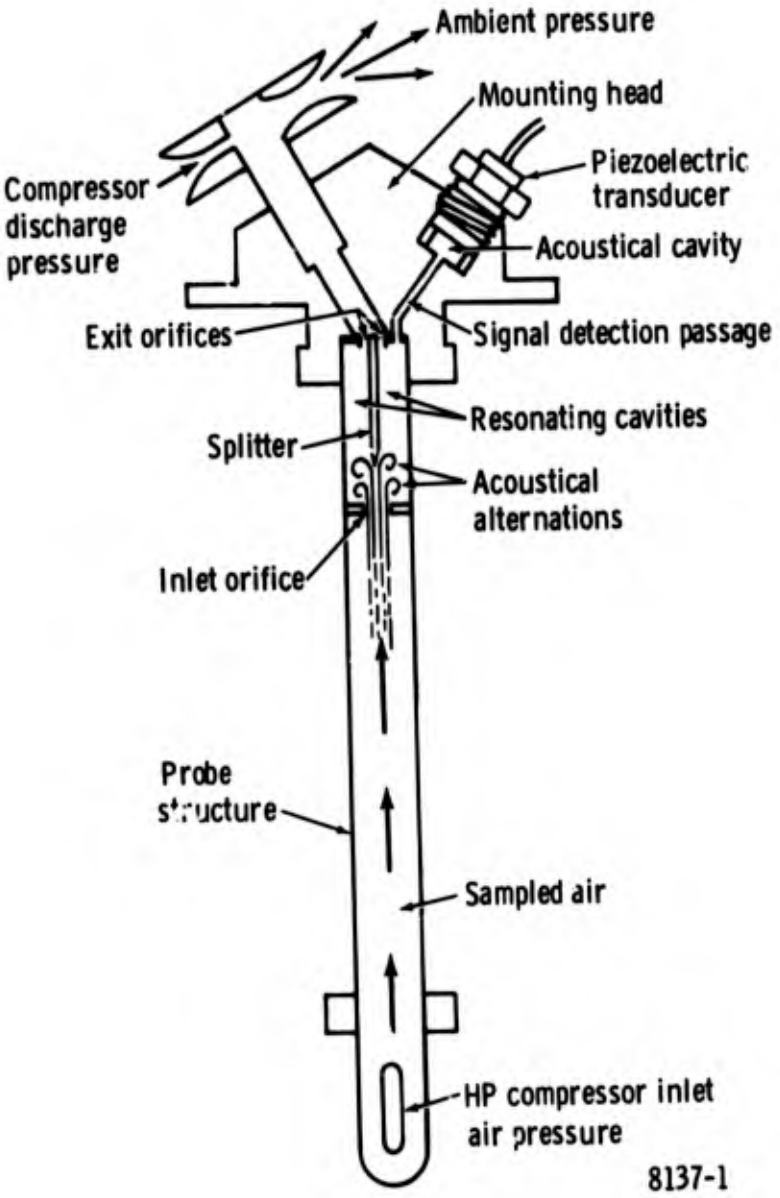

Figure 1. Fluidic temperature sensor/air injection schematic.

The temperature sensor configuration illustrated in Figure 2 was designed to mount on the TF41 turbofan engine at the HP compressor inlet station. The probe geometry is similar to that of total pressure probes that have been engine tested and proved.

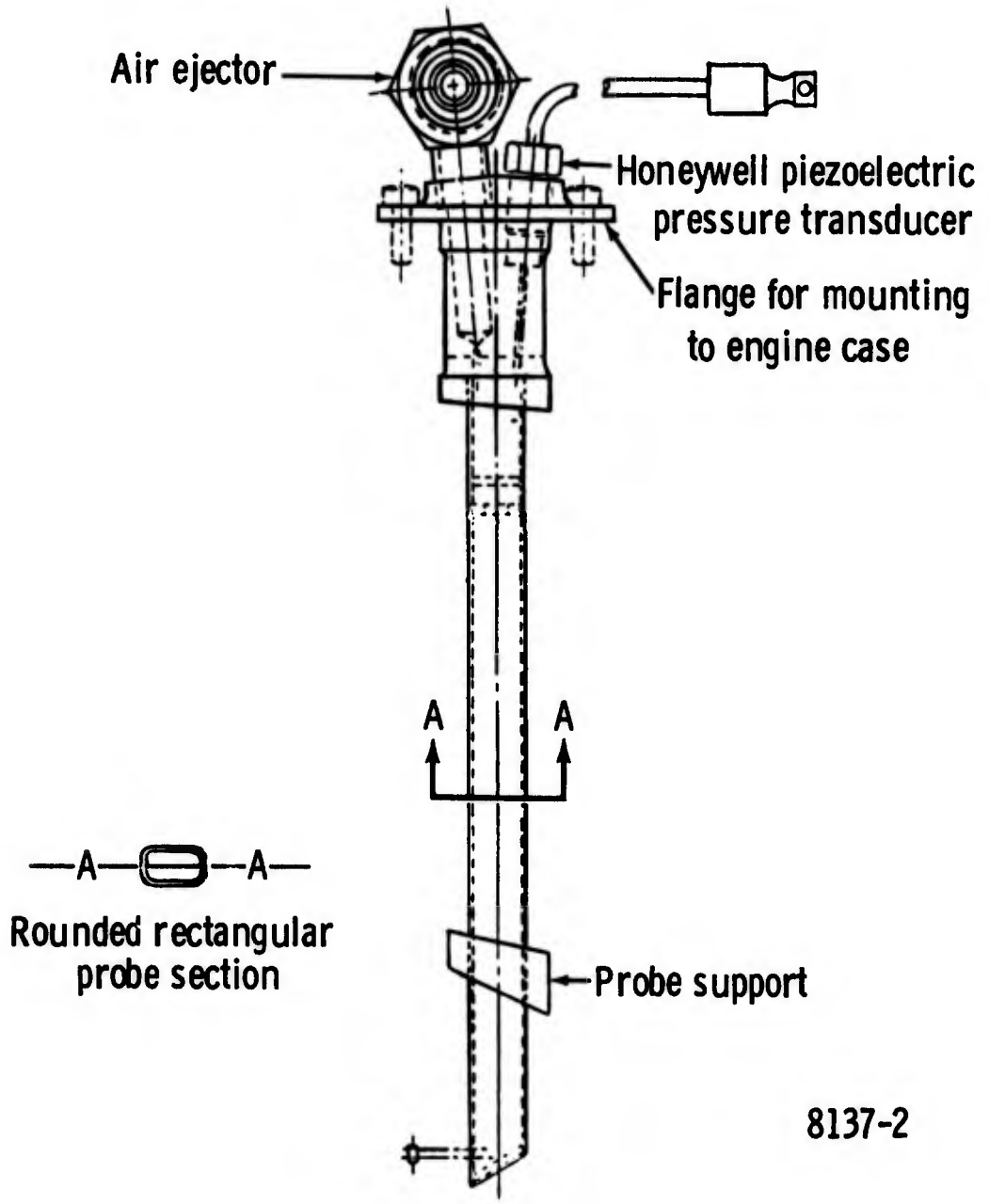

Figure 2. Fluidic temperature sensor/air ejector (P/N EX-112219).

Features of the sensor design are (1) a thin-walled (0.028 in.) probe of high structural integrity, (2) a minimum probe cross section for reduced flow blockage, (3) an edgetone resonator integrally built into the probe, (4) an attached air ejector, and (5) the use of a prototype low-cost, high-performance Honeywell transducer. The Honeywell transducer employs a lithium niobate crystal to transform dynamic pressure into electrical voltage. This piezoelectric pressure transducer has an operating pressure range of 0 to 400 psia and can be used satisfactorily in temperature environments to 1400°F. The physical construction of the transducer is such that it will withstand a 20-g vibration force.

PERFORMANCE VERIFICATION OF EDGETONE RESONATOR CAVITY

Under USAF Contract F33615-71-C-1882, Project 3066, DDA acquired experience with an edgetone resonator concept developed by the Air Force Aero Propulsion Lab (AFAPL). DDA used the AFAPL concept in an immersed probe fluidic temperature sensor which performed successfully in a 3000°F burner rig test.

The edgetone resonator used in this sensor design employed a rectangular cross section with rounded corners as compared with the AFAPL circular, cross-section resonator previously tested. A comparison of these edgetone resonator shapes is shown in Figure 3.

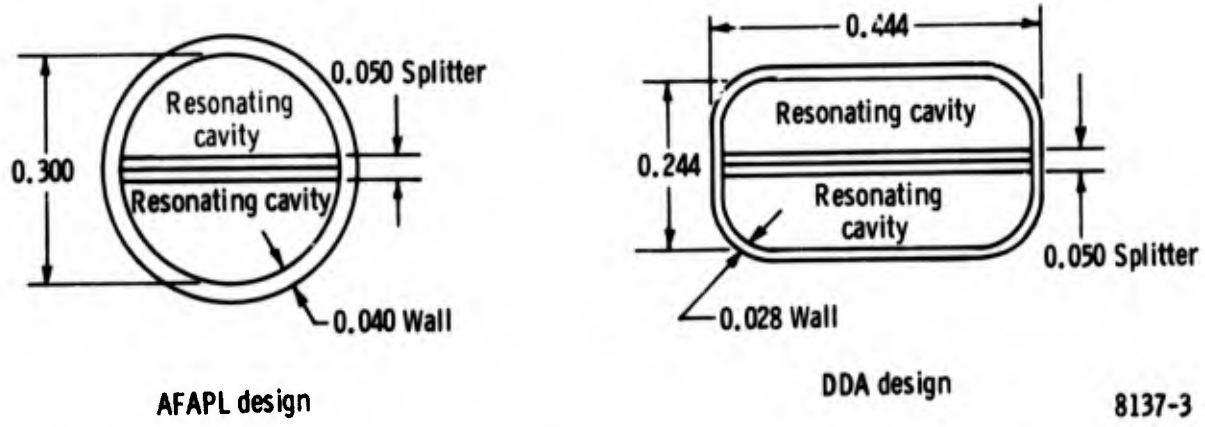

Figure 3. Comparison of AFAPL and DDA sensor section configurations.

To verify that the new resonator cavity shape would provide sufficient acoustical output to be properly detected by a pressure transducer, a sensor edgetone resonator test model was fabricated. The model component parts, shown in Figure 4, consisted of the resonator test section and two sets of entrance and exit orifice plates. The test setup, shown in Figure 5, consisted of:

- Sensor geometry test model
- 601L Kistler pressure transducer
- 504 Kistler charge amplifier
- Tektronic oscilloscope
- Pressure regulator

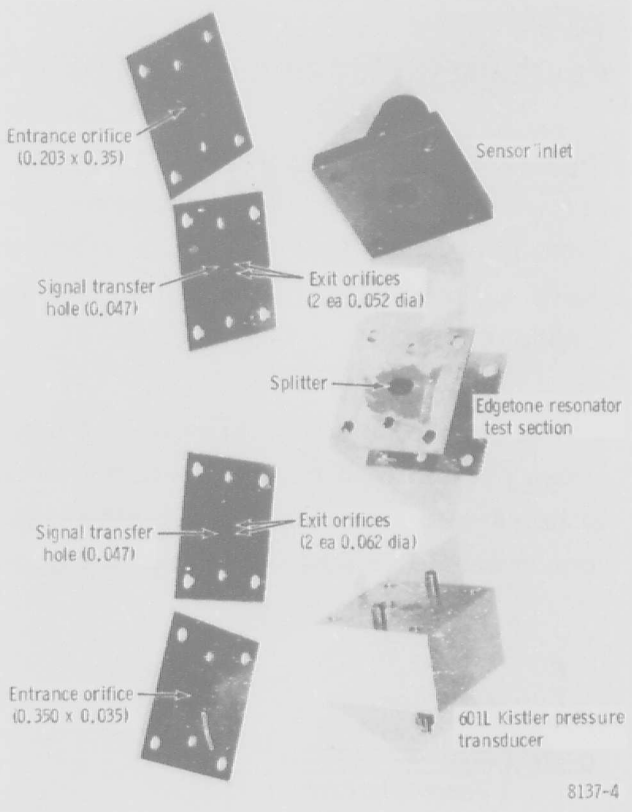

Figure 4. Sensor geometry test model.

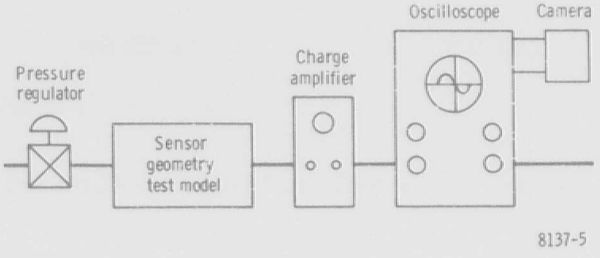

Figure 5. Test setup for evaluating sensor geometry model.

Three test sensor combinations of entrance and exit orifice area ratios were evaluated at an inlet supply pressure of 20 psig. Results of the test, as shown in Figure 6, indicated that the entrance-to-exit orifice area ratio test combination 1 best tuned the new resonating cavity. This combination of entrance-to-exit orifices selected for the fluidic temperature sensor/air ejector design was dimensionally the same as those used in the original AFAPL resonator.

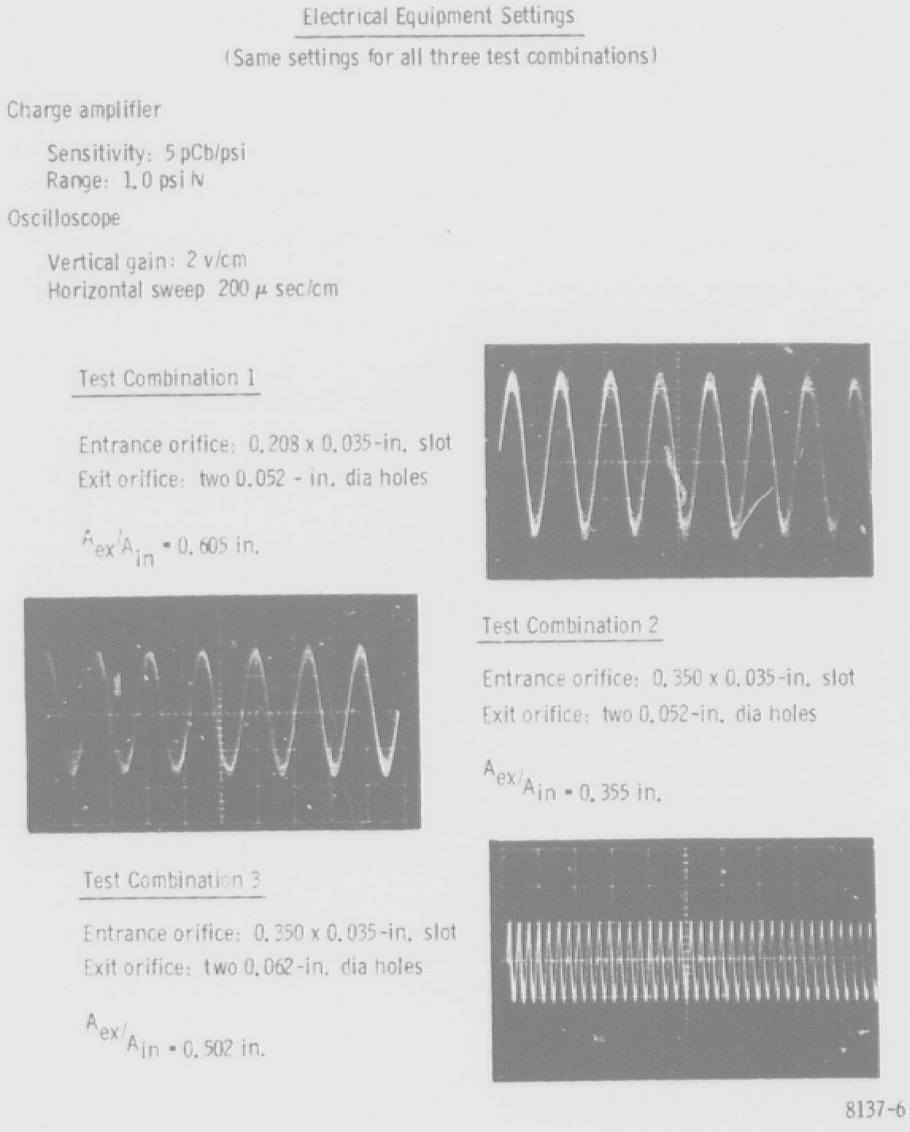

Figure 6. Results of sensor geometry model test evaluation.

FABRICATION

Two fluidic temperature sensor/air ejector assemblies, as shown in Figure 2, were fabricated for this program. The subassembly shown in Figure 7 indicates the dimensional aspects of the sensor probe structure. Figure 8 shows details of the air ejector components used. All elements of the sensor assembly, identified in Figure 9, were made from AMS-5566 stainless steel using conventional machining methods.

Joining of these sensor elements into an assembly was accomplished by the use of laser beam welding and step brazing techniques. Nickel braze alloys, which melted at different temperatures, were used to step braze the entrance orifice plate, splitter, and mounting head into an integral structure. The technique followed in step brazing these sensor elements is shown in Figure 10. Excess material on the entrance orifice locating lugs and edgetone splitter was trimmed off after the final brazing operation.

The completed fluidic temperature sensor assembly, shown in Figure 11, was machined to accept a Honeywell transducer and mount on the intermediate compressor case of the TF41 turbofan engine. Figure 12 illustrates the sensor mounted at the HP compressor inlet station.

HEAT TRANSFER PREDICTIONS OF SENSOR PERFORMANCE

A heat transfer analysis (using the simplified nodal pattern described in Appendix A) was made prior to the completion of sensor fabrication to (1) predict the transient response of the sensor under test conditions and (2) investigate areas for improving the sensor response. An initial analysis was performed on a previously tested short-probe, iridium-rhodium, high-temperature, fluidic sensor to check out the validity of the mathematical predictions.

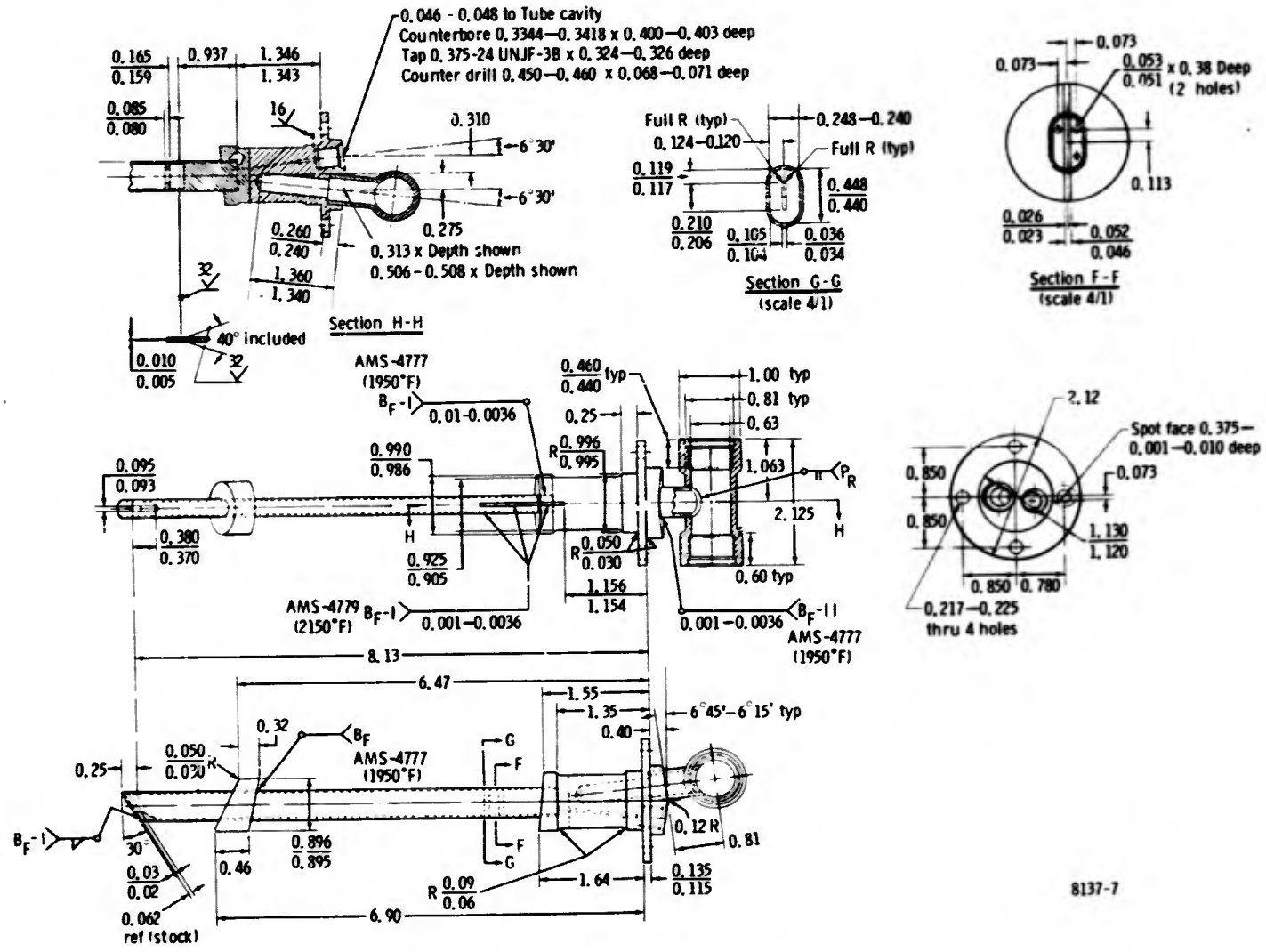

Figure 7. Details of sensor probe structure.

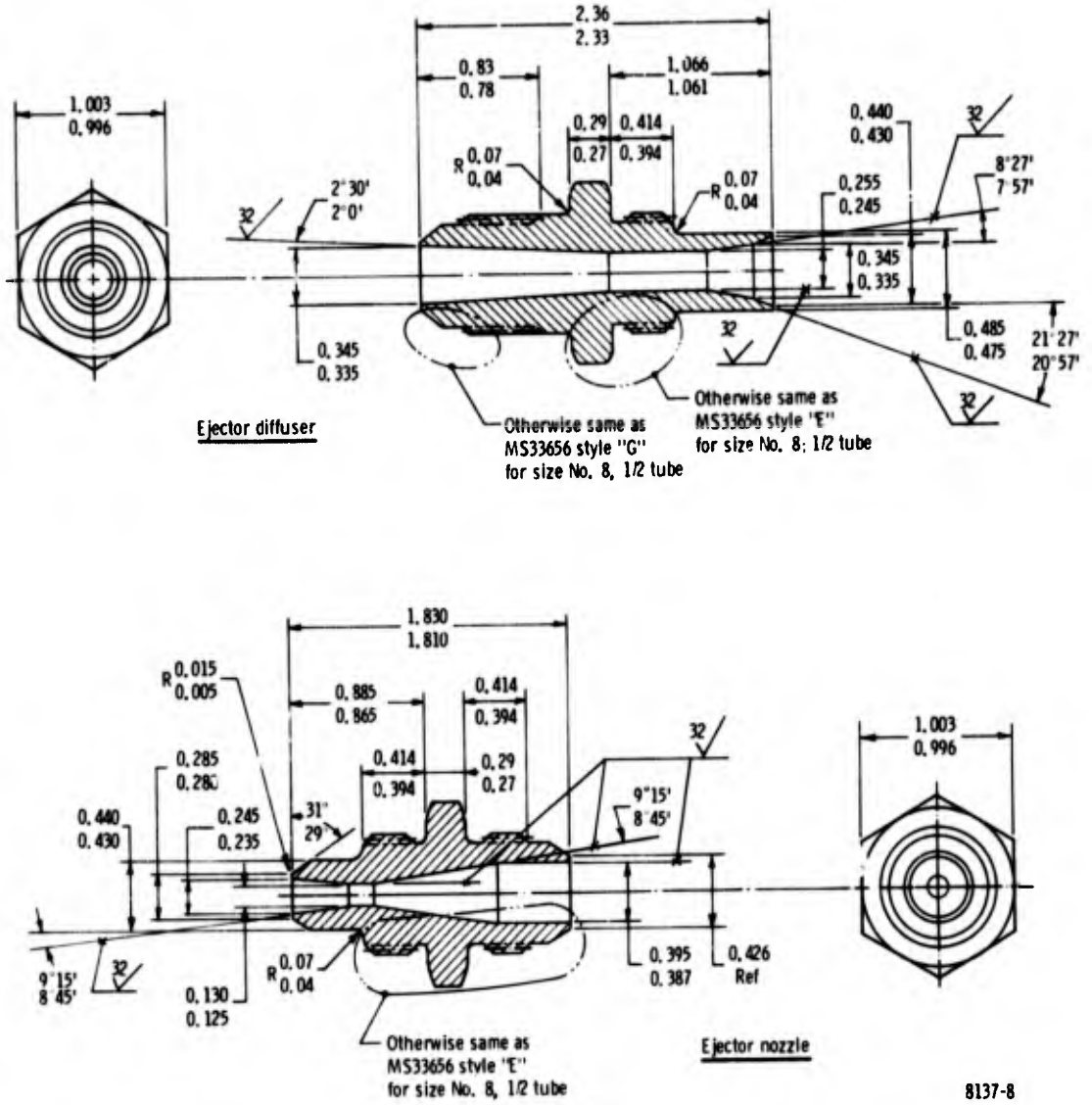

Figure 8. Details of air ejector components.

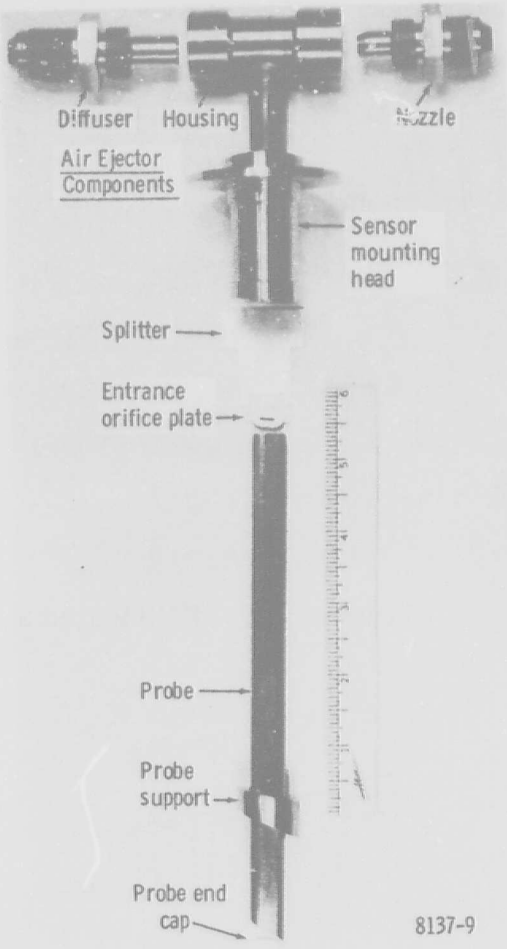

Figure 9. Elements of sensor assembly.

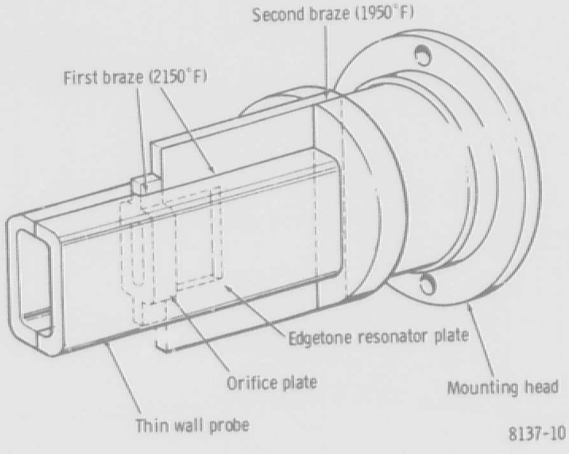

Figure 10. Sensor step brazing technique.

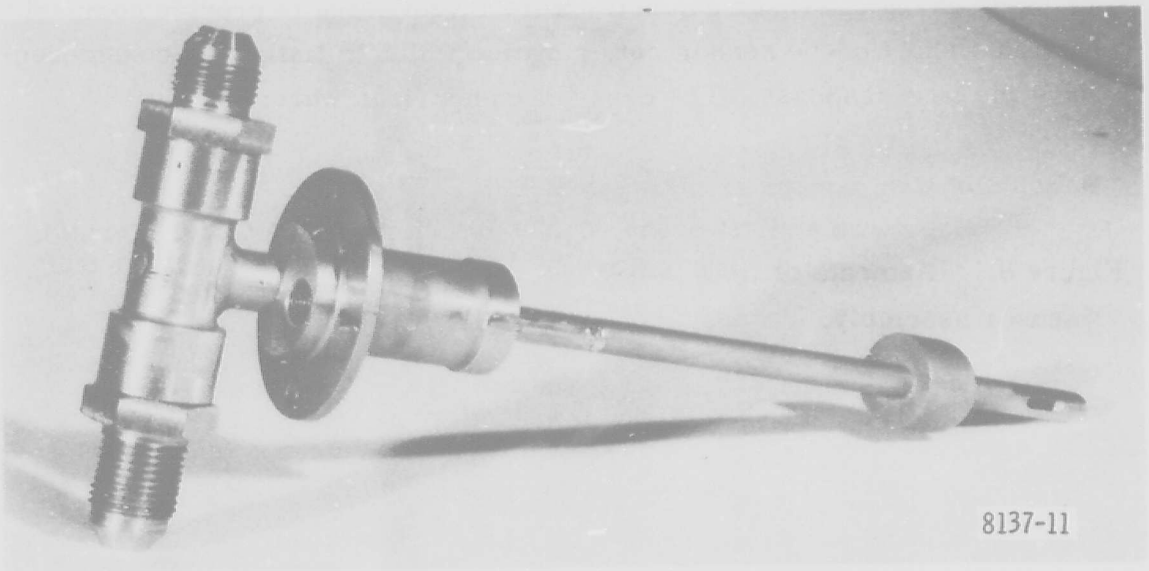

Figure 11. Fabricated sensor assembly.

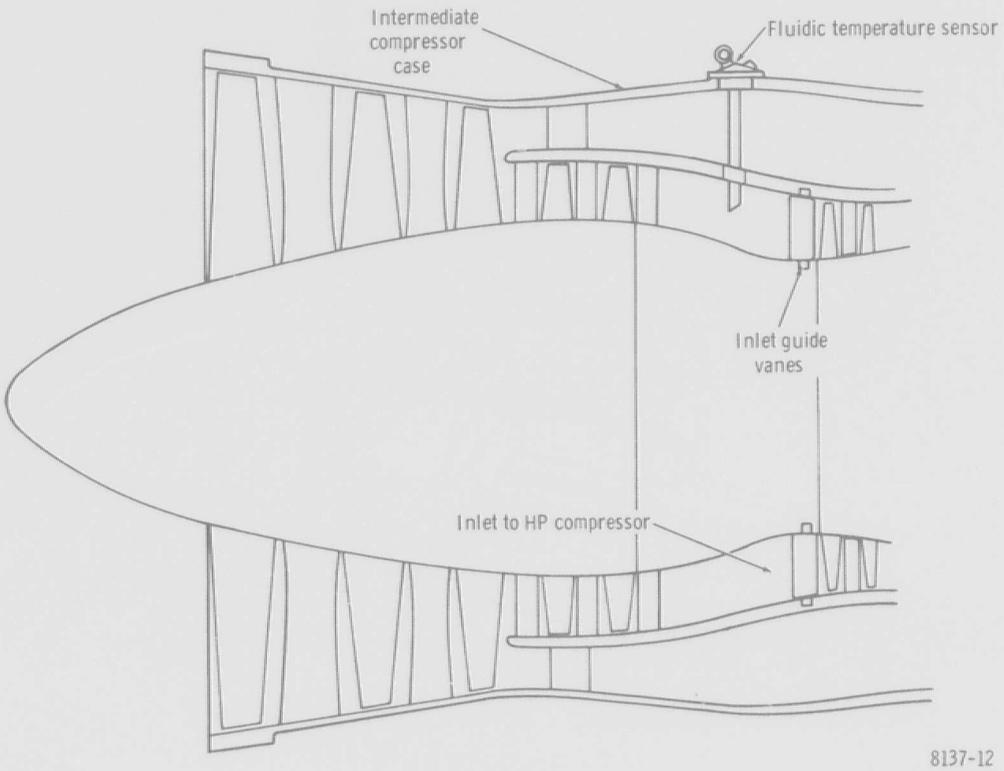

Figure 12. Fluidic temperature sensor mounting on TF41 turbofan engine.

Four basic cases of sensor geometry were investigated to provide comparisons with a short probe sensor configuration which initially was considered to have the best response. The cases of comparison were:

- Basis of Comparison
  - Sensor with a short probe, 0.050 in. thick splitter, and operating under low mass flow
- Sensor Geometry Variations
  - Sensor with a long probe, 0.050 in. thick splitter, and operating under both a low mass flow and a high mass flow
  - Sensor with a long probe, 0.010 in. thick splitter, and operating under low mass flow
  - Sensor with a long probe, 0.050 in. thick splitter, and with liner variation investigated at low mass flow conditions (concentric liners that were 0.001, 0.002, and 0.004 in. thick; diamond-shaped liner that was 0.001 in. thick)

The analysis indicated that a thin metal liner with dead air space behind it would decrease the initial step response to a slight temperature change, but would improve the overall time response of the sensor to a point where it was almost as good as the short probe configuration. Comparisons of sensor outputs to a step temperature change are shown in Figure 13: a sensor with a long probe and no liner, a sensor with a diamond-shaped liner in a long probe, and a sensor with a short probe.

The decision was made, based on the results of the heat transfer analysis, to evaluate a 0.001 in. thick, diamond-shaped, stainless steel liner upstream of the sensor entrance orifice on sensor No. 2 (Figure 14). Air space behind the diamond-shaped liner was sealed off from the incoming airflow at both ends by a high temperature RTV silicone rubber capable of withstanding 600°F.

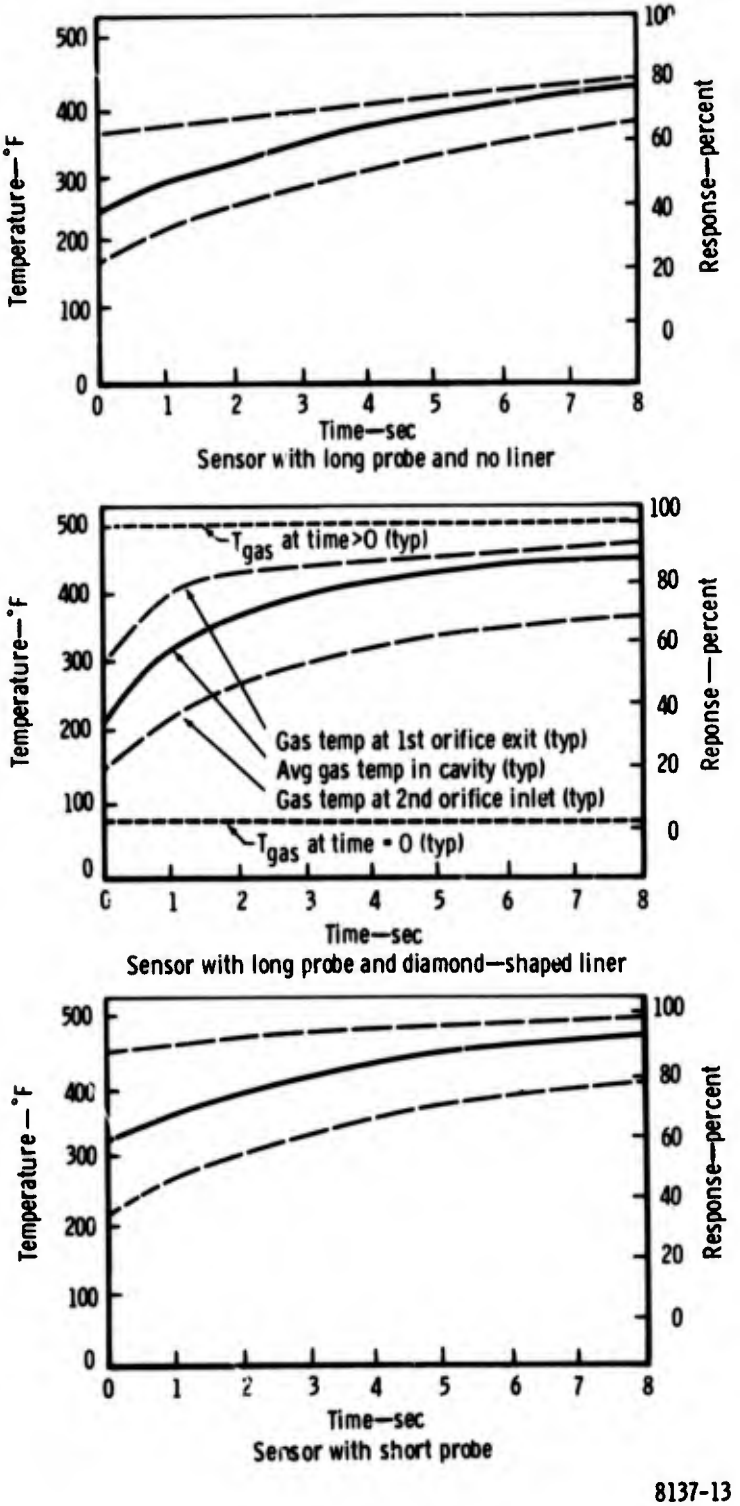

Figure 13. Results of heat transfer analysis.

The decision also was made that for this analysis to become meaningful for future sensor development work, sensor No. 1 without a liner should be instrumented with thermocouples (Figure 15) at key heat transfer nodal stations to record the sensor metal response. The data obtained from sensor No. 1 test evaluation could be compared with the prediction.

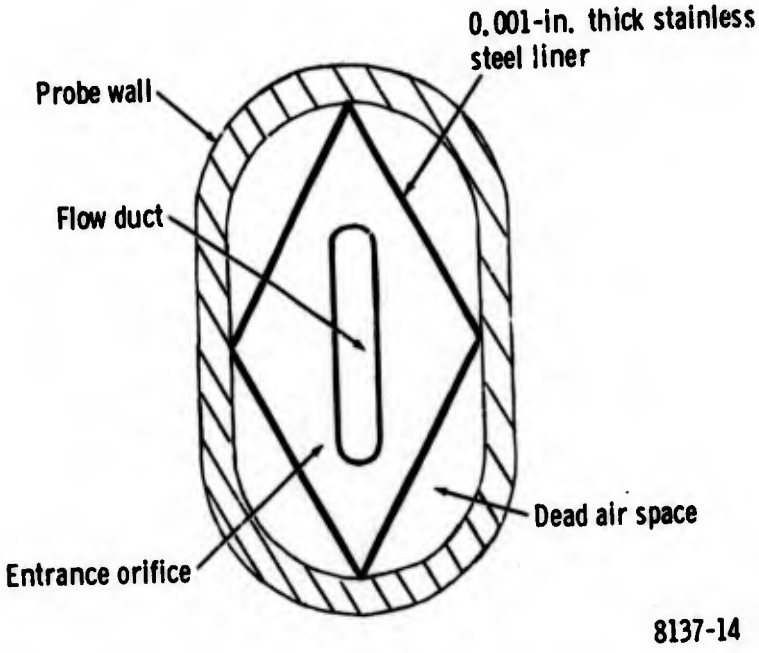

Figure 14. Diamond-shaped liner installed in probe.

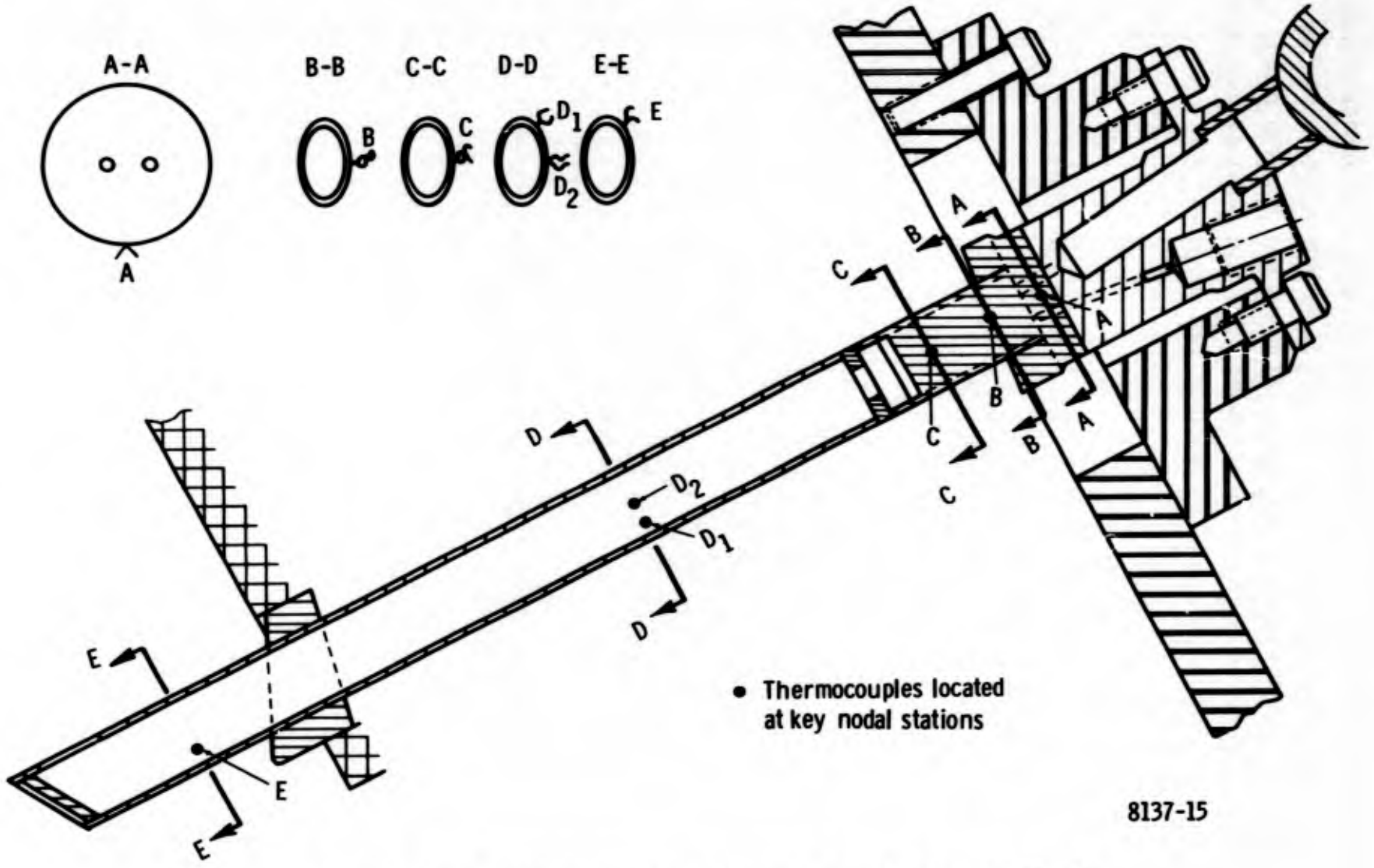

Figure 15. Thermocouple instrumentation on sensor No. 2.

III. BENCH TEST OF PROTOTYPE SENSORS

Two prototype fluidic temperature sensors were given a bench performance checkout test in preparation for evaluation rig testing. Initial bench testing disclosed that neither sensor would produce a discernible signal output frequency at sensor inlet pressures up to 90 psig.

Since the sensors did not function in a bench performance checkout test, it was necessary to remove both long probes as shown in Figure 16 just forward of the entrance orifice plate. Investigation of the sensor heads revealed that the registration of each orifice plate had shifted during the brazing operation in such a manner to cause misalignment between the inlet orifice and the splitter knife edge. Under these conditions, it was impossible for a good edgetone frequency to be generated and acoustically amplified. Figure 17 depicts the observed misalignment of the entrance orifice plates on Sensors No. 1 and 2.

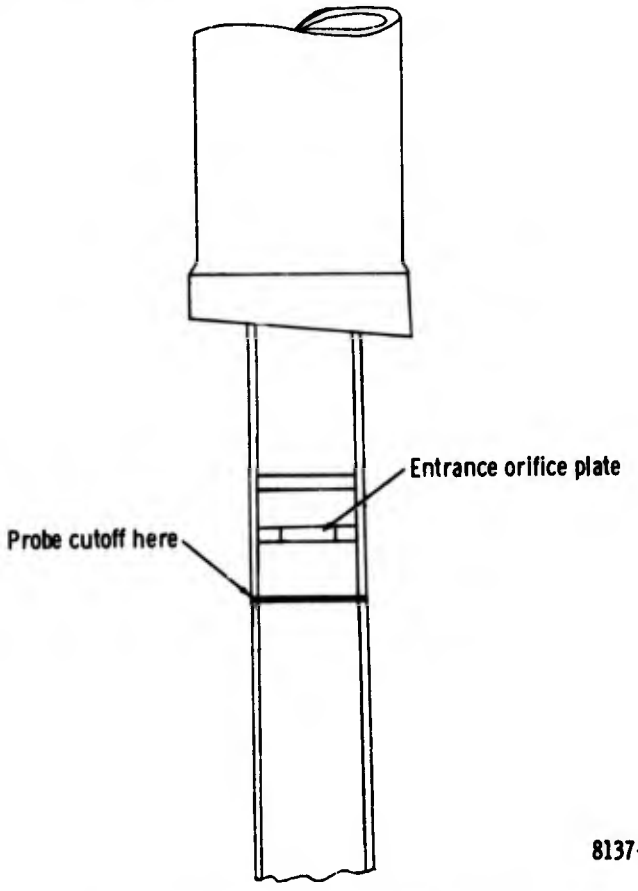

Figure 16. Sensor with long probe removed.

Sensor No. 1 entrance orifice was both tilted and offset from the center line of the splitter and could not be hand reworked by filing the orifice. Sensor No. 1 was repaired by laser beam welding a new entrance orifice plate insert into the sensor entrance end and then subsequently rejoining the long probe by laser beam welding.

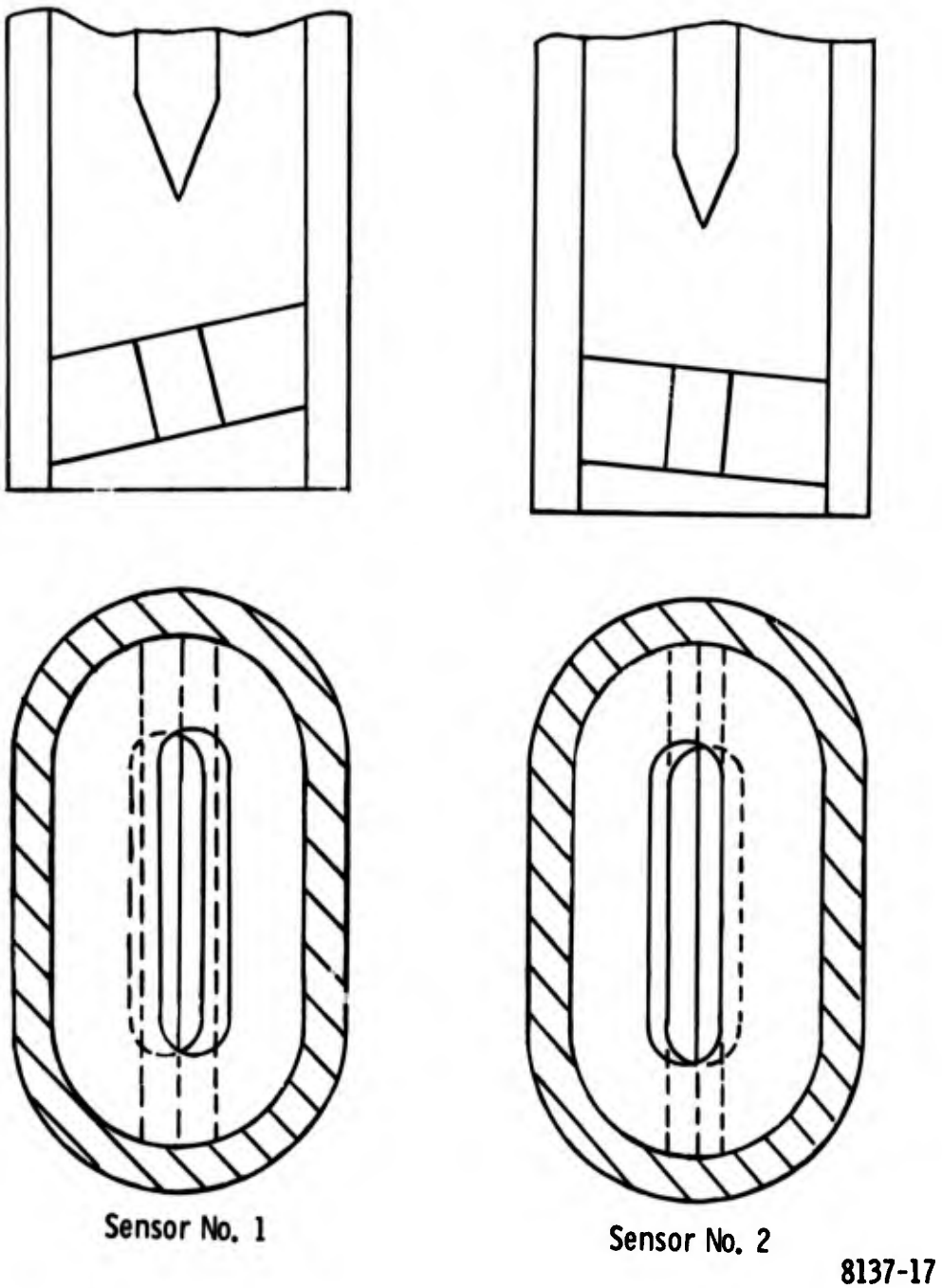

Figure 17. Entrance orifice misalignment.

Sensor No. 2 was restored to operational status by lightly hand filing the sides of the entrance orifice so that they were parallel to the splitter. After the repair work had been performed, the sensor head was refitted to the probe by laser beam welding and the diamond-shaped, 0.001-in. thick stainless steel liner was installed in the probe.

After restoration of the sensors had been completed, a final test was made to verify their performance. The test setup as shown in Figure 18 was used in the bench evaluation. Both sensor assemblies were tested at room temperature when powered by air supplied directly to the probe inlet and by air supplied directly to the air ejector. Each sensor functioned satisfactorily from atmospheric pressure to 105 psia. Tuning of the transducer in each sensor was accomplished by adjusting the acoustical cavity formed between the transducer face and the sensor mounting head (Figure 1) until the signal output amplitude was at a maximum. Both Honeywell transducers were easily tuned to the sensors and performed without problems. Figure 19 shows a linear increase of peak-to-peak voltage of the sensor signal output with increasing sensor supply pressure. All electronic gains on the oscilloscope and charge amplifier were held constant. Oscilloscope pictures taken of the sensor signal output with air supplied to the air ejector only and air supplied to the sensor probe only are shown in Figure 20.

Air consumption of the sensor air ejector was determined on the bench by measuring the pressure drop across a pair of calibrated orifices of 0.200-in. dia and 0.250-in. dia under shop air temperature conditions. The air consumption of a sensor air ejector for varying supply pressures is shown in Figure 21. It is estimated from the data shown in Figure 21 that the consumption of engine compressor discharge air by the sensor air ejector at 400 psig maximum engine operating conditions would not represent any significant loss in engine performance.

The difficulty encountered with both sensors pointed up some shortcomings in the sensor design or process fabrication techniques that were originally

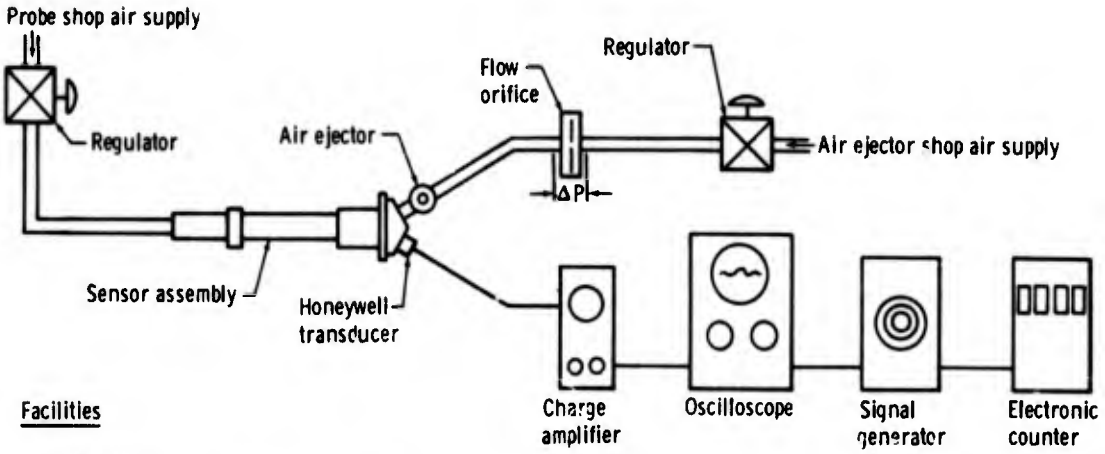

Facilities

- Shop air
- Flow measuring orifice—range (0.5 to 2 lb/min

Electronic equipment

- Dual trace scope with camera
- Charge amplifier (Kistler 504)
- Signal generator
- Electronic counter

8137-18

Figure 18. Bench test setup for prototype sensors.

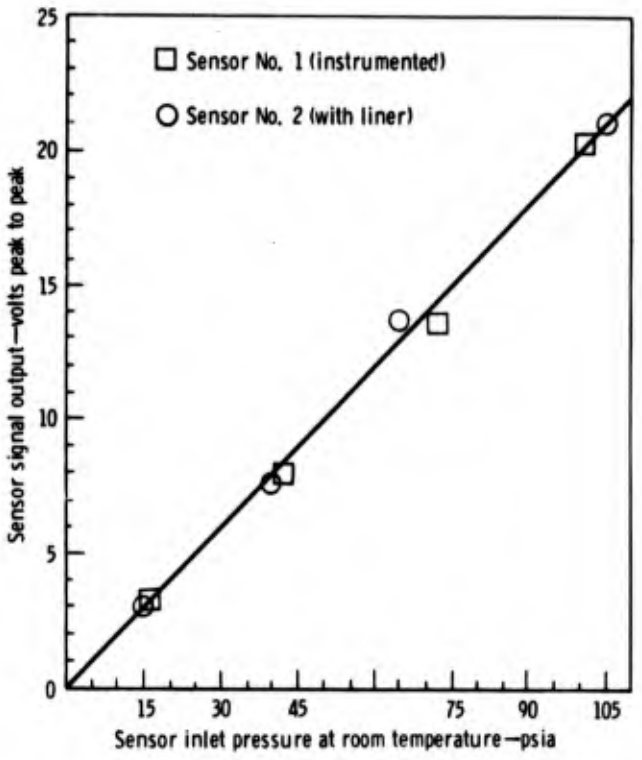

8137-19

Figure 19. Sensor No. 2 signal output test results.

Electrical Equipment Settings

Charge amplifier

Sensitivity: 0.2 pCb/psi
Range: 1.0 psi/v

Oscilloscope

Vertical gain: 5 v/cm
Horizontal sweep: 0.2 millisec/cm

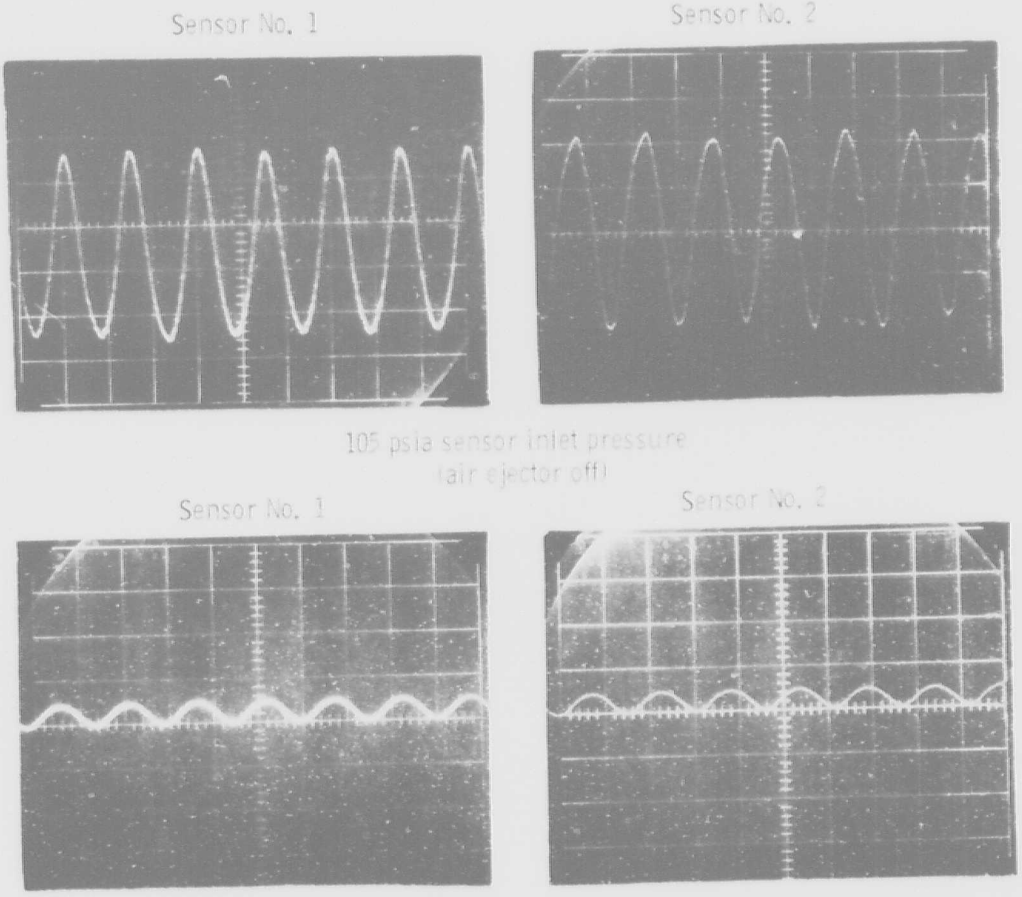

Figure 20. Signal output of prototype sensors.

used. However, repairs made to the sensor using laser beam welding technique produced high weld joint integrity. With this joint integrity, both repaired sensors had sufficient structural soundness to permit their use on the TF41 engine.

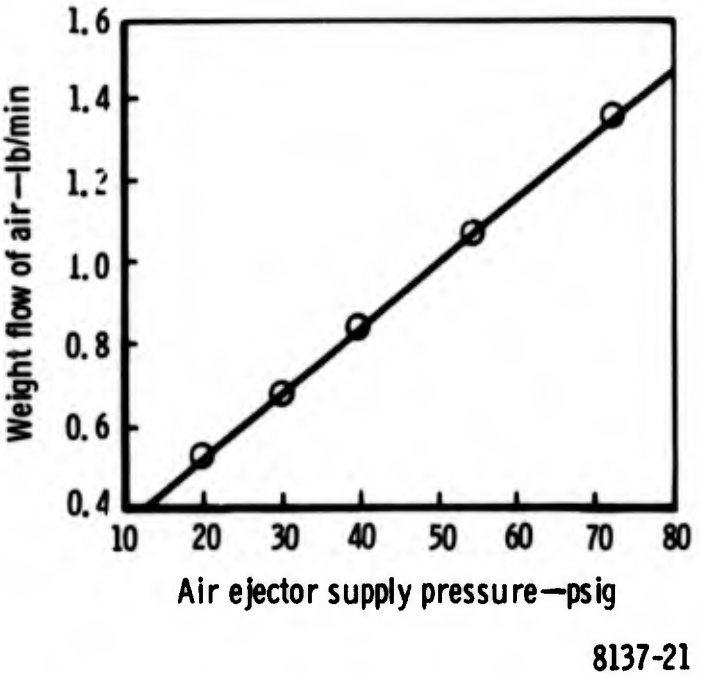

Figure 21. Air ejector air consumption.

IV. EVALUATION TEST FACILITY

TEST RIG DESCRIPTION

A new test section was fabricated for the evaluation of the long probe fluidic temperature sensor and the assembly was installed in the research combustion facility. Figure 22 shows the system relationships of airflow control valves, flow measuring orifices, electric heaters, and the sensor test section in the test rig setup.

All sensor evaluation testing was performed with this basic test rig setup. Operation of the test rig set up for each of the sensor evaluation tests is discussed in the following paragraphs.

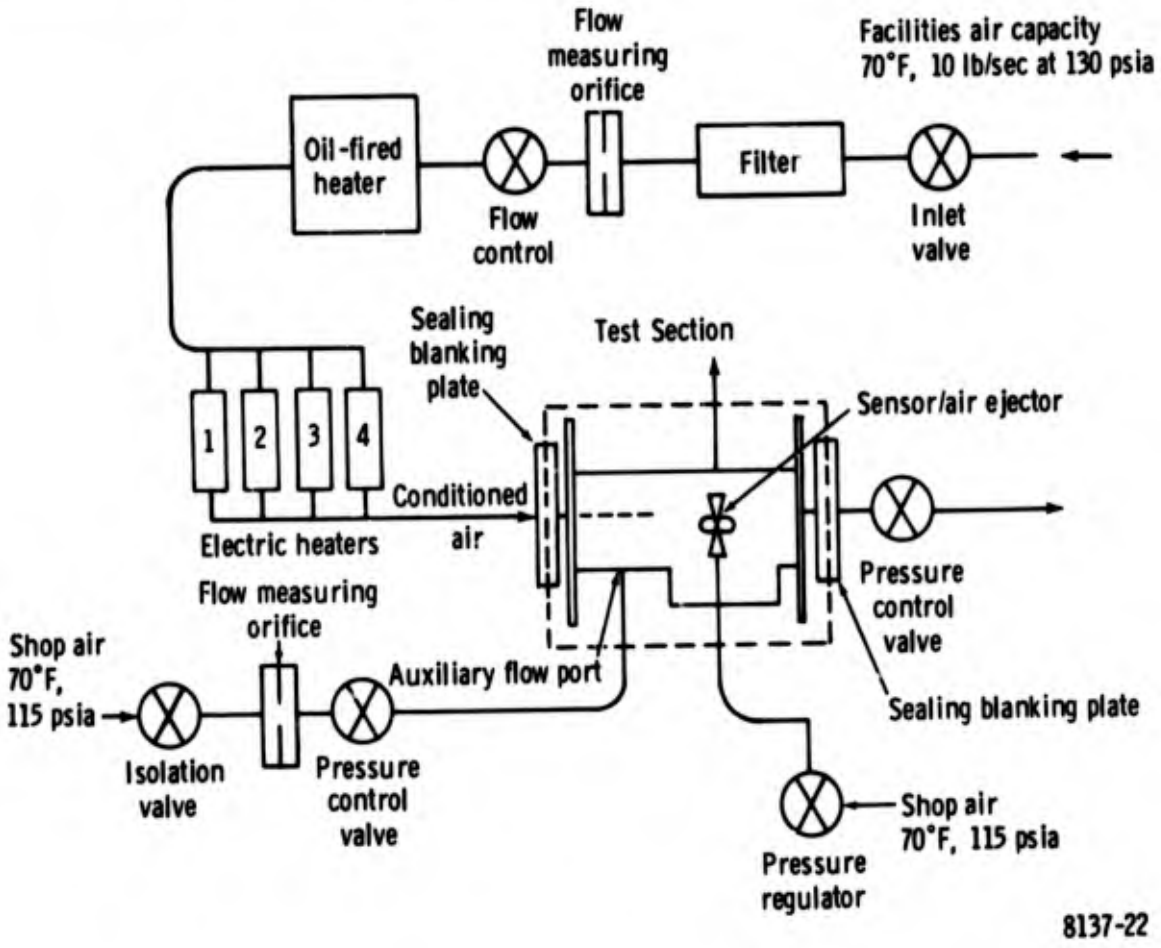

Figure 22. Test setup schematic.

Sensor Air Ejector Evaluation

Sealing blanking plates were installed on both ends of test section to provide a no airflow chamber. Absolute pressure ranging from 10 to 25 psia was produced within the test section. To develop a negative pressure in the test section, the auxiliary airflow port was capped and the inside pressure was lowered by running the sensor air ejector. During positive pressure operation of the test section, regulated air pressure was supplied to the auxiliary airflow port. Regulated shop air was furnished to the sensor air ejector. (See Figure 22.)

Sensor Calibration

Conditioned entrance air from the facility was permitted to pass unobstructed through both air ducts in the test section by flow-aligning the shutter doors and capping off the auxiliary airflow port. Regulated shop air was supplied to the sensor air ejector. (See Figure 23.)

Sensor Transient Test

Conditioned entrance air from the facility was allowed to pass through one air duct of the test section only by installing a flow blocking plate at the entrance of the other test section air duct. The flow-blocked air was then furnished with metered shop air through the cold airflow port. Regulated shop air was supplied to the air ejector. (See Figure 23.)

The test section shown in Figure 24 was designed and fabricated to provide a representative exposure of the long probe fluidic temperature sensor to airflow conditions that would be encountered at the inlet to the high pressure compressor of the JTDE. Airflow conditions accommodated by the test section were airstream velocities to 0.15 M_N, airstream temperatures to 500°F, and airstream pressures ranging from 10 to 75 psia.

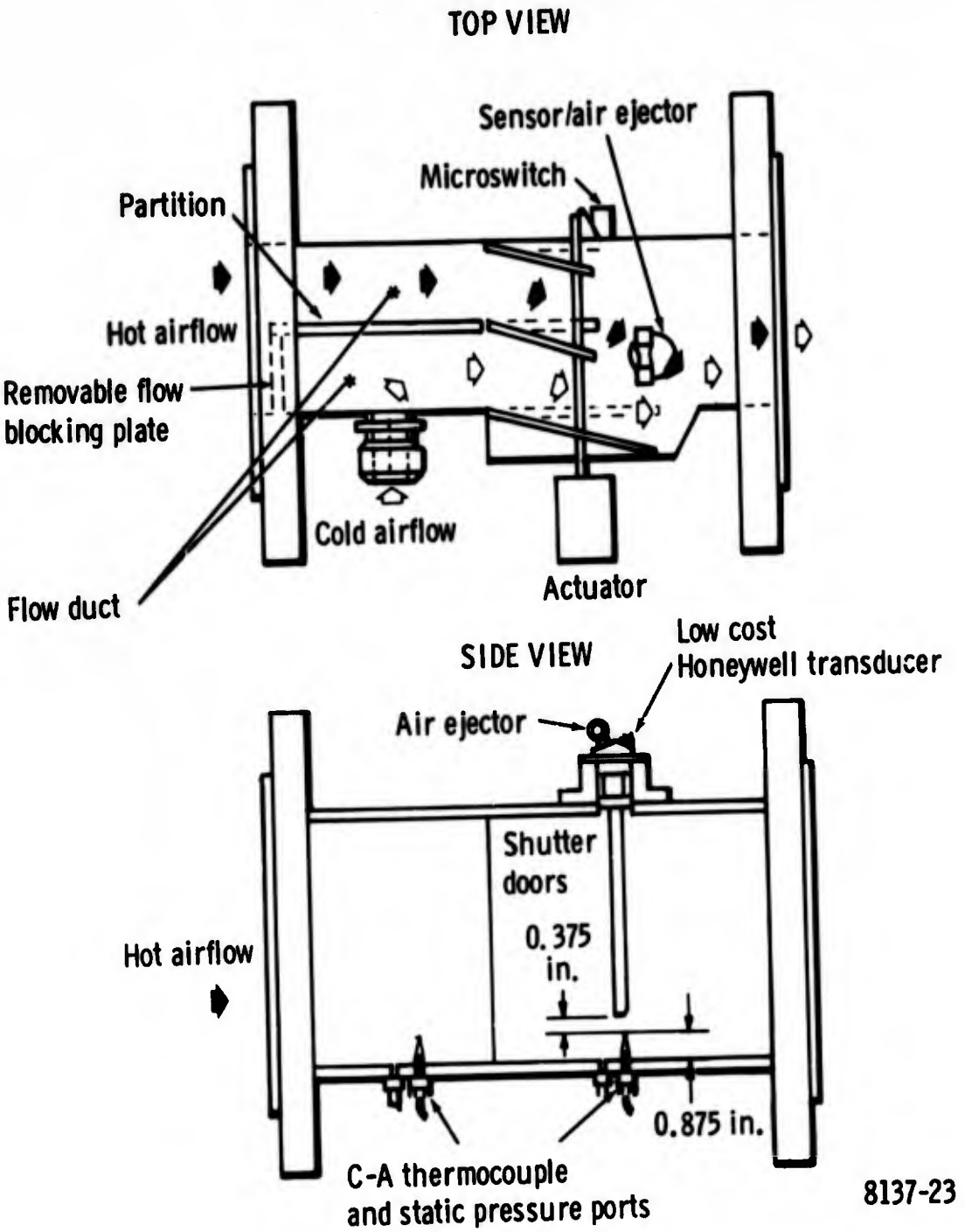

Figure 23. Test section geometry.

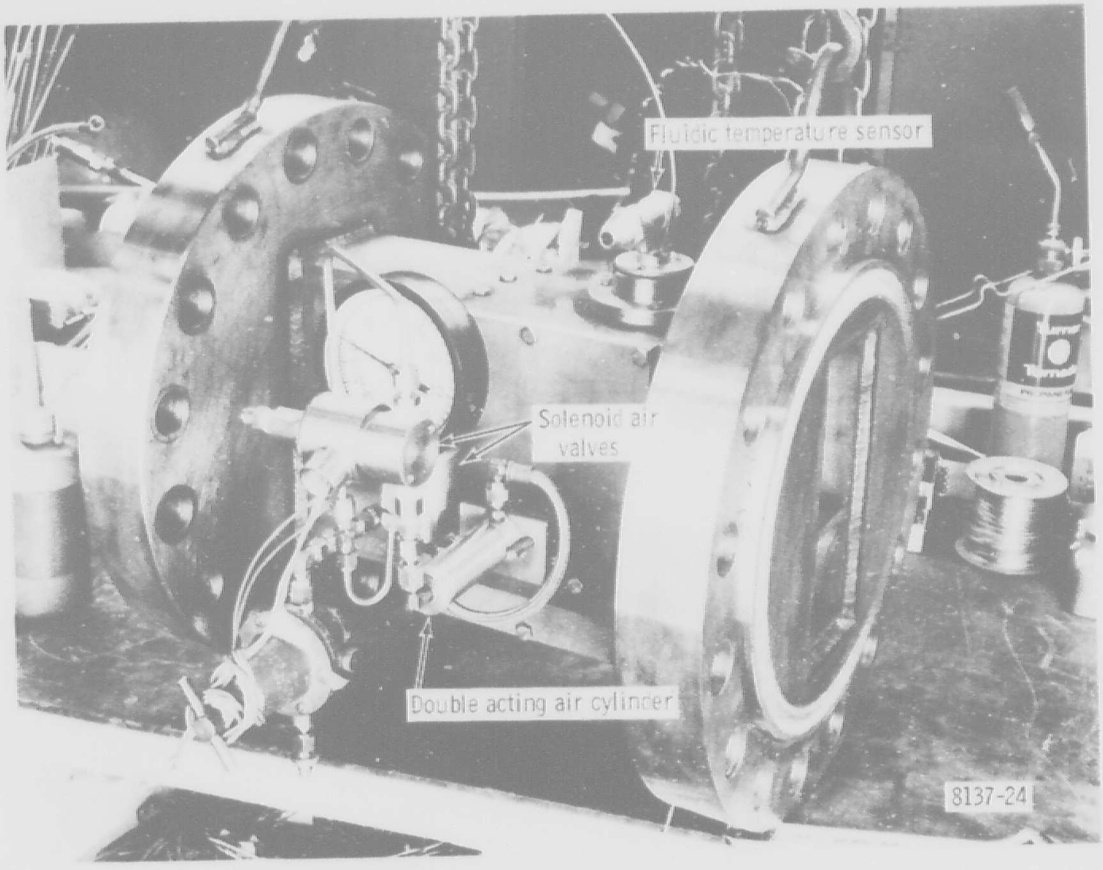

Figure 24. Test section.

Figure 23 shows the geometry of the test section and the mechanical arrangement of the movable shutter doors which were aligned with the direction of airflow during calibration testing and actuated during temperature response testing of the sensor.

Calibration of the sensor was accomplished by removing the flow blocking plate and capping the cold airflow port which permitted entrance air to the test section to flow through two rectangular ducts past flow-aligned shutter doors into the sensor test chamber. Static pressure taps and chromel-alumel (C-A) thermocouples were located in each flow duct and the test chamber. The thermocouple positioned under the sensor probe in the test chamber served as a reference for sensor performance evaluation.

When performing temperature response testing of the sensor, the flow blocking plate was installed in the cold air duct and shop air was connected to the cold air port to provide both hot and cold airflow into the sensor test chamber. With the test section set up in this manner, the sensor was subjected to rapid air temperature changes by moving the shutter doors to divert either hot or cold airflow onto the sensor probe. Figure 25 is a view of exit end of the test section showing the shutter doors diverted to allow hot airflow past the sensor. The shutter doors were powered by a double-acting air cylinder which was directed by two solenoid air valves as shown in Figure 24.

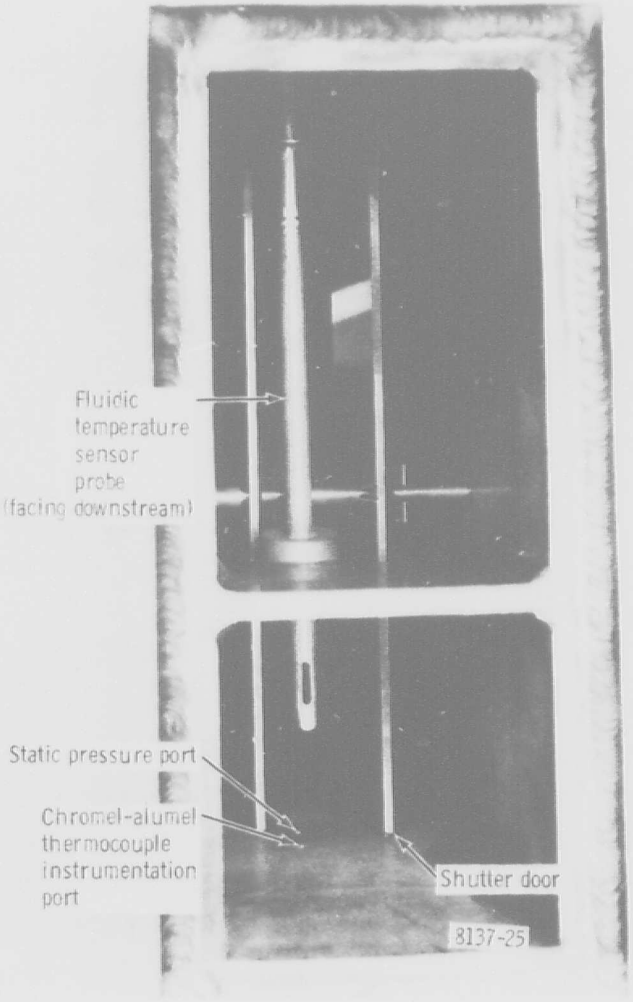

Figure 25. Test section shutter doors.

The speed of shutter door actuation depended on the supply pressure furnished to the air cylinder. During the sensor transient temperature response test, 90 psig air pressure was supplied to the air cylinder. This supply pressure produced a shutter door actuation time faster than the initial response time of the fluidic temperature sensor.

TEST INSTRUMENTATION AND DATA ACQUISITION

Test Thermocouple Instrumentation

C-A bare tip thermocouples were used to measure the air temperature in the test section and the metal temperature on the fluidic temperature sensor assembly. Thermocouples that were used to measure the air temperature in the test section had a bare tip exposure of 0.140 in. and were made from 0.025-in. dia C-A wire that was fused to form a 0.035-in. dia junction bead. The thermocouples that were used to measure metal temperatures of sensor probe assembly were made from 0.005-in. dia C-A wire that was spot welded to the structure. All thermocouple C-A wires were encased in a stainless steel sheath filled with magnesium oxide.

Air Ejector Evaluation Instrumentation

The output from a Honeywell piezoelectric transducer was amplified by a 501 Kistler charge amplifier for display on a Tektronix oscilloscope. A schematic of the instrumentation is shown in Figure 26.

Sensor Calibration Instrumentation

A Hewlett-Packard, 200-channel, automatic data acquisition and reduction system was used for rig control and obtaining data. The system operates on the following principles. A cross-bar scanner steps through the data channels on command and feeds signals to a digital voltmeter which is interfaced with a computer. The computer reduces the raw data to engineering

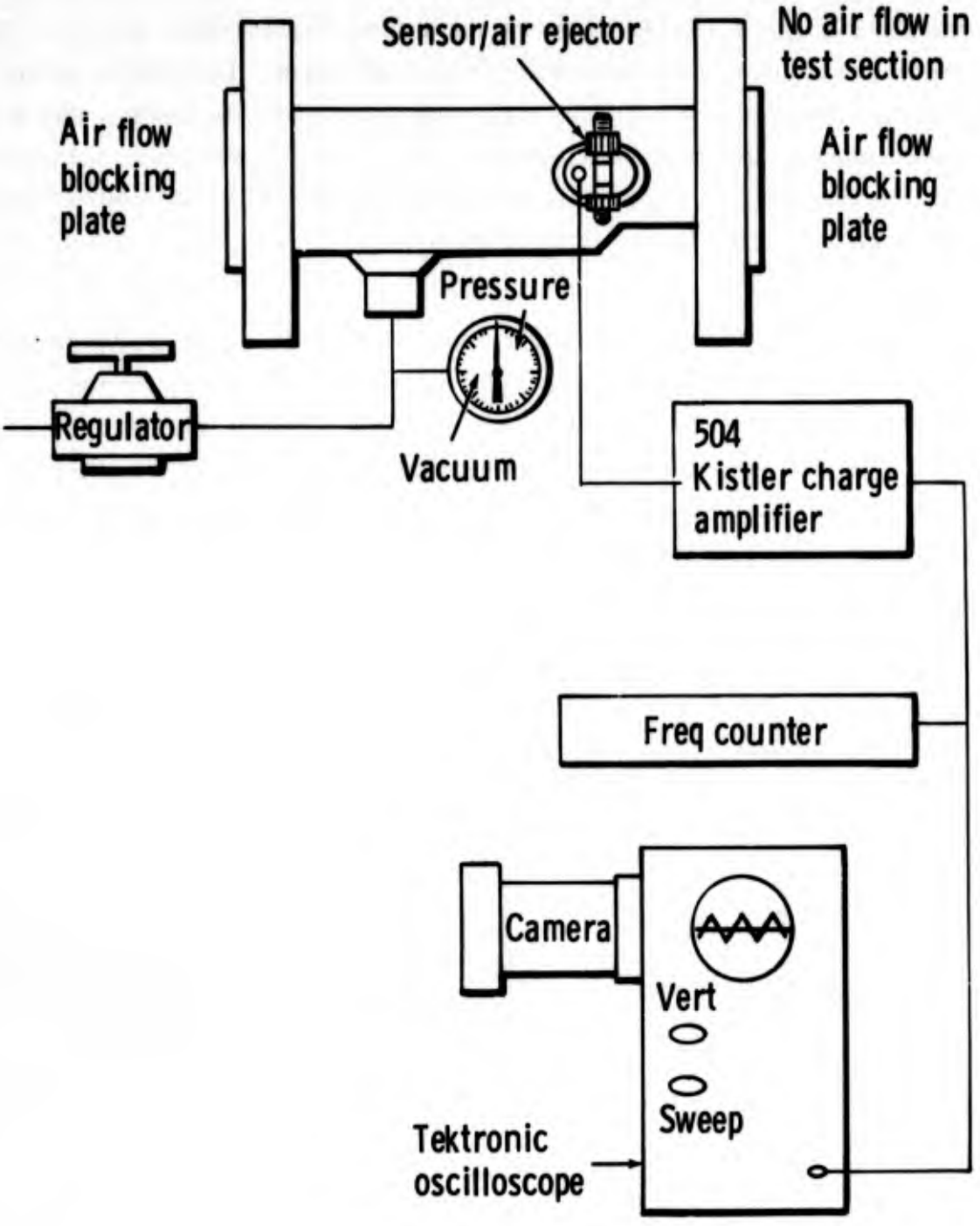

Figure 26. Sensor air ejector evaluation instrumentation schematic.

units. It also operates on the data to calculate Mach numbers and other parameters desired. Selected operating data and calculated values are then printed by teletype in approximately 15-sec intervals. Detailed readings can be obtained when desired and are logged on punched paper taper. These data are subsequently listed by an on-line printer. Readings taken at steady-state conditions are shown in Appendix B. Figure 27 shows the data acquisition devices located in the laboratory control room.

To verify the sensor output quality at each calibration point, pictures were taken. These pictures were identified with each run of the computer representing a calibration point. Electronic equipment shown in Figure 28 was the same as that employed in the air ejector evaluation with the exception of the additional band pass filter. The band pass filter was needed to blank out 60 Hz and 220 Hz signal interference.

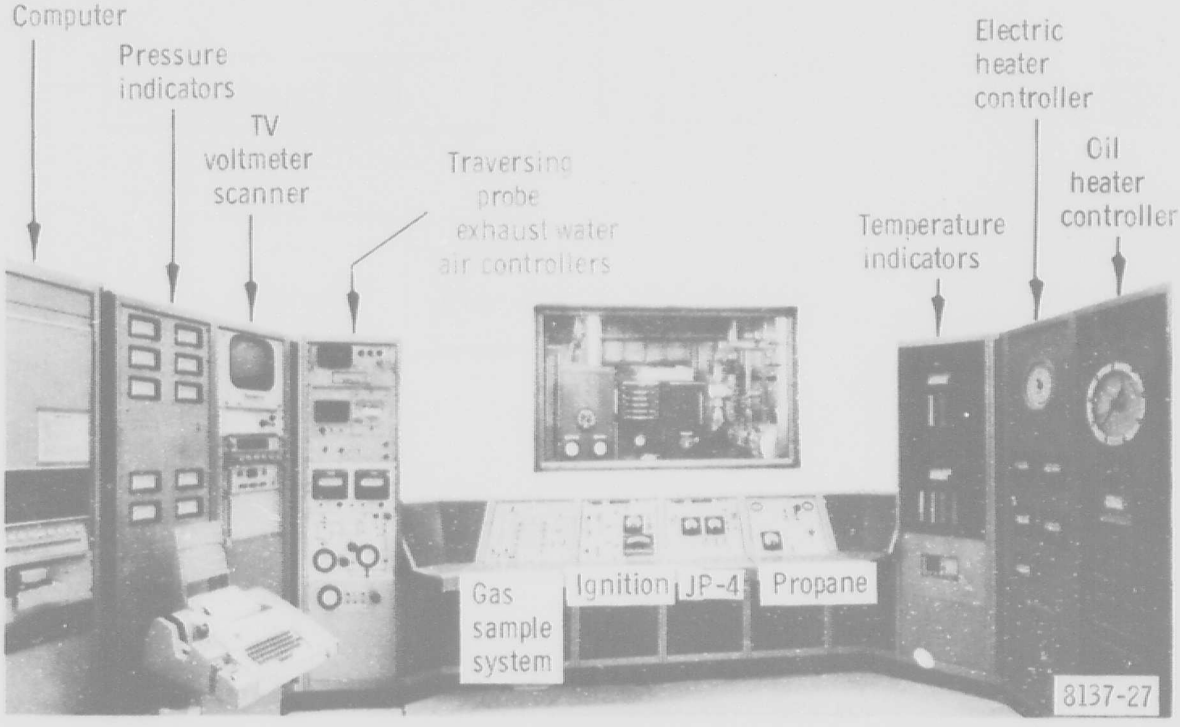

Figure 27. Data acquisition devices in laboratory control room.

Sensor Transient Response Instrumentation

A schematic of the system for processing the fluidic sensor output frequency and obtaining transient response data is shown in Figure 29. The transient response was recorded on an 8-channel Offner recorder. During a step temperature change, the event was detected by a microswitch on the shutter door mechanism of the test section and recorded on the Offner.

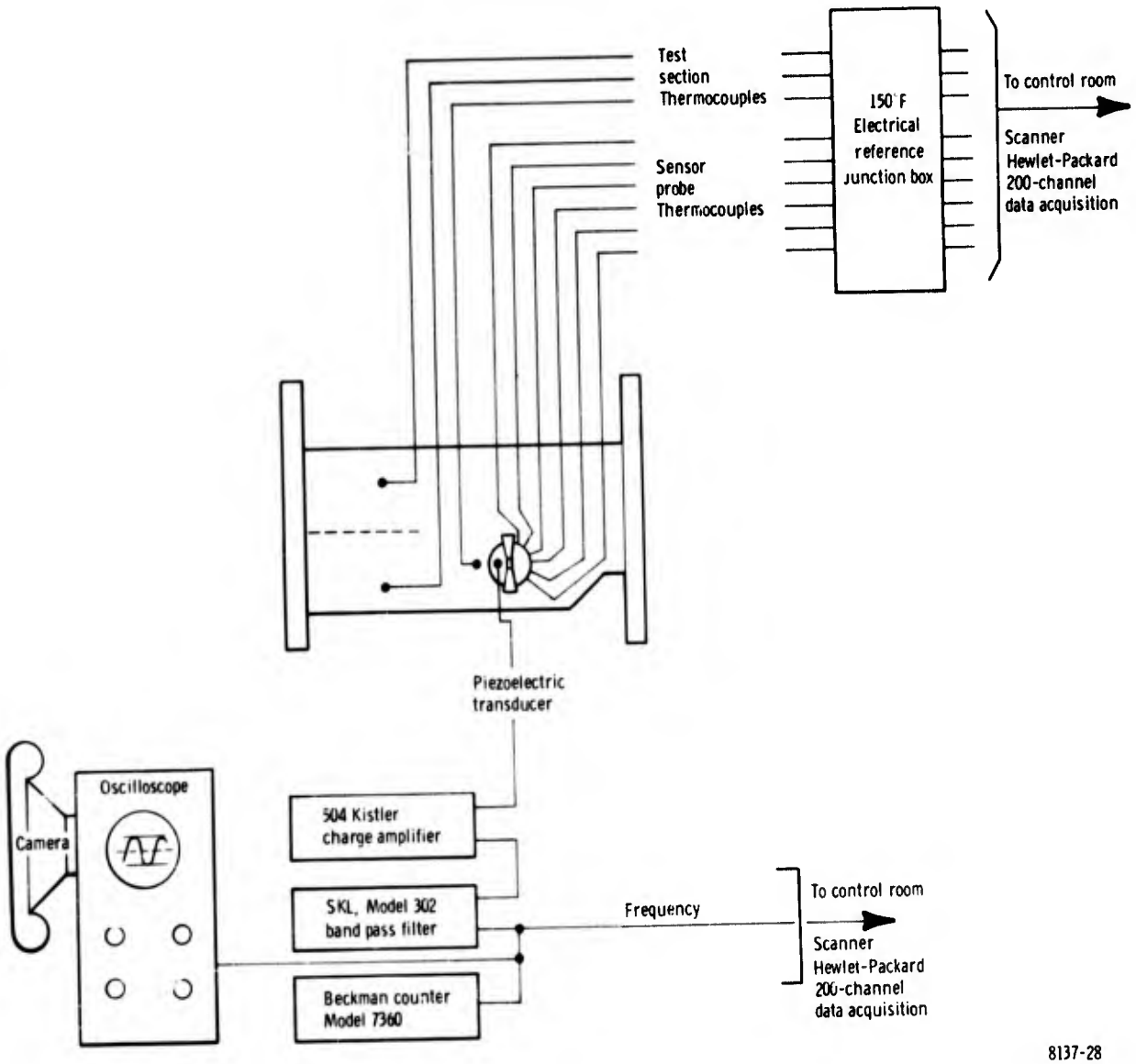

Figure 28. Sensor calibration instrumentation.

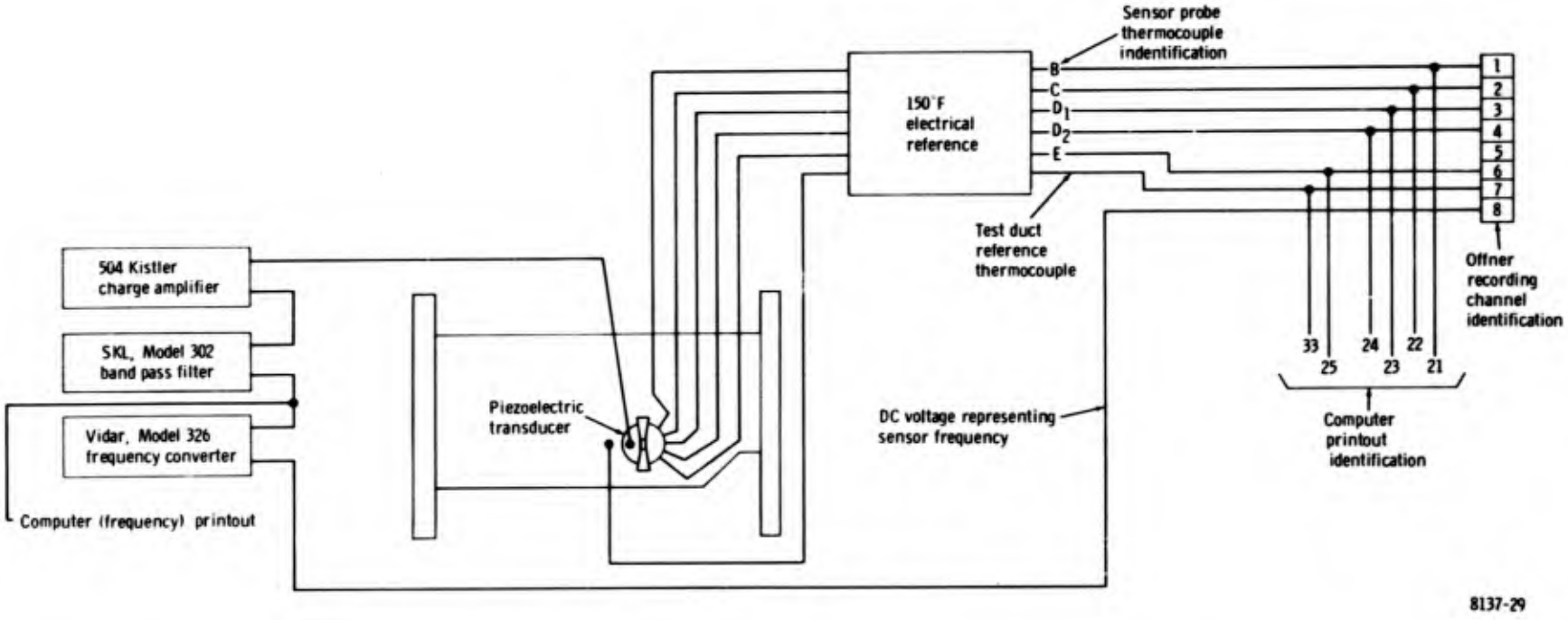

Figure 29. Sensor transient test instrumentation.

V. FLUIDIC TEMPERATURE SENSOR EVALUATION

Evaluation of the sensor involved performance air ejector tests, steady-state calibration, and transient temperature response tests. These tests were made to (1) determine the capability of the air ejector to develop the required sensor pressure ratio for pressure insensitive operation below a sensor inlet pressure of 30 psia at sea level, (2) determine the accuracy of each sensor in producing an output frequency indicative of the sensed air stream temperature, and (3) compare the response of the sensor to a step temperature change to that of a C-A bare tip thermocouple. These tests, within the limitations of the facility, simulated conditions that might result in marginal operation of the sensor in the turbofan JTDE.

SENSOR AIR EJECTOR EVALUATION

The objective of this test was to determine (1) a minimum sensor inlet pressure in which sensor pressure insensitive operation could be achieved by use of the air ejector and (2) the supply pressure necessary for optimum performance of the air ejector. The effectiveness of the air ejector when operated over varied conditions of sensor inlet pressure was measured by photographing amplitude changes of the sensor signal output. The test results are listed in Table 1.

Figure 30 is a summary of the air ejector test results. The plot in Figure 30 shows the signal output amplitude measured in volts (peak to peak) of the sensor performance at various static stream pressures with different levels of air supplied to the air ejector. The effectiveness of the air ejector to improve sensor performance at each static stream condition is discussed in the following paragraphs.

TABLE 1. EFFECTIVENESS OF THE SENSOR EJECTOR

Static stream pressure (psia)*	Ejector supply pressure (psig)	Sensor No. 1		Sensor No. 2	
		Freq (Hz)	Amplitude (v, peak to peak)	Freq (Hz)	Amplitude (v, peak to peak)
25	75	3506	4.25	3460	4.0
	55	3506	4.25	3458	4.1
	25	3506	4.30	3458	4.2
	15	3505	4.40	3458	4.4
	0	3505	4.40	3458	4.4
20	75	3503	3.00	3450	3.0
	55	3503	3.00	3451	3.1
	25	3504	3.00	3451	3.1
	15	3507	2.60	3467	2.6
	0	3523	2.00	3470	2.2
14.7	75	3487	1.60	3452	2.0
	55	3480	1.60	3452	2.1
	25	3400/3500	1.50	3455	2.1
	15	None	None	None	None

*Stream temperature was not measured.

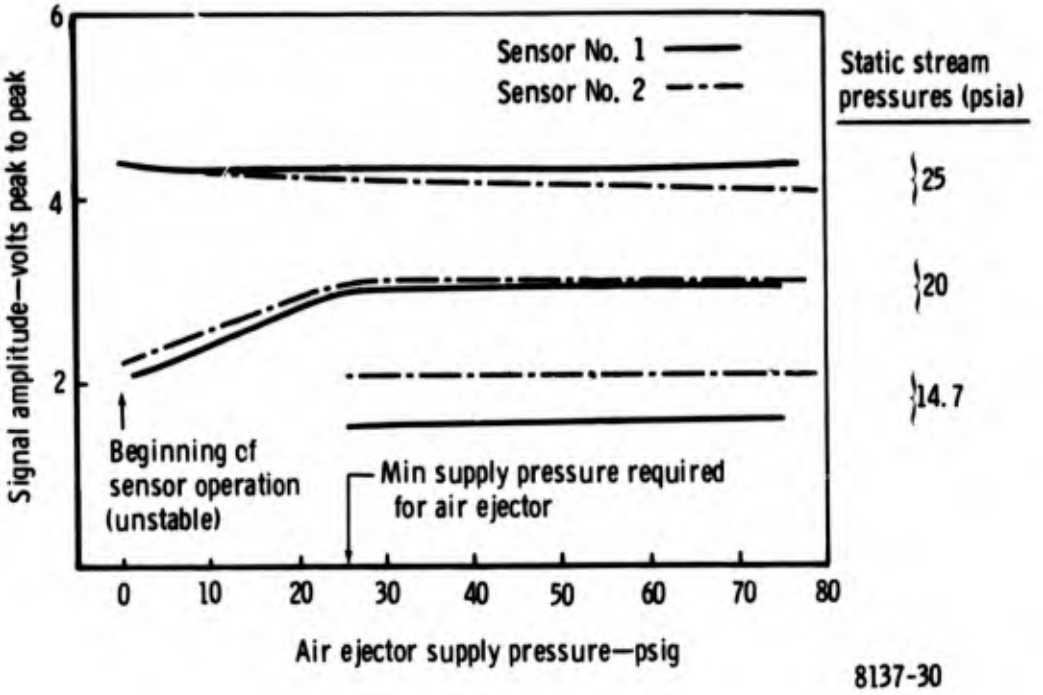

Figure 30. Effectiveness of air injector.

25 Psia Stream Pressure

The need for an air ejector at this test condition is not readily apparent since the signal output amplitude for each sensor remains fairly constant over the range of 0 to 75 psig air ejector supply pressure.

20 Psia Stream Pressure

As the air ejector supply pressure is increased from 0 to 25 psig, the signal output amplitude at the beginning point of sensor operation also increases. Above 25 psig, further increases in supply pressure to the air ejector have no effect on the signal output amplitude. At 25 psig, further increases in the ejector supply pressure become ineffective in increasing the signal output amplitude, which indicates an optimum condition for operation of the air ejector. Both sensors appear evenly matched in performance.

14.7 Psia Stream Pressure

This was an unreal case for sensor operation, but it demonstrated that the capacity of the air ejector at 25 psig supply pressure was sufficient to produce the required pressure ratios in the sensor for pressure insensitive operation. This test condition confirmed the opinion that the optimum (25 psig) supply pressure to the air ejector is adequate for proper sensor operation even in a static airstream. At a 14.7 psia stream pressure, the air ejector operating at 25 psig supply pressure was capable of lowering the sensor exhaust pressure to 7.17 psia. Shown in Figure 31 is the required sensor exhaust pressure needed for proper sensor operation at various inlet pressures. This defines the required ejector performance.

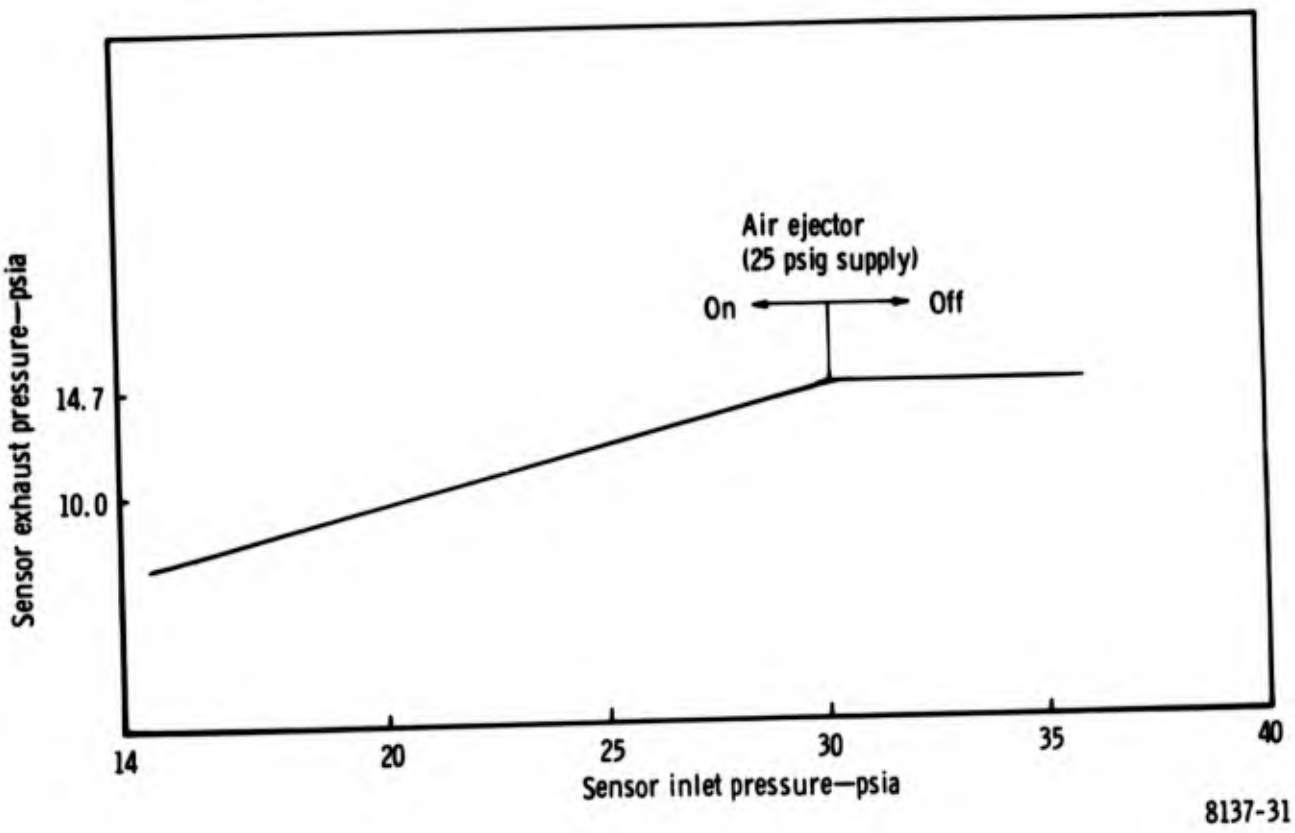

Figure 31. Predicted air ejector suction capacity.

Sensor No. 2 was mounted in the test section with its probe inlet facing downstream to the direction of flow during calibration testing. At the conclusion of the calibration test evaluation at 400°F, a temperature coastdown was initiated to gradually cool the electric facilities. During the temperature coastdown process, the facilities airflow to the test section was allowed to slowly decay to a point where the stream airpressure was below 30 psia, and with the air ejector off, a loss in the sensor's signal output occurred at 19.2 psia stream pressure. However, the sensor signal output was regained as shown in Figure 32 after the air ejector was supplied with 25 psig air pressure. Views A, B, C, and D of Figure 33 were taken during the temperature coastdown. All electronic gains on the oscilloscope and charge amplifier were held constant.

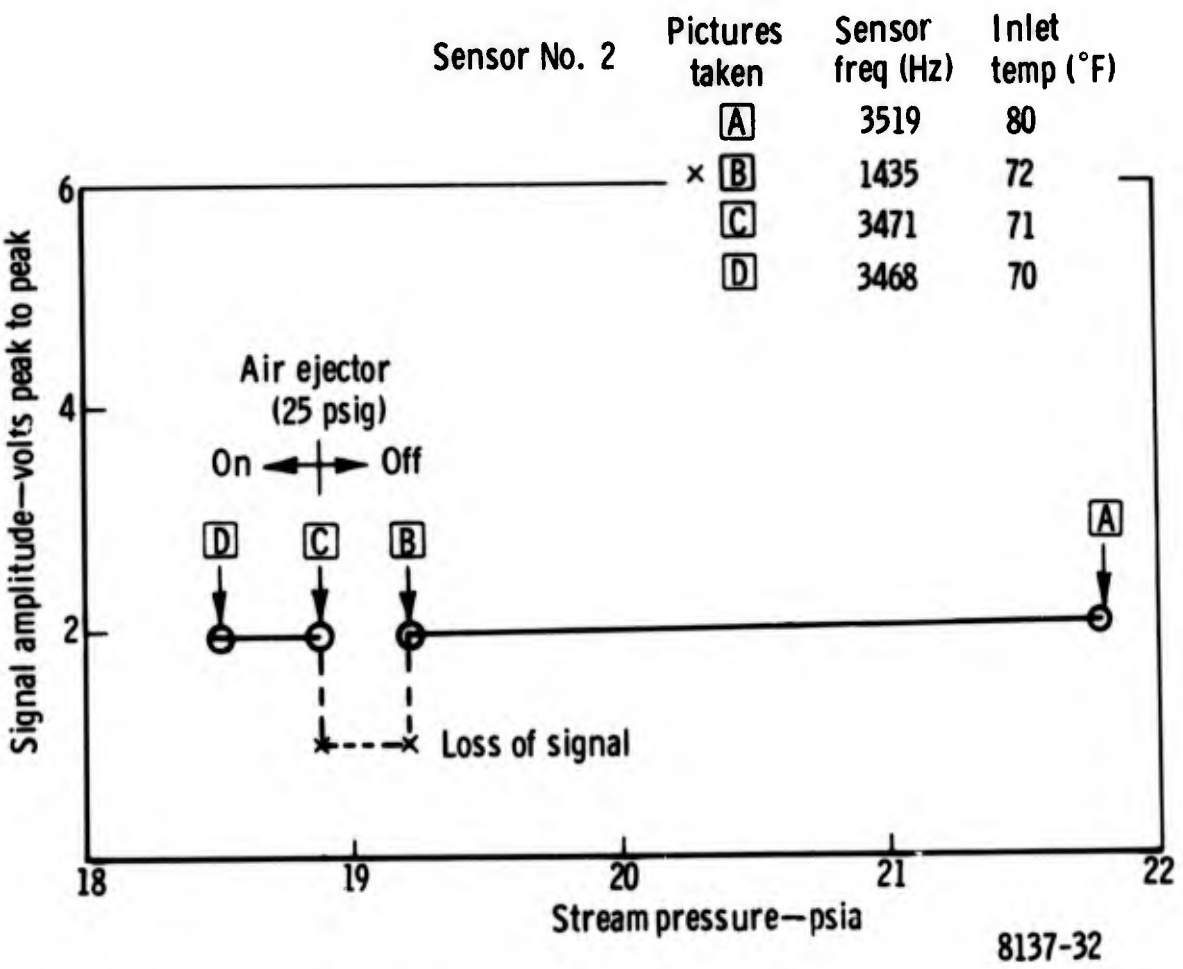

Figure 32. Facilities air temperature coastdown.

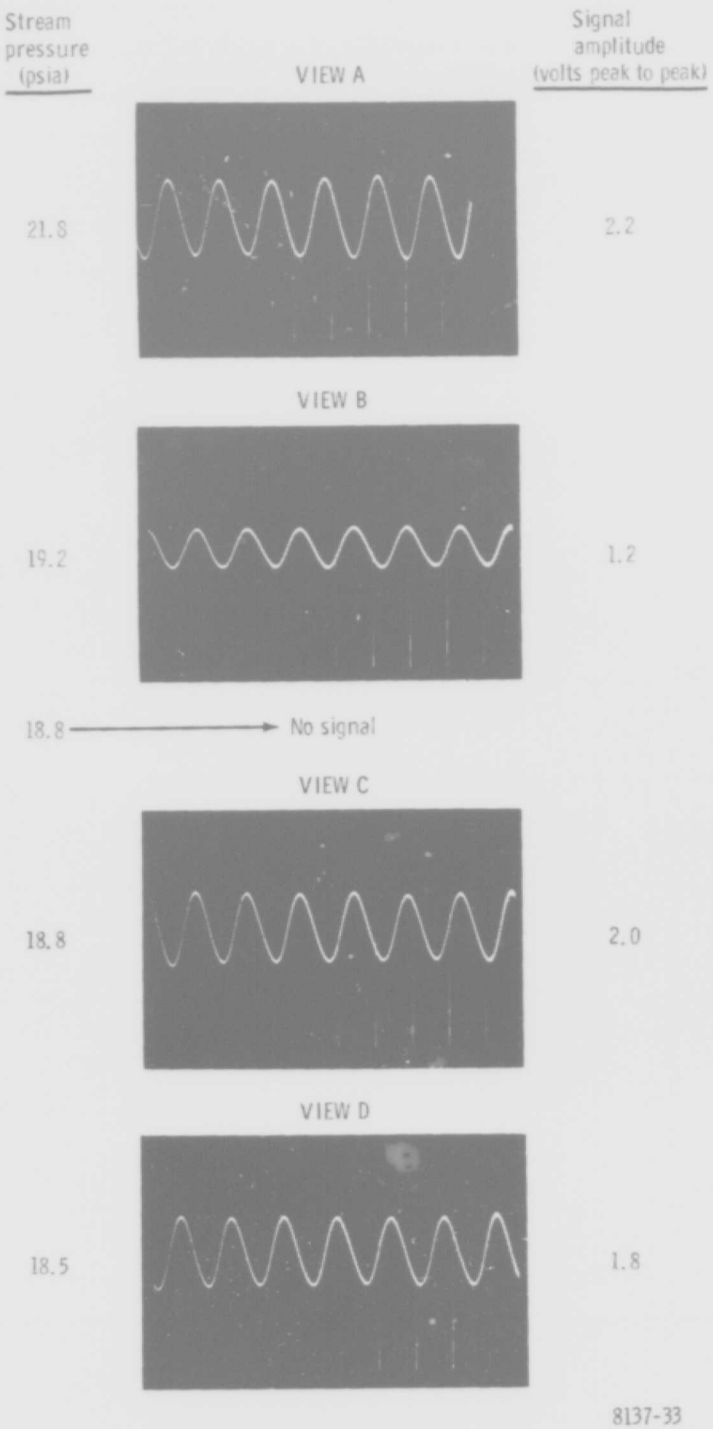

Figure 33. Sensor signal output views.

The effectiveness of the air ejector to increase the operating range of the fluidic temperature sensor was demonstrated during evaluation testing. The test results indicated that the sensor could operate with an inlet pressure of 14.7 psia with the air ejector on. During the temperature coastdown of the calibration rig, Sensor No. 2 was operated with the air ejector on under stream conditions equal to a P_1/P_a ratio of 1.26. This pressure ratio of P_1/P_a (sensor inlet pressure to ambient pressure) is one of the engine operating conditions for the sensor. Figure 34 shows that the sensor with the aid of the air ejector can operate at any of the engine conditions and that the optimum pressure ratio (CDP/P_a = 2.70) across the air ejector is less than the compressor requirements at any condition.

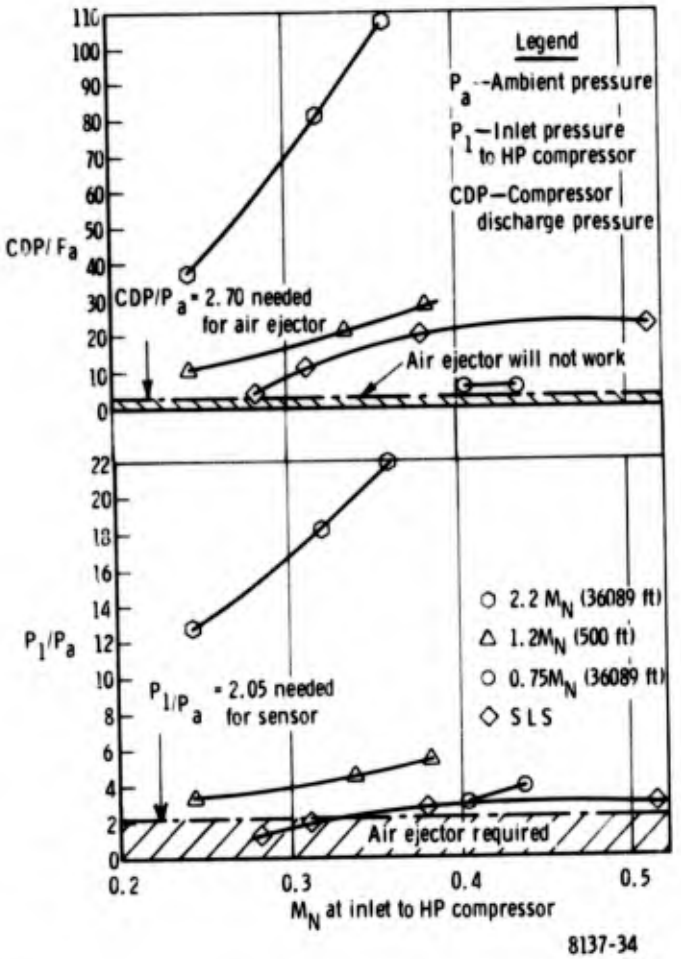

Figure 34. Sensor engine operating conditions.

SENSOR CALIBRATION

A total of 94 runs were obtained from Sensors No. 1 and 2 during calibration testing. A sampling of computer printouts of these runs contained in Appendix B were acquired under the test conditions outlined in Table 2. Runs are listed in Table 2 with regard to the position of the probe inlet relative to the direction of stream flow, i.e. facing upstream or downstream.

The original test format was altered during the course of the testing to (1) accommodate a facilities shop air pressure reduction, and (2) eliminate those test runs at various ejector supply pressures that showed little change in sensor performance. Initial calibration data gathered from Sensor No. 1 with the probe inlet facing upstream indicated that sensor performance was not affected by operation of the air ejector below 25 psig and remained virtually unchanged at higher supply pressures. Because of these indications of sensor performance and a reduction of supply pressure to the air ejector, calibration readings were taken for the remainder of the test at 0, 25, and 55 psig air ejector supply pressures. Those runs obtained with 55 psig air supplied to the ejector were not used in the sensor calibration determination, but were taken for monitoring purposes only.

The order of testing indicated by the progression of calibration reading run numbers was entirely a matter of the stand operator's choice of changing the airflow conditions to the test section. Calibration readings were obtained from Sensor No. 1 with its probe inlet facing both upstream and downstream to the direction of airflow through the test section. Sensor No. 2 calibration readings were obtained with the probe inlet in the downstream position only. Photographs were taken at each of the calibration points to monitor the quality of the sensor signal output. Metal temperatures obtained from thermocouple instrumentation attached to the probe of Sensor No. 1 were acquired for all conditions of calibration testing for a reference in later analysis.

TABLE 2. SENSOR CALIBRATION

Test section condition				Sensor air ejector	Sensor No. 1		Sensor No. 2
Stream press. (psia)	Stream temp (°F)	Airflow (lb/sec)	M_N	Supply press. (psig)	Run No. Upstream	Run No. Downstream	Run No. Downstream
				0	29	70	97
				15	30		
	Amb	3.0	0.115	25	31	71	98*
				55	32	72	99
				75	33		
				0	34	73	100
				15	35		
30	120	3.0	0.120	25	36	74	101
				55	37	75	102
				75	38		
				0	39	76	103
				15	40		
	240	3.0	0.130	25	41	77	104
				55	42	78	105
				75	43		
				0	44	87	112
				15	45		
	Amb	3.0	0.057	25	46	86	113*
				55	47	85	114
				75	48		
				0	49	84	109
				15	50		
60	180	3.0	0.062	25	51	83	110
				55	52	82	111
				75	53		
				0	54	81	106*
				15	55		
	360	3.0	0.070	25	56	80	107
				55	57	79	108*
				75	58		
				0	69	88	115
				15			
	Amb	3.0	0.045	25	68	89	116*
				55	67	90	117
				75			
				0	66	91	118
				15			
75	200	3.0	0.050	25	65*	92*	119
				55		93	120
				75	64		
				0	63	94	121
				15	62		
	400	3.0	0.058	25	61	95	122
				55	60	96	123
				75	59		

* computer printouts contained in Appendix B.

The line plots and sensor performance expressions presented in Figure 35 are the predicted relationships of sensed air temperature to output frequency, i.e., $T°_R = a\,(f)^b$. These line plots were used as a base line for later comparisons and represent the least squares solution of data from all calibration readings taken with the air ejector off. All individual data points fit the least squares solution with a maximum deviation of 3.5°F.

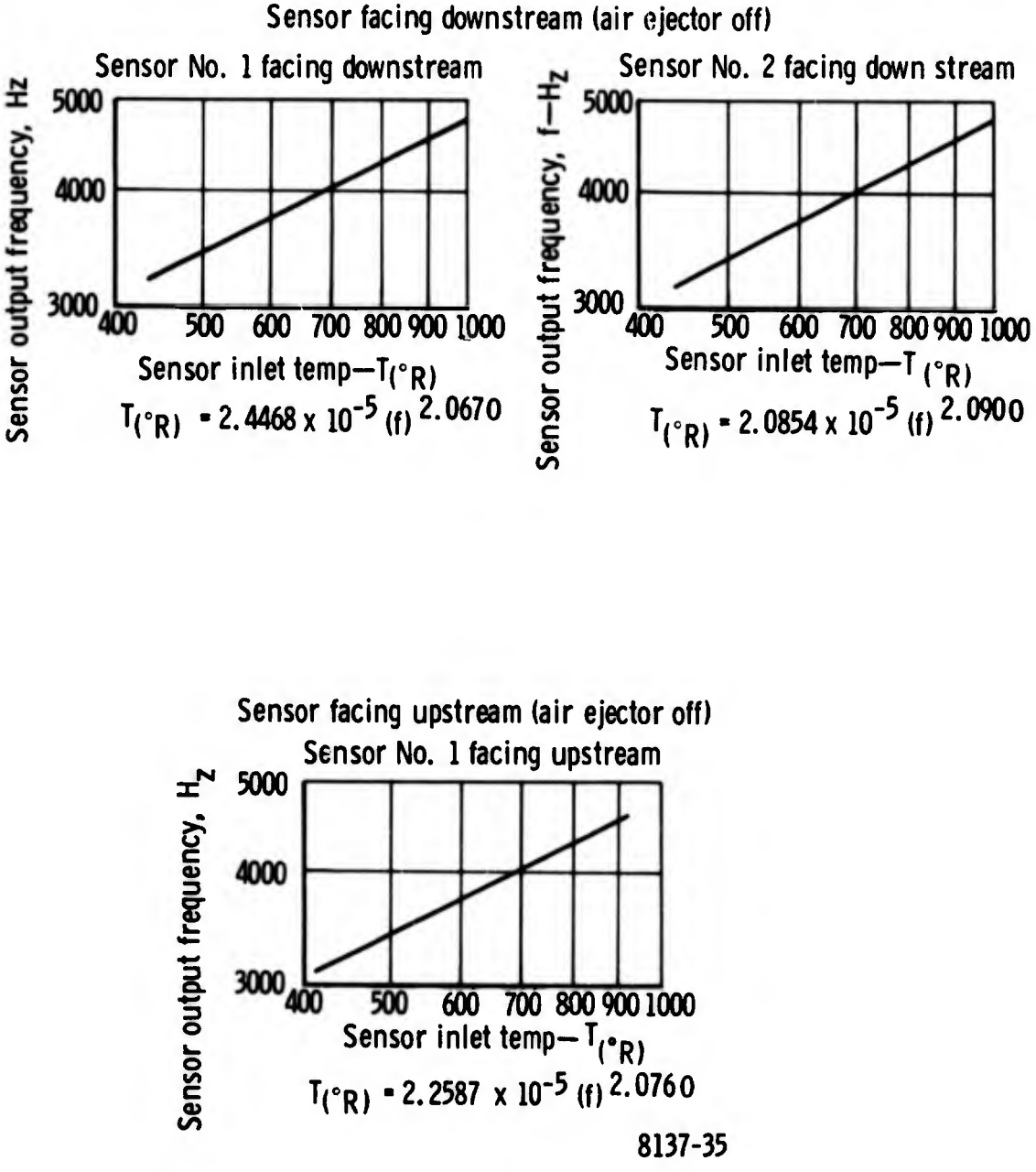

Figure 35. Base-line sensor performance.

Table 3 presents base-line comparisons of the performance between Sensors No. 1 and 2 facing downstream and comparisons of Sensor No. 1 performance based on the direction the probe inlet is facing. All comparisons were made with the air ejector off. The comparisons show that a maximum performance deviation of 3.36% (or 29°F) exits between Sensors No. 1 and 2 at 4460 Hz and that Sensor No. 1 performance is virtually unaffected by the orientation of the probe inlet in the airflow field. The maximum performance deviation of Sensor No. 1 was 0.17% (or 0.9°F) at 3521 Hz.

TABLE 3. BASE-LINE COMPARISONS OF SENSOR PERFORMANCE

Sensors No. 1 and 2—Probe Inlet Facing Downstream (Air Ejector Off)

$T_{°R} = a\,(f)^{b}$

Sensor No. 1 $T_A = 2.4468\ 10^{-5}\,(f)^{2.0670}$

Sensor No. 2 $T_B = 2.0854\ 10^{-5}\,(f)^{2.0900}$

Freq (Hz)	T_A (°R)	T_B (°R)	Dev (%)
3521	524.3	539.2	2.84
4460	854.6	883.3	3.36

Sensor No. 1—Probe Inlet Facing Upstream/Downstream (Air Ejector Off)

Upstream $T_A = 2.2587 \times 10^{-5}\,(f)^{2.0766}$

Downstream $T_B = 2.4468 \times 10^{-5}\,(f)^{2.0670}$

Freq (Hz)	T_A (°R)	T_B (°R)	Dev (%)
3521	523.4	524.3	0.17
4460	855.2	854.6	0.07

The effect of air ejector operation on sensor performance at all stream conditions was found to be very slight. Performance of each sensor with 25 psig air pressure supplied to the ejector when compared with the ejector off (base line) sensor performance is within 5°F.

Stream pressure had a greater effect on sensor performance than sensor orientation in the test section or operation of the air ejector. Expressions of sensor performance (derived by the least squares method) for all stream pressures versus sensor performance for 30 psia stream conditions only are given in Table 4. Calibration readings used in this comparison were taken with the probe inlet facing downstream and 25 psig air pressure supplied to the ejector. Both sensors show the effect of changes in stream pressure on their performance.

TABLE 4. EFFECT OF STREAM PRESSURE ON SENSOR PERFORMANCE

Sensor No. 1—Probe Inlet Facing Downstream (Air Ejector On, 25 psig)

$T_{°R} = a\,(f)^b$

All stream pressures: $T_A = 2.1763 \times 10^{-5}\,(f)^{2.0811}$

30 psia stream pressure: $T_B = 1.8268 \times 10^{-5}\,(f)^{2.1031}$

Freq (Hz)	T_A (°R)	T_B (°R)	Dev (%)
3521	523.2	525.8	0.50
4460	844.8	864.5	1.03

Sensor No. 2—Probe Inlet Facing Downstream (Air Ejector On, 25 psig)

All stream pressures: $T_A = 2.3314 \times 10^{-5}\,(f)^{2.0760}$

30 psia stream pressure: $T_B = 1.4770 \times 10^{-5}\,(f)^{2.1325}$

Freq (Hz)	T_A (°R)	T_B (°R)	Dev (%)
3521	539	540	0.28
4460	880.5	894.8	1.59

One index of sensor performance is its sensitivity at various temperatures, i.e., its change in frequency per unit change in temperature. Expression denoting this characteristic for Sensors No. 1 and 2 are presented in Tables 5 and 6, respectively. These expressions were derived from least squares solutions representing calibration readings taken at the various stream and air ejector conditions. Tables 5 and 6 contain examples of solutions to these expressions within the appropriate temperature span. These values exhibit the trends of decreasing sensitivity with temperature increases.

TABLE 5. TEMPERATURE SENSITIVITY OF SENSOR NO. 1
(PROBE INLET FACING DOWNSTREAM)

Air to ejector	Sensor expression
Off	$T_{(A)} = 2.4468 \times 10^{-5} (f)^{2.0670}$
	$\frac{dT_{(A)}}{df} = 5.0500 \times 10^{-5} (f)^{1.0670}$
On (25 psig)	$T_{(B)} = 2.1762 \times 10^{-5} (f)^{2.0811}$
	$\frac{dT_{(B)}}{df} - 4.5250 \times 10^{-5} (f)^{1.0811}$

Sensor Operating Span

Stream temperature ranges (°F)	70	200	360	400
Sensor frequencies (Hz)	3550	3940	4370	4488
$\frac{1}{\frac{dT_{(A)}}{df}}$ (cycles/°R) = $\frac{df}{dT_A}$	3.22	2.88	2.58	2.51
$\frac{1}{\frac{dT_{(B)}}{df}}$ (cycles/°R) = $\frac{df}{dT_B}$	3.20	2.87	2.56	2.49

TABLE 6. TEMPERATURE SENSITIVITY OF SENSOR NO. 2
(PROBE INLET FACING DOWNSTREAM)

Air to ejector	Sensor Expression
Off	$T_{(A)} = 2.0854 \times 10^{-5} (f)^{2.0900}$
	$\frac{dT_{(A)}}{df} = 4.3600 \times 10^{-5} (f)^{1.0900}$
On (25 psig)	$T_{(B)}$ 1 $2.3314 \times 10^{-5} (f)^{2.0760}$
	$\frac{dT_{(B)}}{df} = 4.8350 \times 10^{-5} (f)^{1.0760}$

Sensor Operating Span

Stream temperature (°F)	70	200	360	400
Sensor frequencies (Hz)	3550	394	4370	4480
$\frac{1}{\frac{dT_{(A)}}{df}}$ (cycles)°R) = $\frac{df}{dT_{(A)}}$	3.10	2.76	2.48	2.39
$\frac{1}{\frac{dT_{(B)}}{df}}$ (cycles/°R) = $\frac{df}{dT_{(B)}}$	3.04	2.80	2.50	2.46

The filtered output frequency from both sensors was of good quality and of sufficient amplitude to permit counting and frequency conversion to a dc level. A band pass filter was needed to remove 60-cycle and 220-cycle interferences which occurred intermittently throughout the test. The source of the electrical interference was judged to have originated from the facilities' electric heaters. The quality of the sensor signal output was typical of that shown in Figure 36 of Calibration Run No. 91. Both Honeywell piezolelectric transducers performed very well under all stream test conditions.

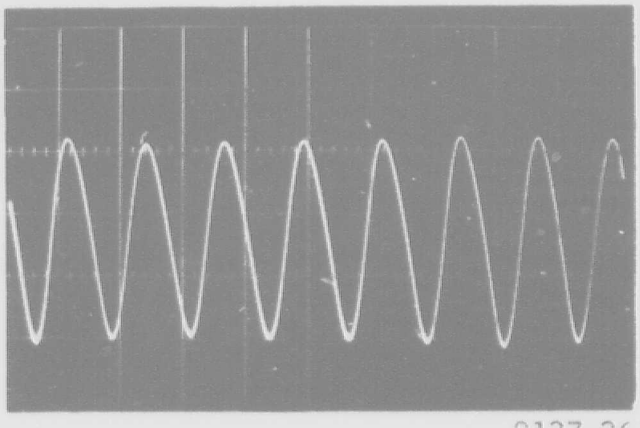

Figure 36. Typical oscilloscope view of sensor signal output during calibration testing.

SENSOR TRANSIENT TEMPERATURE RESPONSE TEST

Because of facilities limitations on the airflow capacity of shop air, stream pressure in the test section was restricted to 30 psia and Mach numbers were also quite low. Since all of the temperature response characteristics obtained in this test were at low stream pressure and velocity conditions, the test results were indicative of an engine operating condition which might be marginal for sensor operation. As will be shown later in the postanalysis, the response of the sensor to temperature changes is improved at higher stream pressures and airflows so the results obtained from this test represent a minimum in sensor performance.

In conjunction with a heat transfer analysis that was made prior to completion of the sensors, a heat transfer liner was installed in the probe of Sensor No. 2 and Sensor No. 1 was instrumented with thermocouples at various key nodal

positions along its sensor probe. The purpose of this earlier work was to determine under transient temperature conditions any improvement in the performance of Sensor No. 2 over Sensor No. 1 and to obtain node temperature data for later use in a heat transfer analysis.

Test evaluation of both sensors was performed under conditions shown in Table 7. Each sensor was tested for its response over temperature ranges of 70 to 500°F, 70 to 250°F, and 70 to 150°F at a stream pressure of 30 psia. Step increases and decreases were made at the three temperature ranges. The air ejector was operated at its optimum supply pressure (25 psig) at all test conditions. Again because of shop air limitations, the weight flow and Mach number of air in the cold air duct could not be matched to that of the hot air duct in the test section. Differences in sensor performance related to this mismatch of airflows are discernible in the test results.

Transient response runs at the three temperature ranges were taken with the probe inlet of Sensor No. 1 facing upstream and downstream to the direction of flow through the test section. Sensor No. 2 was only evaluated with its probe inlet facing downstream. With the probe inlet of Sensor No. 1 facing upstream, Offner strip chart recordings were taken at the three temperature step ranges. The actual temperatures sensed by the reference thermocouple in the test section are given for each step and the representative run numbers associated with the step in Table 8. Because of instrumentation problems that occurred during the testing, reruns of a particular condition were necessary, and, as a result, number identification of the run does not show order of test.

Offner strip chart recordings of both sensors facing downstream were also taken at the three temperature step ranges. However, since the extreme temperature step range of 70 to 500°F was needed to define sensor performance, only those pertaining to this temperature step is given in Table 9.

TABLE 7. SENSOR TRANSIENT TEST CONDITIONS

Test section condition				Sensor Air ejector	Test information
Stream press. (psia)	Stream temp (°F)	Airflow (lb/sec)	M_N	Supply press. (psig)	No. of temp steps made
30	70	0.597	0.0456	25	2
	500	0.449	0.0457		
30	70	0.619	0.0468	25	2
	250	0.453	0.0397		
30	70	0.597	0.0450	25	2
	150	0.434	0.0353		

TABLE 8. IDENTIFICATION OF REPRESENTATIVE RUNS WITH SENSOR NO. 1 FACING UPSTREAM

Reference thermocouple readings (°F)		Size of temperature step (°F)	Run No.	Figure No.
84*	472	388	11	38
472	83	389	10	39

*Cold air was not conditioned, but taken as is from the facilities shop air source.

TABLE 9. IDENTIFICATION OF REPRESENTATIVE RUNS TAKEN WITH BOTH SENSORS FACING DOWNSTREAM

Reference thermocouple readings (°F)		Size of temperature step (°F)	Run No.	Figure No.
		Sensor No. 1		
84	477	393	33	40
477	84	393	34	41
89	477	388	35*	42
		Sensor No. 2		
83	477	394	27	43
477	94	383	28	

*Increased airflow in hot temperature duct only.

Extra Run No. 35 was made with increased airflow to the hot air duct in the test section for subsequent transfer analysis.

The mechanics of conducting the temperature response test involved converting the frequency output of the sensor into a dc signal and recording this information along with dc outputs from the reference thermocouple in the test section and the thermocouples attached to the sensor probe onto an eight-channel Offner strip chart recorder. With both entrance ducts of the test section being supplied continuously with hot and cold air, the Offner recorder was started just prior to each run and the test section shutter doors were actuated to divert either hot or cold air onto the sensor. Movement of the shutter door actuating rod was detected with a microswitch and recorded by an event marker on the strip chart.

The criteria for judging the performance of a fluidic temperature sensor as shown in Figure 37 is concerned with the rapidity of recognition of a step temperature change, the response of the recognition in terms of the total temperature excursion, and the time it takes after the initial response to reach a stabilized temperature. The first temperature response of the sensor has been determined experimentally to be in the order of 5 to 40 milliseconds and is followed by a longer time response. The initial time response of the sensor (referred to as flushing time constant) is related to the time required to flush air from the edgetone resonator cavity. The slower response time that follows (referred to as thermal inertia time constant) is associated with the loss of the sampled air energy to the sensor structure. Because the sensor output will always be in error until the structure is brought up to sampled air temperature, the higher the first step in response, the less effect thermal inertia of the structure has on reaching the final stabilized temperature.

Table 10 in Section VI summarizes all of the previously discussed sensor performance criteria for all conditions of test runs listed in Tables 8 and 9. Offner strip chart recordings of these runs are shown in Figures 38 through 43.

The following observations can be derived from the summary.

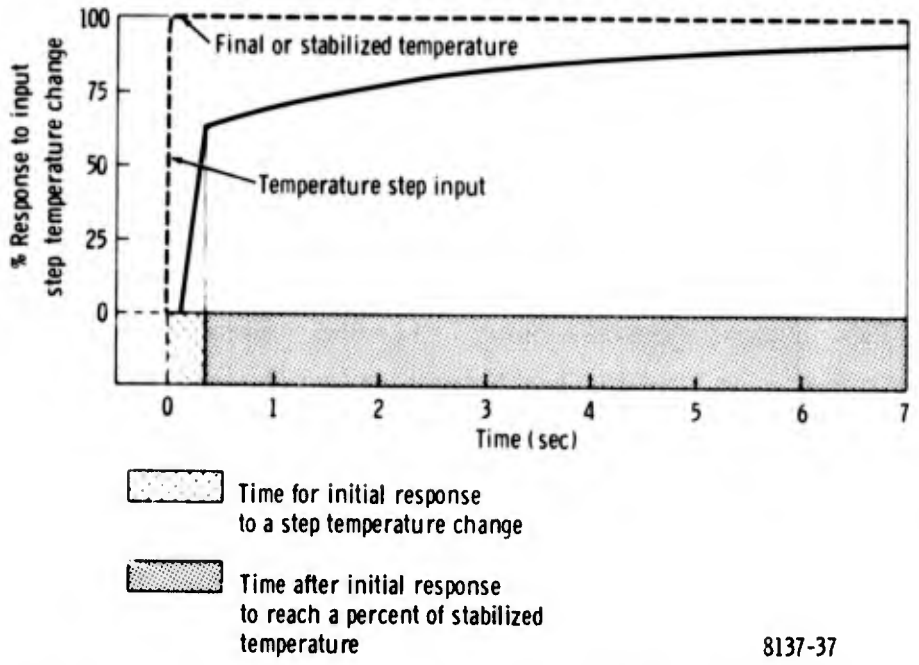

Figure 37. Fluidic temperature sensor response.

Only small differences of step response occurred because of the sensor probe orientation with respect to the airflow in the test section. Since these differences were small, it was concluded that the sensor could operate in an engine application with its probe inlet facing downstream to avoid contaminate pickup.

Sensor No. 2 with the heat transfer liner was not as responsive to step temperature changes as Sensor No. 1. The lower values for step response were not unexpected and were caused in part by the increased heat transfer coefficient caused by a reduced area sampled air passageway. The smaller flow area of the liner that was presented to the sampled airflow increased the air velocity, causing more heat transfer initially to the surrounding surface (liner). Sensor No. 1 without the liner presented a larger flow area to the sampled airflow which resulted in a lower air velocity in the probe and corresponding reduction in heat transfer to the structure, hence the larger initial response step.

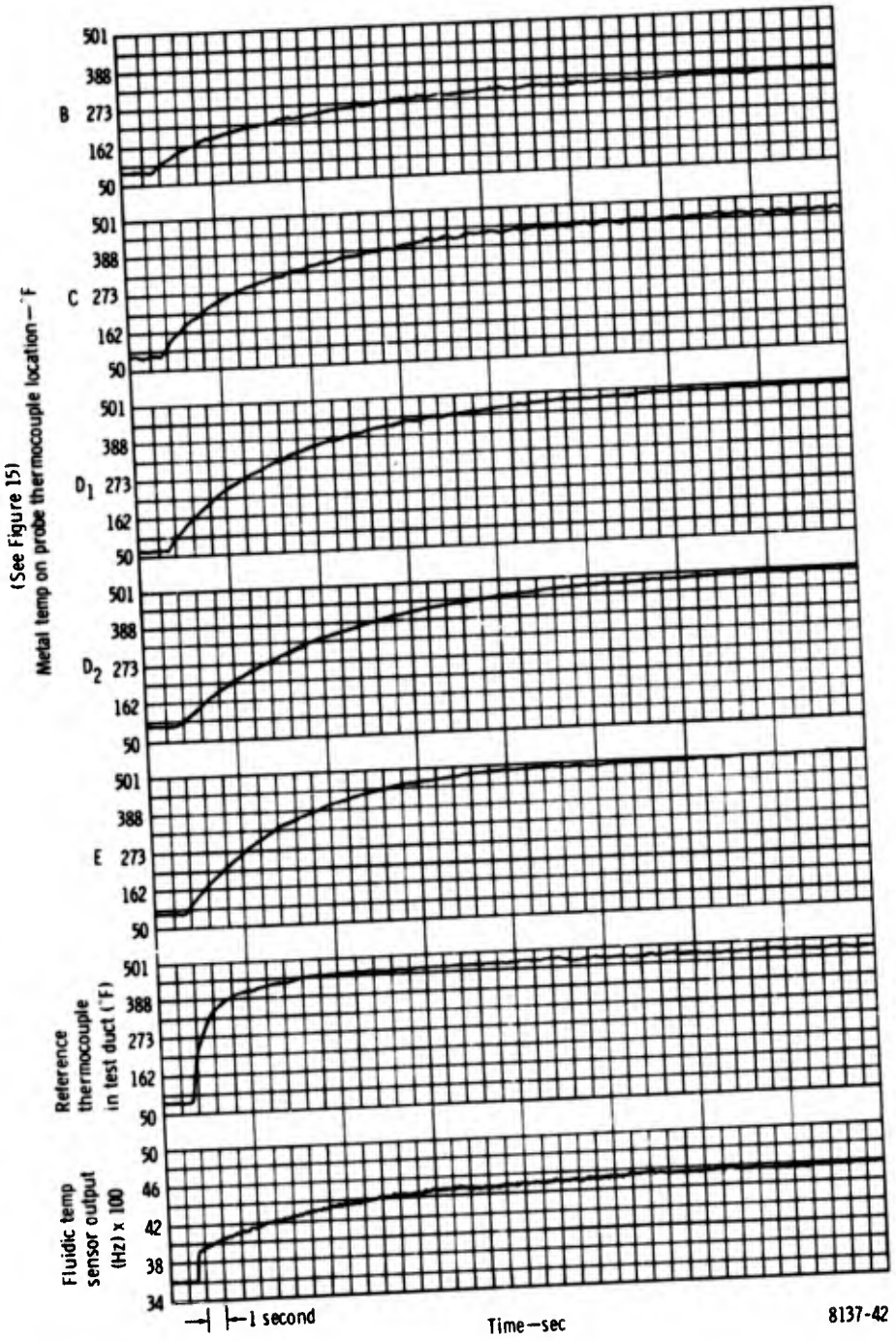

Figure 38. Run No. 11: sensor No. 1 facing upstream—step 70°F to 500°F.

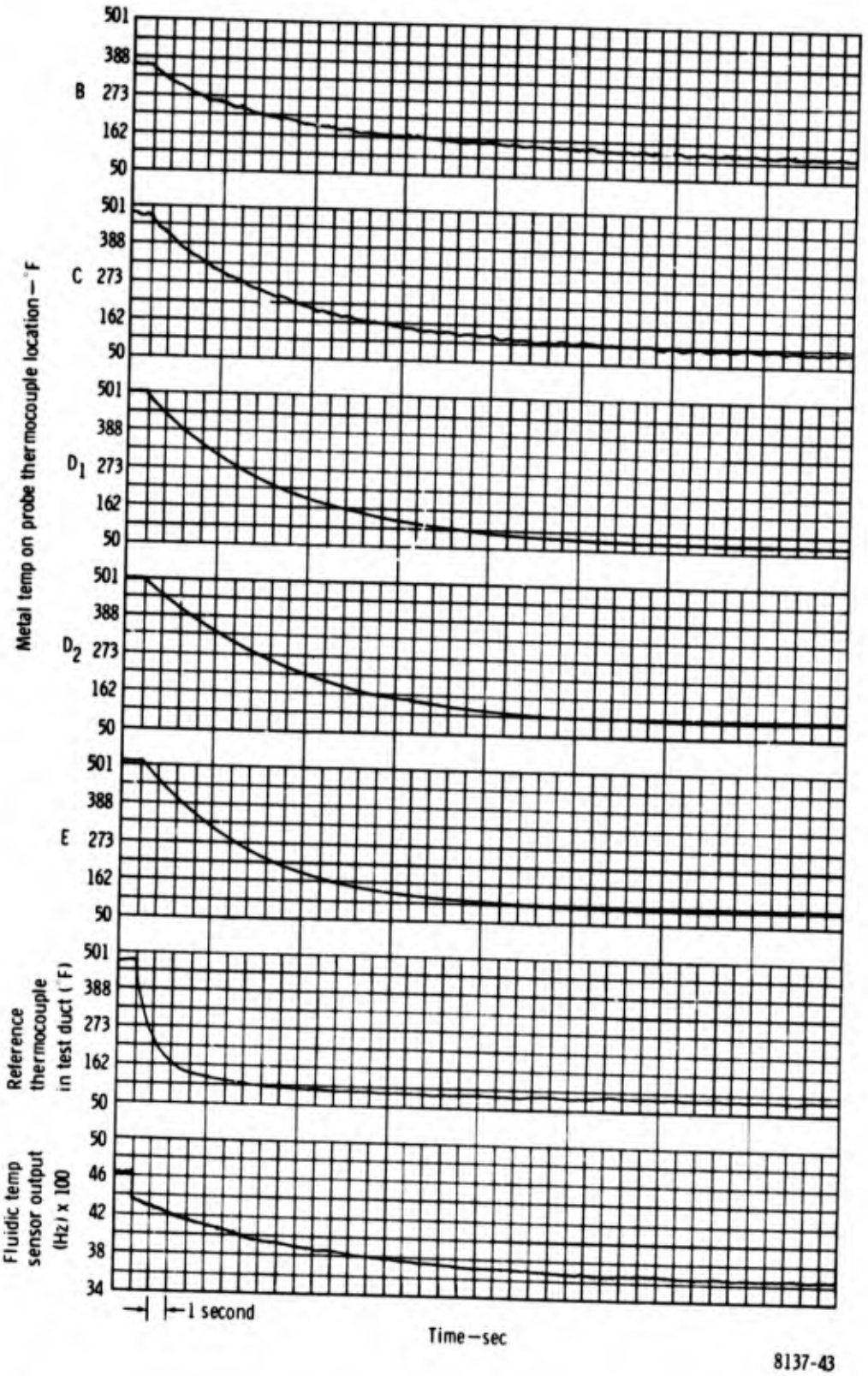

Figure 39. Run No. 10: sensor No. 1 facing upstream—step 500°F to 70°F.

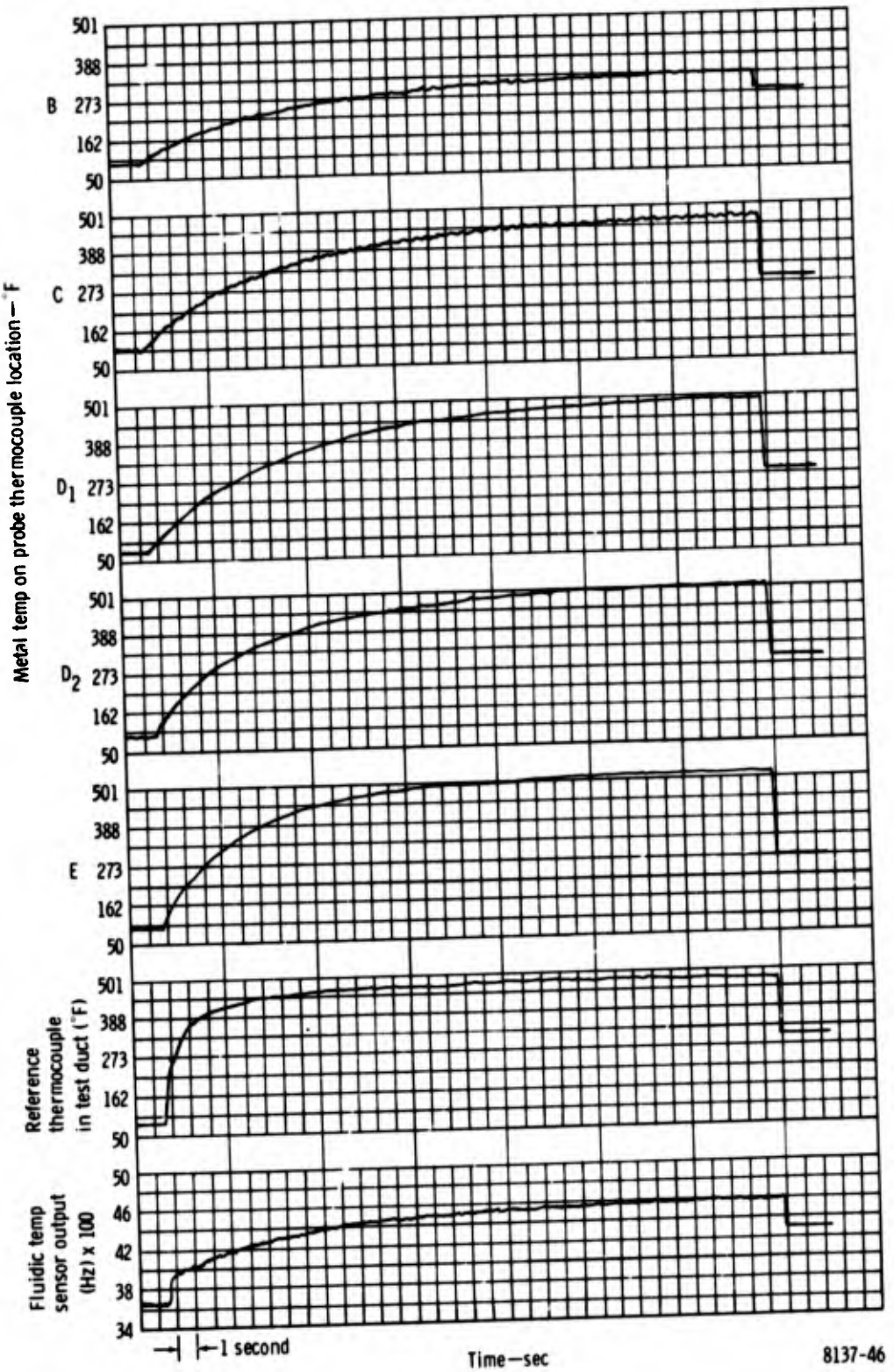

Figure 40. Run No. 33: sensor No. 1 facing downstream—step 70°F to 500°F.

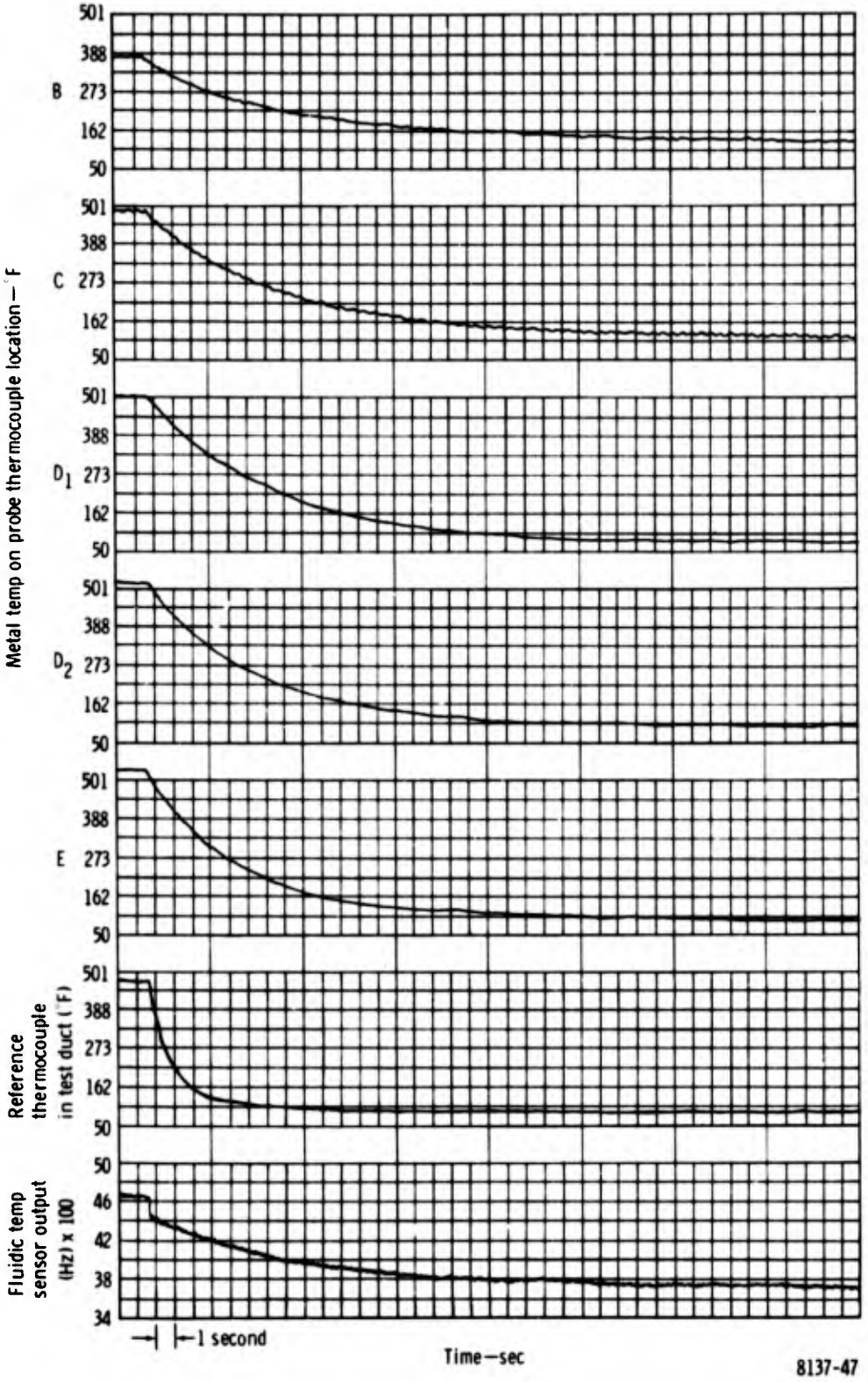

Figure 41. Run No. 34: sensor No. 1 facing downstream—step 500°F to 70°F.

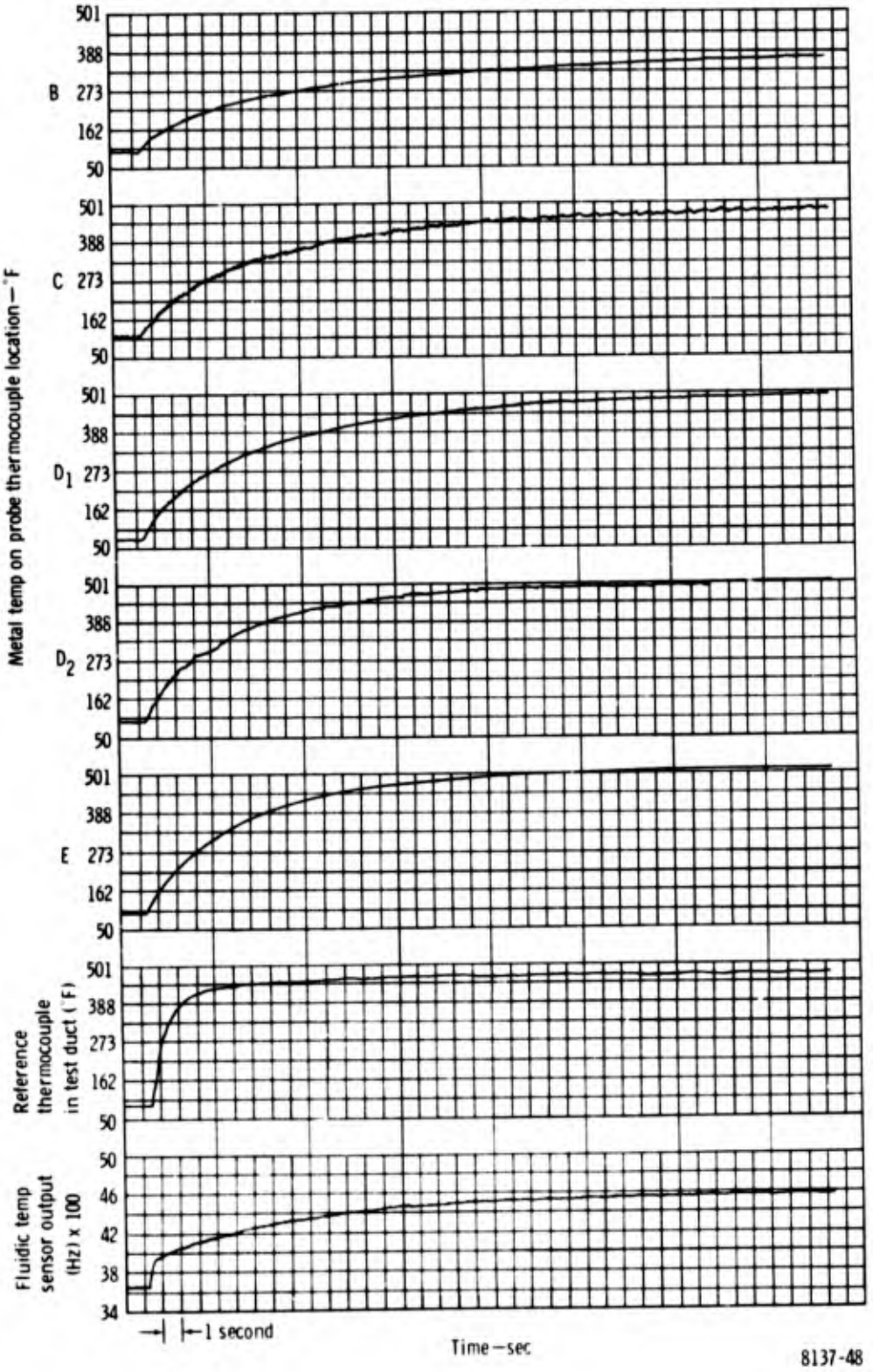

Figure 42. Run No. 35: sensor No. 1 facing downstream—step 70°F to 500°F.

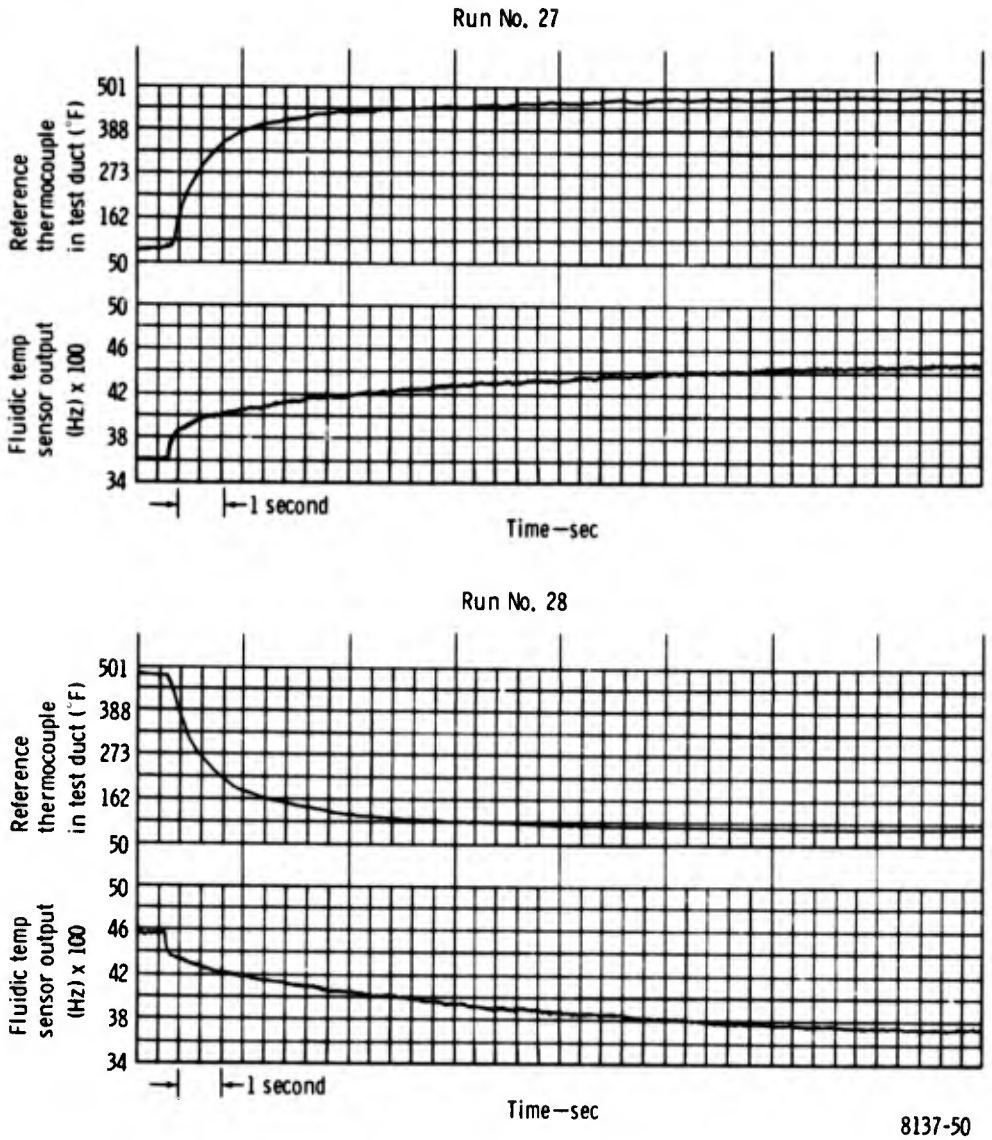

Figure 43. Runs No. 27 and 28: sensor No. 2 facing downstream—step 500°F to 70°F and 70°F to 500°F.

Sensor No. 2 with the heat transfer liner installed in its probe was suspected during early transient testing of having a ruptured liner. Because no differences in performance were observed to that of Sensor No. 1, the sensor was removed from the test section and two 0.062-in. dia holes were drilled through the probe wall just beyond the liner sealing point. The soundness of the liner was tested by blowing smoke into the probe inlet. As smoke was passed into the probe it exited via the small (0.062 in. dia) holes that had been drilled into the probe; this indicated the liner was ruptured. Because there was no time to make a new liner before transient temperature test resumption, Sensor No. 2 was reinstalled for further testing. The test evaluation of Sensor No. 2 that followed did indicate that the ruptured liner was capable of lowering the time to stabilize at 90% over that of its companion Sensor No. 1. The two 0.062-in. dia holes provided a pressure balance internally across the liner, thereby allowing most of the sampled air to pass inside the liner with a minimum heat loss to the probe structure.

Both sensors produced an initial fast step response ranging from 23% for Sensor No. 2 to 35% for Sensor No. 1. The time to make the initial step response for the sensors was estimated to be 20 milliseconds, which was much faster than response from the reference thermocouple. The reference thermocouple did not show any response within the 20 millisecond time period. A time period of 1 sec was required by the thermocouple to respond to 63% of the final temperature. However, neither sensor could match the thermocouple in the time to stabilize at 90% of a final temperature. The time to statilize to 90% of final temperature ranged from 15.5 sec for Sensor No. 2 to 28.3 sec for Sensor No. 1 as compared with 5 seconds for the reference thermocouple.

Run 35 was an experiment which was performed on Sensor No. 1 during the last stages of transient temperature response testing. To determine the effects of an increased flow on sensor performance, the weight flow of air in the hot air duct of the test section was increased from 0.449 lb/sec shown in Table 7 to 1.637 lb/sec and a step increase in temperature was made from

100 to 500°F. The results of this experiment indicated an initial step response of the sensor of 35% and time to stabilize to 90% final temperature of 12.5 sec. This time stabilize to 90% final temperature was faster than the times previously recorded for Sensor No. 1. Previous transient testing at the lower airflow conditions indicated that the average time for Sensor No. 1 to stabilize to 90% final temperature was 21.5 sec. This test indicated that higher weight flow surrounding the immersed probe structure reduced the thermal inertia time constant of the sensor.

Metal temperature recordings of Sensor No. 1 probe structure were taken to provide additional information on the heat transfer that occurred from the sampled air to its surrounding structure. These recordings taken at predetermined nodal stations on the probe were used in the subsequent heat transfer analysis to adjust the original mathematical model of the sensor.

VI. POSTANALYSIS OF SENSOR PERFORMANCE

To review briefly, the heat transfer analysis that was made prior to test evaluation, indicated that the long probe fluidic temperature sensor could not achieve the response capabilities of a short probe sensor design. However, improvements in performance could be expected if a heat transfer liner was installed in the long probe. The predictions indicated that with a 500°F temperature step, the long probe sensor with liner installed would respond initially to 34% of the final temperature and would stabilize to 88% of the final temperature in 8 sec. These predictions were based on the assumption that the frequency generated in the edgetone resonator was reacting to the average air temperature in the resonator cavities, i.e. the average of air temperature between the sensor inlet and exit orifices. However, the results of the temperature response test indicated that these predictions were not true. Figure 44 shows a comparison to the predictions of the test results obtained from Sensor No. 2 (Run No. 27) with a heat transfer liner installed and Sensor No. 1 (Run 33) without a liner. The comparison shows that actual performance of Sensor 2 was much lower than had been expected.

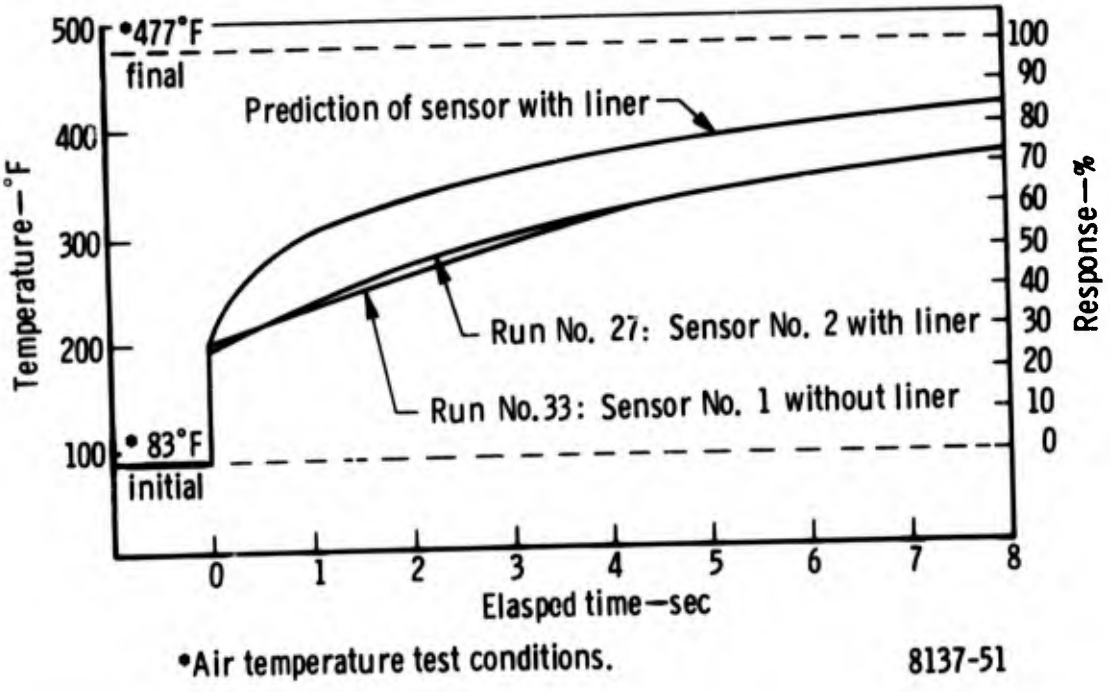

Figure 44. Comparison of predicted response to actual response of sensors.

A postheat transfer analysis, reported in Appendix C, was performed to realign the math model used in the predictions to the test results and investigage design changes that would improve the response. The analysis used test information gathered from the runs listed in Table 10.

TABLE 10. SENSOR RUNS USED IN POSTHEAT TRANSFER ANALYSIS

Sensor No.	Run No.	Probe orientation	Step	Airflow
1	33	Downstream	70 to 500°F	Table 6
1	35	Downstream	70 to 500°F	3.35 × Table 6 (hot air only)
2	27	Downstream	70 to 500°F	Table 6

The largest source of error in the math model was in the assumptions that were made regarding the flow field around the sensor probe. Thermocouple instrumentation attached to Sensor No. 1 indicated that the highest air temperature in the test section occurred in the middle of test chamber. Because of boundary layer conditions in the test chamber the reference thermocouple and the sensor probe inlet did not sense true upstream test duct temperatures. Other sources of error were related to uneven weight flow of hot and cold air in the test section. In the process of adjusting the model to account for these errors, the best correlation between predicted and measured sensor response output was obtained by using an air temperature near the exit orifices. After correcting the model to the actual flow field conditions, a computer run was made simulating the response of Sensor No. 1 and Sensor No. 2 with an ideal liner.

Figure 45 shows the comparison of the measured response from Sensor No. 1 and No. 2 operating with a ruptured liner to corrected model predictions. As the comparison shows, the sensors are close in performance and the predicted response was slightly more optimistic than the measured response.

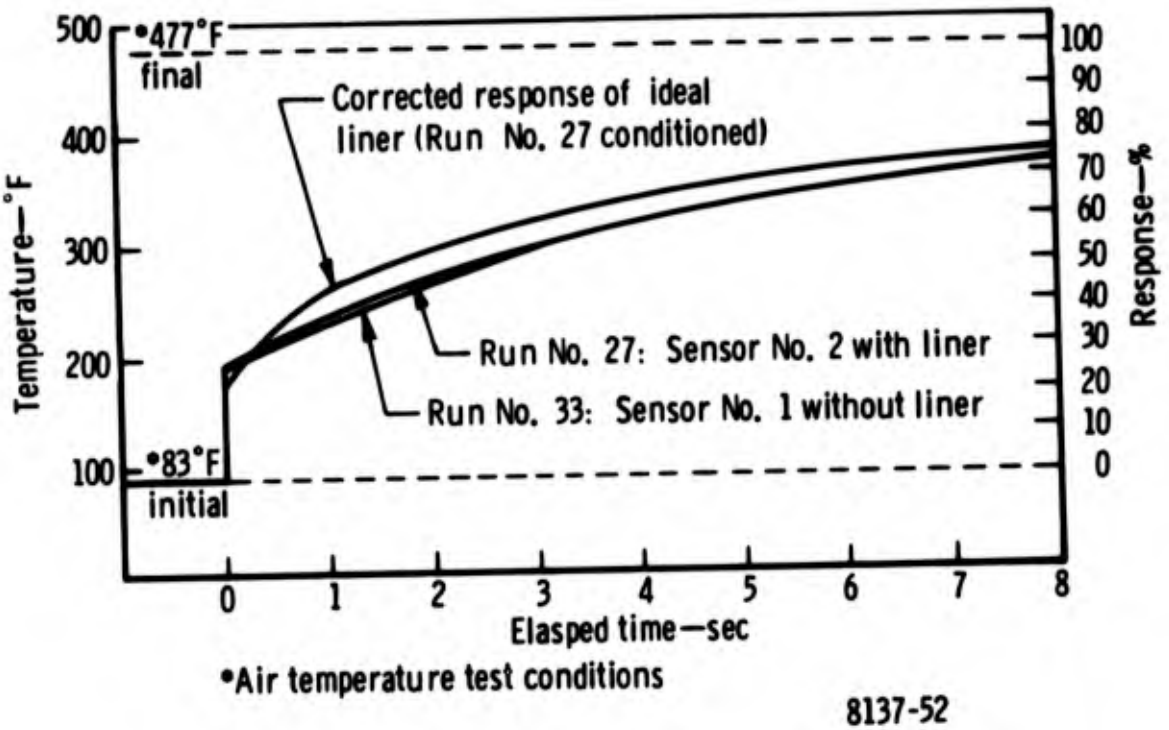

Figure 45. Comparison of corrected sensor model performance to measured response.

Because the response of the sensor that was fabricated for this program could not be improved with an ideal liner, other sensor design modifications were investigated. The objective of this investigation was to realistically determine what design modifications to the sensor would improve the response enough to make it attractive for engine use. To obtain the very best performance, the design modifications that evolved out of this investigation are:

- Relocation of the edgetone resonator cavity from the sensor mounting head location to the end of the probe to obtain a short-probe type of sensor performance
- Reduction of the present edgetone resonator wall thickness from 0.028 to 0.014 in. and thinning the resonator splitter from 0.050 to 0.025-in. thickness

- Doubling the airflow through the edgetone resonator by increasing the areas of the inlet and exit orifices

A comparison is shown in Figure 46 between a 0.040-in. dia, bare-tipped C-A thermocouple and a fluidic temperature sensor with and without improvements. The thermocouple used for comparison purposes is representative of those that have been used in similar gas turbine engines applications. Figure 46 indicates that under the test conditions of Run No. 33, a sensor with the aforementioned design modification would show substantial improvements in response over the present sensor geometry and would be superior to a 0.040-in. dia, bare-tipped C-A thermocouple for 3.5 sec. Following this elapsed time of 3.5 sec, the thermocouple would stabilize to 98% of the finalized temperature in 8 sec as compared with 92% for the sensor in the same time period.

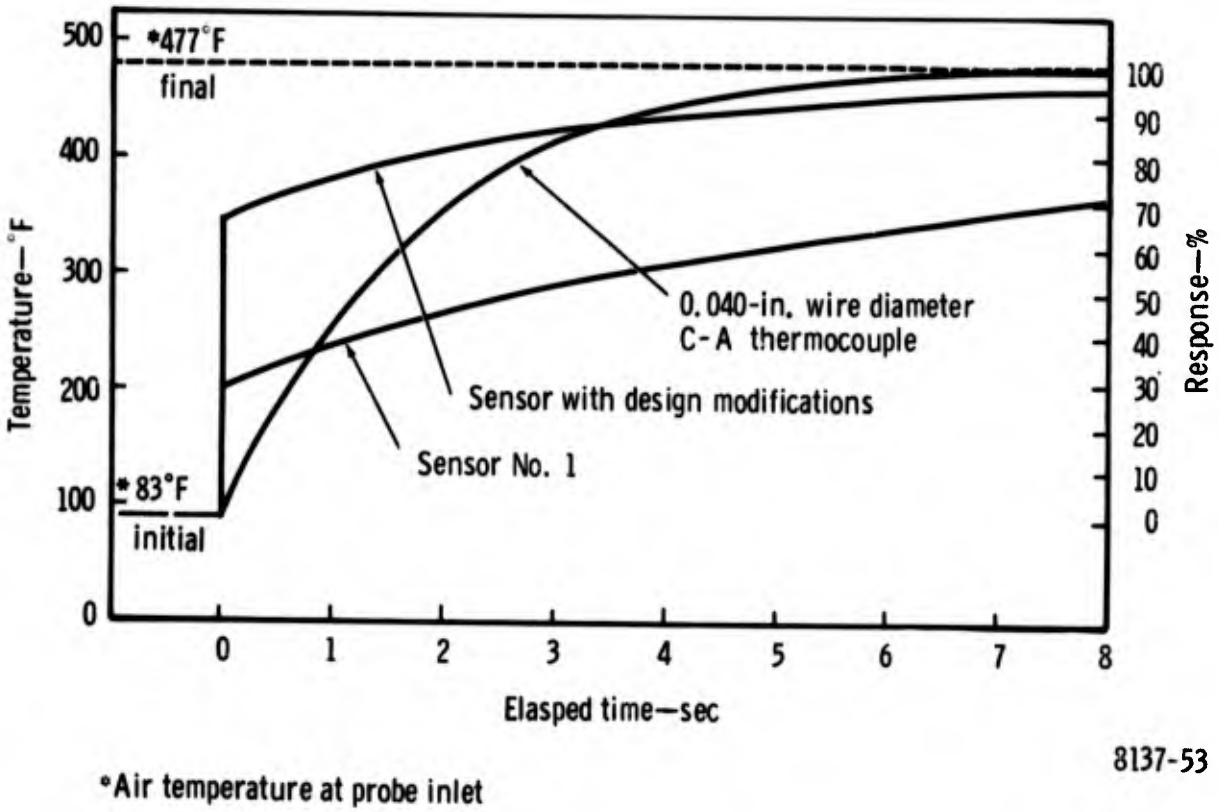

*Air temperature at probe inlet

Figure 46. Improved sensor response predictions.

To determine if the improved sensor is worth the system implementation on a JTDE, an open loop analysis was made to identify engine performance advantages. This qualitative analysis, documented in Appendix D, compares the fluidic sensor with the 0.040-in. dia, bare-tipped thermocouple in scheduling the HP compressor vanes during engine transients. The HP compressor vanes are scheduled by corrected high pressure rotor speed. The compressor inlet temperature is used to correct high pressure rotor speed. The analysis shows that the fluidic probe produces less error in scheduling the HP compressor vanes during an engine acceleration than that produced by the thermocouple probe. An increase in the amount of error in scheduling the HP compressor vanes during the engine transient will result in affecting the engine response time and the possibility of less HP compressor surge margin. Consequently, the fluidic probe has a slight engine performance advantage over the thermocouple probe.

VII. CONCLUSIONS AND RECOMMENDATIONS

The fluidic temperature sensor/air ejector designed and fabricated in this program was intended as a candidate for ultimate use on the turbofan engine technology demonstrator. Additional analysis work was performed during the course of this program to establish the basis of performance for this sensor geometry. Evaluation testing of the sensors, together with heat transfer and simulated engine transient analysis yielded significant findings regarding its use for JTDE application. Conclusions drawn from the program findings follow.

1. The response performance of the sensor tested was less than expected and less than that required to control the inlet guide vanes on the advanced engine. The application of actual test data to a heat transfer model indicated that the sensor response could not be substantially improved using an insulating heat transfer liner in the probe.

2. The air ejector was effective in producing stable sensor operation at a stream air pressure of 18 psia which was representative of those found in the engine operating envelope. Performance of the sensor at air stream conditions above its threshold (30.1 psia) was not affected by operation of the air ejector at supply pressures up to 75 psig.

3. Extensive design modifications to the sensor would be necessary to achieve significant performance improvements for engine use. The necessary modifications to the sensor would consist of relocating the edgetone resonator in the end of the probe, removing 50% of the metal mass in the edgetone resonator geometry, and doubling the airflow through it by increasing the inlet and exit orifice areas. These modifications to the sensor will require new fabrication techniques and substantiation of the proper sensor operation at increased sensor mass flow.

4. Incorporating the design modifications mentioned in 3., the response of the sensor to changes in HP compressor inlet temperature shows a minimum improvement over an exposed junction thermocouple (0.040-in. dia chromel-alumel) which could be used for this same purpose. Because of the dollar costs and development time needed to mature the fluidic temperature sensor to a comparable level with today's thermocouple technology, this approach does not appear to be worthwhile for substantially improving compressor geometry control. If the ground rules change and either (1) a very fast temperature sensor is needed for surge control or (2) a digital output sensor is needed for direct input to a digital computer controller, then the fluidic temperature sensor with appropriate signal conditioning may represent a significant advantage.

APPENDIX A

THERMAL ANALYSIS OF A FLUIDIC SENSOR PROBE FOR MEASURING COMPRESSOR INLET TEMPERATURE

APPENDIX A

THERMAL ANALYSIS OF A FLUIDIC SENSOR PROBE FOR MEASURING COMPRESSOR INLET TEMPERATURE

(The following discussion is based on Detroit Diesel Allison Technical Data Report AX. 1260-025 by R. E. Chupp, Detroit Diesel Allison Heat Transfer Section, Mechanical Research.)

The DDA Heat Transfer Section analyzed the fluidic sensor probes under test conditions. The analysis performed was much simpler than a previous one on a water-cooled probe.[1] * This report presents the results of that analysis and shows the effect of design changes. These design changes were made, and some have been included in the hardware. This report includes the analysis results, the method of analysis, and heat transfer considerations.

A typical response curve for a fluidic sensor with a step change in gas temperature is shown in Figure A-1. A fluidic sensor responds almost instantaneously to gas temperature changes as shown by the initial response in this illustration. This time period is so short that the probe wall temperature distribution remains essentially constant. Consequently, heat transfer between the gas and probe walls causes the gas temperature in the resonance cavity to lag behind the gas stream temperature. Thus, the measured initial response (Δoutput) is only about half of the gas temperature change (Δ temp). After the initial change, the measured gas temperature increases gradually with time as the probe walls respond. Characteristically, a fluidic sensor has a much faster initial response than does a thermocouple, but a slower subsequent response. In designing a fluidic sensor it is important to maximize the initial response change and minimize the time lag in the subsequent response. Heat transfer considerations in designing a probe are discussed later in this appendix.

---

*Superscript numbers correspond to publications listed under References.

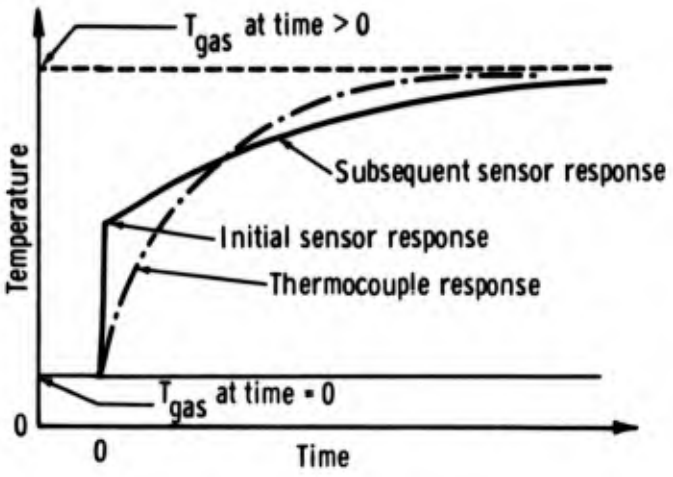

Figure A-1. Typical response curves for fluidic sensor and thermocouple probe.

ANALYSIS RESULTS

The fluidic sensor probe was analyzed using the nodal network shown in Figure A-2. Transient metal and air temperatures were determined for a variety of flow and geometric conditions with a fixed step change in gas temperature of 70 to 500°F. Table A-1 lists the flow and geometric variations considered. Plots of air temperature in the cavity region versus time are given in Figure A-3. The time considered was for the first 8 sec after the step in gas temperature occurs. Three air temperature variations are plotted: One for the cavity inlet, one for the cavity exit, and one for the average air temperature within the cavity. The shaded region in Figure A-3 represents the overall air temperature variation within the cavity versus time. The actual air temperature that the sensor responds to is unknown, but the average air temperature in the cavity was considered to represent the sensor response. Figure A-3 also shows the numerical value of the initial response of the average air temperature for each case considered.

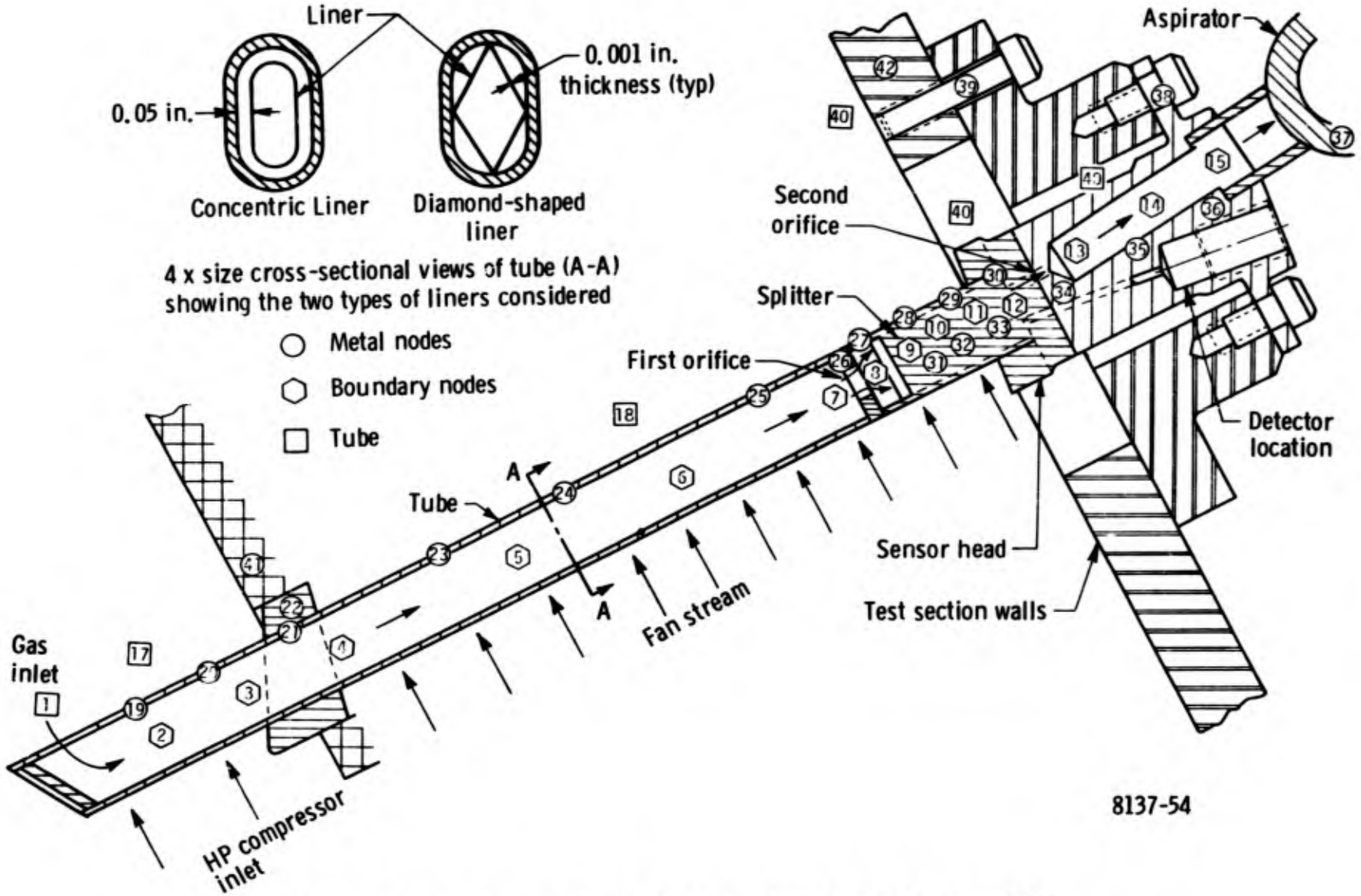

Figure A-2. Nodal pattern for heat transfer analysis—P/N EX-112219 fluidic temperature sensor (Mgn: 2X).

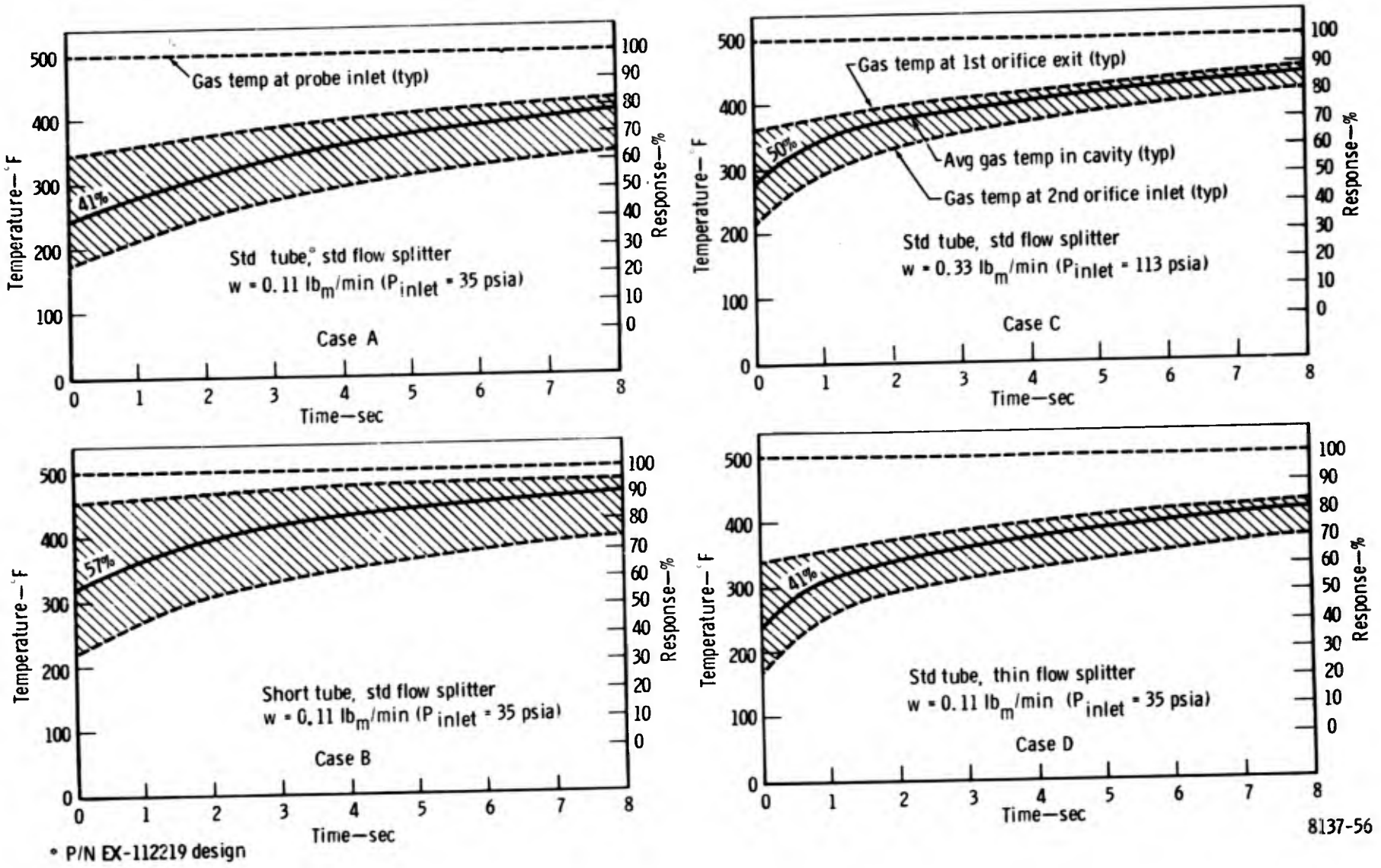

Figure A-3. Predicted response of fluidic sensor.

TABLE A-1. RESPONSE RESULTS FOR CASES INVESTIGATED

Case	Condition	Percent of response** at 0 sec	2 sec	8 sec
A	Base line*	41	56	78
B	Short tube	57	76	90
C	Higher flow rate (3* base value)	50	72	88
D	Thin flow splitter	41	62	79
E	Concentric liner (0.001 in. thick)	34	69	89
F	Diamond-shaped liner (0.001 in. thick)	34	69	88
G	Concentric liner (0.002 in. thick)	34	65	88
H	Concentric liner (0.004 in. thick)	34	59	85

*Base line is the P/N EX-112219 design with 0.110 lbm/min flow rate through the sensor.

**Percent of response corresponds to that of the average air temperature in the sensor cavity.

Four different cases are illustrated in Figure A-3. These are the first four cases listed in Table A-1 and are denoted as A through D. Table A-1 also includes response values of the average temperature at 0, 2, and 8 sec taken from Figure A-3. Case A represents the base line. This case is for the probe as designed with a flow rate that is typical for the proposed test conditions. The initial response of 41% is lower than that of previous designs[2] because of the longer delivery tube. The response at later times is also worse than the previous design. To prove that the delivery tube is the cause, Case B is for a shorter tube. The initial response for this case is increased to 57%, which is comparable to that of previous designs.[2] Case C is the same as Case A except the flow rate through the probe is three times larger. The increased flow rate improves the response considerably. Case D is the same as Case A except a thinner flow splitter is considered. Heat transfer to the splitter is high so a thinner splitter decreases the lag of the air

temperature variation. The initial response for Case D is identical to Case A but the subsequent response is better.

Several possible design modifications to improve the response in addition to those previously discussed were investigated. Shortening the delivery tube (Case B) significantly improved the response, but solving the mechanical problems associated with placing the sensor head in the gas stream was considered to be beyond the scope of the program. Instead of shortening the tube, inserting a metal liner inside the delivery tube was considered. A liner creates an insulating air space and is thin so that it reacts faster to gas temperature changes than the tube wall. Two liner shapes as shown in Figure A-2 were investigated. Transient air results are given in Figure A-4 for four different liner designs. Cases E, G, and H are for a concentric liner shape with wall-thicknesses of 0.001, 0.002, and 0.004 in., respectively. Case F is for a diamond-shaped liner which touches the tube wall at its four corners. Response results for these cases are also listed in Table A-1.

The data indicate that inserting a metal liner in the tube decreases the initial response, but significantly improves the subsequent response. For example, the response for the two 0.001 in. thick liner designs (Cases E and F) is better than without a liner (Case A) after the first one-half second. Thus, the liner is effective. This approach makes the long delivery tube more acceptable. However, the response of a long tube with a liner never exceeded that of a short tube. Both the long and short tube designs could be improved if a larger cross-sectional area were employed.

Another modification investigated was the removal of material from the sensor head. Removing about one-third of the mass of the head had no effect on the air temperature response for the first 8 sec. The primary concern is to improve the response in the first few seconds; thus, there is little need to lighten the sensor head.

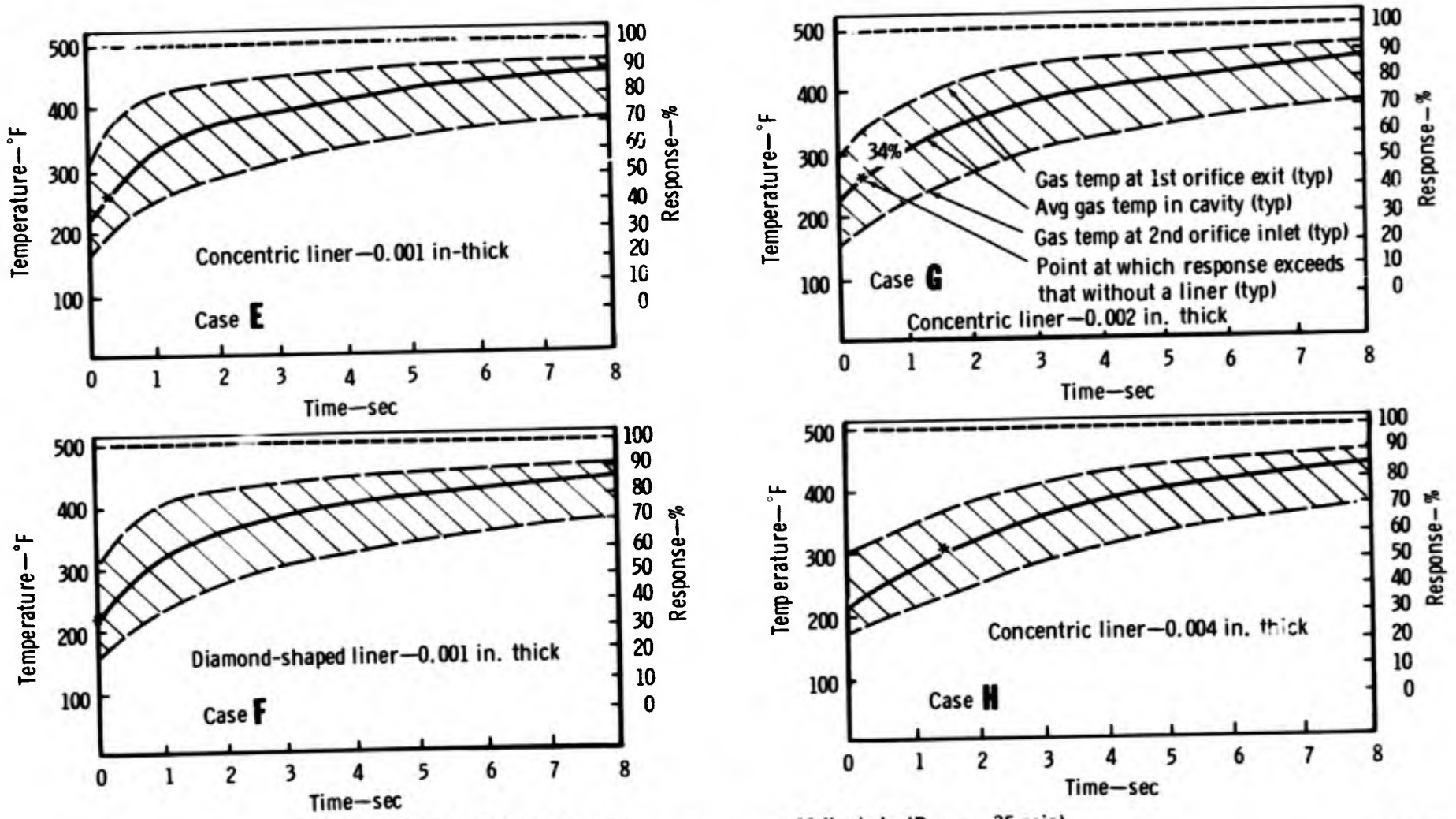

Figure A-4. Predicted response of fluidic sensor for tube with inner liner.

In summary, the results presented show that the expected response of the fluidic sensor is not as good as previous designs because of the longer delivery tube. The response could be improved, however, by inserting a metal liner inside the tube.

METHOD OF ANALYSIS

The heat transfer analysis was performed by subdividing the sensor into nodes as shown in Figure A-2. The material nodes are assumed to be isothermal and the fluid nodes represent axial locations at which the fluid temperature is evaluated. The nodal temperature variations with time were evaluated using computer program EJ-8.[3] This program uses a simple, explicit approach to determine the transient temperature distribution. The fluid node temperatures are evaluated from a quasi-steady-state heat balance, i.e., the fluid temperatures are assumed to respond much faster than the metal temperatures. This assumption is valid for the sensor probe since the time for air to pass through the sensor (residence time) is of the order of 0.01 sec compared to a minimum time constant of 0.5 sec for the metal nodes.

The heat transfer boundary conditions were calculated from standard "pipe flow" correlations for all regions except along the splitter where a "flat plate" correlation was employed. The first orifice forms a jet of air which impinges on the splitter knife edge. The mass velocity thus used in the flat plate correlation was that through the first orifice. The variation of flow rate through the sensor versus upstream pressure was adapted from cold flow calibration data. The second orifice is always choked so that the downstream pressure has no effect on the flow rate.

An initial analysis was performed on a sensor probe which had already been tested.[2] This probe had a short delivery tube so that response lag was primarily caused by heat transfer in the cavity region. The heat transfer model employed is similar to that shown in Figure A-2. An initial response of the

average air temperature in the cavity was predicted to be 65% compared with a 55% measured response. The difference could be caused by the air temperature to which the sensor responds. The 55% initial response would correspond to that of the air near the cavity exit. Intuitively, the sensor would respond to some average air temperature rather than the exit temperature. Thus, the difference between the predictions and measurements were attributed to enhanced heat transfer at the cavity's outer wall because of the locally high air velocities after the air impinges on the splitter. The heat transfer coefficient along these walls had been predicted from a pipe flow correlation with an average mass velocity in the cavity. By increasing the predicted heat transfer coefficient by 75%, the predicted initial response step matched the measured value. No doubt, the air velocities along the cavity walls are higher than the average value and heat transfer should be higher. Thus, the 75% correction was applied to the cavity walls in analyzing the new probes.

The conditions assumed in the analysis were those for the test and are listed in Table A-2. The test provides a step change in gas temperature which can be easily modeled analytically. Any intended engine application will have a less severe gas temperature change. The gas stream Mach number modeled in the test (0.05) is the highest that could be run. The probes external dimensions matched those of the thermocouple probe in the inlet of the TF41 HP compressor.

HEAT TRANSFER CONSIDERATIONS

In designing a fluidic sensor probe, the heat transfer characteristics of a sensor should be understood in order to maximize response. The heat transfer problem in a sensor probe has two parts: (1) A quasi-steady-state transfer of heat from the gas stream to the probe walls at any given time, and (2) the transient response of the probe walls. The first part determines the sensor's initial response; both parts affect the subsequent response.

TABLE A-2. CONDITIONS ASSUMED IN THE ANALYSIS

Gas conditions outside tube

T_g = 500°F $t > 0$, T_g = 70°F $t \leq 0$
P_g = 30 to 90 psia
M_{N_g} = 0.05

Orifice conditions

First orifice: A = 0.00702 in.^{2}
M_N = 0.083 (for second orifice choked)
C_D effective = 0.66 (from flow calibration data)

Second orifice: A = 0.00424 in.^{2}
M_N = 1.0
C_D effective = 0.66 (assumed same as first orifice)

Heat transfer coefficients for W = 0.11 lbm/min

Btu/hr ft^2 °F
(independent of W)

Outside tube	= 32
Inside tube	= 14
Beginning of splitter	= 150
End of splitter	= 103
Cavity outer walls	= 35

The concept of thermal effectiveness is useful in understanding the heat transfer problem. Thermal effectiveness, η_t, is defined as

$$\eta_t = \Delta T \text{ gas}/(T_{walls} - T_{gas\ in}) = 1 - e^{-\frac{hA}{Wcp}} \qquad (1)$$

for a constant wall temperature case, where h is the heat transfer coefficient, A the surface area, W the flow rate, and Cp the air specific heat. The initial percent response listed in Figures A-3 and A-4, and Table A-1, is simply

$$\text{Percent of initial response} = (1 - \eta_t) \cdot 100\% \qquad (2)$$

because the probe walls are essentially at the initial gas temperature. To improve the initial response, the heat transfer effectiveness, η_t, must be minimized. However, minimizing η_t will slow down the response of the probe walls and the subsequent sensor response. Thus, improving one part of of the response slows down the other part.

The approach taken in considering possible design changes to the probe was to to allow the initial response to drop in order to improve the subsequent response. This was done specifically in investigating the effect of a tube inner liner. The cross-sectional flow area was diminished; this increased the air velocity, heat transfer coefficient, and η_t for a given flow rate but caused the initial response to drop from 41% to 34% for the lower flow rate case. However, the 0.001 in. thick liner walls responded much faster than the 0.028-in. thick tube walls and the subsequent response was much faster. The response with a liner could be improved if a larger cross-sectional area were employed.

The same effect as a metal liner could be obtained if the inner tube walls were insulated. However, the air side surface of the insulation should be smooth so that convection is not enhanced. This could be accomplished by attaching a metal foil to this surface of the insulation.

APPENDIX B

SAMPLING OF CALIBRATION DATA
FROM SENSORS NO. 1 AND NO. 2

RUN 65

```
1624:18
JANUARY 23, 1974    -FLUIDIC SENSOR TEST-  B/U  1, SERIES -A
  WA      PRESS    TEMP.      REF      SENSOR
LB/SEC    PSIA     DEG F     MACH #  SIGNAL-HZ
  2.95    74.68     199.     .05006     3937.
SENSOR TC'S:
  #21 = 196.  #22 = 196.  #23 = 197.  #24 = 196.
  #25 = 198.  #26 = 192.  #
  2.95    74.63     199.     .05017     3937.
SENSOR TC'S:
  #21 = 196.  #22 = 196.  #23 = 197.  #24 = 196.
  #25 = 198.  #26 = 191.  #
  2.95    74.62     198.     .05010     3936.
SENSOR TC'S:
  #21 = 196.  #22 = 196.  #23 = 197.  #24 = 196.
  #25 = 198.  #26 = 191.  #
  2.95    74.59     198.     .05014     3935.
SENSOR TC'S:
  #21 = 196.  #22 = 196.  #23 = 197.  #24 = 196.
  #25 = 197.  #26 = 191.  #
  2.94    74.59     199.     .05008     3937.
SENSOR TC'S:
  #21 = 197.  #22 = 197.  #23 = 198.  #24 = 197.
  #25 = 199.  #26 = 191.  #
1625:38 END RDG.
```

Preceding page blank

RUN 92

```
1238:49
JANUARY 24, 1974   -FLUIDIC SENSOR TEST-  B/U  1, SERIES -A
  WA      PRESS    TEMP.      REF      SENSOR
LB/SEC    PSIA     DEG F     MACH #  SIGNAL-HZ
  3.01    74.56     198.     .05113     3937.
SENSOR TC'S:
  #21 = 197.  #22 = 198.  #23 = 200.  #24 = 200.
  #25 = 200.  #26 = 190.  #
  3.01    74.55     199.     .05127     3941.
SENSOR TC'S:
  #21 = 198.  #22 = 199.  #23 = 202.  #24 = 201.
  #25 = 200.  #26 = 189.  #
  3.01    74.54     199.     .05126     3942.
SENSOR TC'S:
  #21 = 198.  #22 = 199.  #23 = 202.  #24 = 201.
  #25 = 200.  #26 = 189.  #
  3.02    74.53     199.     .05138     3941.
SENSOR TC'S:
  #21 = 198.  #22 = 199.  #23 = 201.  #24 = 200.
  #25 = 200.  #26 = 189.  #
  3.03    74.56     199.     .05160     3941.
SENSOR TC'S:
  #21 = 198.  #22 = 199.  #23 = 201.  #24 = 200.
  #25 = 200.  #26 = 189.  #
  3.01    74.59     199.     .05131     3940.
1240:16 END RDG.
```

RUN 98

```
1359: 3
JANUARY 24, 1974   -FLUIDIC SENSOR TEST-  B/U  1, SERIES -A
  WA      PRESS    TEMP.      REF      SENSOR
LB/SEC    PSIA     DEG F     MACH #  SIGNAL-HZ
  2.98    29.84      67.     .11346     3478.
  2.99    29.83      67.     .11365     3478.
1359:17 END RDG.
```

RUN 106

1442:59
JANUARY 24, 1974 -FLUIDIC SENSOR TEST- B/U 1, SERIES -A

WA LB/SEC	PRESS PSIA	TEMP. DEG F	REF MACH #	SENSOR SIGNAL-HZ
2.99	59.24	363.	.07160	4316.
2.99	59.21	362.	.07166	4317.
2.99	59.21	363.	.07152	4318.
3.00	59.26	363.	.07186	4318.
2.99	59.32	363.	.07156	4320.
3.00	59.35	363.	.07161	4320.
3.00	59.38	363.	.07158	4318.
2.99	59.35	363.	.07139	4318.

1443:55 END RDG.

RUN 108

1447:46
JANUARY 24, 1974 -FLUIDIC SENSOR TEST- B/U 1, SERIES -A

WA LB/SEC	PRESS PSIA	TEMP. DEG F	REF MACH #	SENSOR SIGNAL-HZ
2.98	59.61	363.	.07084	4317.
2.98	59.69	363.	.07089	4317.
2.98	59.72	363.	.07087	4317.
2.99	59.77	363.	.07096	4317.
2.99	59.84	363.	.07086	4316.
2.99	59.82	362.	.07083	4314.

1448:28 END RDG.

RUN 113

1524: 5
JANUARY 24, 1974 -FLUIDIC SENSOR TEST- B/U 1, SERIES -A

WA LB/SEC	PRESS PSIA	TEMP. DEG F	REF MACH #	SENSOR SIGNAL-HZ
3.03	59.62	69.	.05760	3495.
3.03	59.70	69.	.05772	3496.
3.04	59.70	69.	.05786	3495.
3.03	59.74	69.	.05768	3494.
3.04	59.74	69.	.05780	3494.
3.03	59.78	69.	.05771	3495.

1524:46 END RDG.

RUN 116

1530:21
JANUARY 24, 1974 -FLUIDIC SENSOR TEST- B/U 1, SERIES -A

WA LB/SEC	PRESS PSIA	TEMP. DEG F	REF MACH #	SENSOR SIGNAL-HZ
2.99	75.36	69.	.04505	3497.
2.96	75.45	69.	.04462	3497.
2.98	75.42	69.	.04489	3497.
2.97	75.36	69.	.04483	3497.
2.97	75.31	69.	.04489	3496.

1530:56 END RDG.

APPENDIX C

POST-TEST THERMAL ANALYSIS OF FLUIDIC SENSOR PROBES FOR MEASURING COMPRESSOR INLET TEMPERATURES

(The following discussion is based on Detroit Diesel Allison Technical Data Report AX. 1260-027 by R. E. Chupp, Detroit Diesel Allison Heat Transfer Section, Mechanical Research.)

POST-TEST ANALYSIS

The objectives of the post-test analysis were to:

- Adjust the heat-transfer model so that the predicted temperature response data matched the measured data for Sensor No. 1
- Using the revised model, predict the response of Sensor No. 2 having a liner and compare the results with measured data for Sensor No. 2
- Recommend and analyze an improved probe design

This report presents the results of the post-test analysis. The response characteristics of a fluidic sensor, method of analysis, and heat transfer considerations are described in DDA TDR AX. 1260-025.[4]*

Adjustment of Heat Transfer Model

The model developed in the analysis consisted of a network of nodes (Figure C-1) whose heat capacities were calculated from property data and boundary conditions determined from data correlations. The largest source of error in the model was in the boundary conditions because of uncertainties in the flow field. Thus, only the boundary conditions were adjusted in matching the predicted response with measured data.

---

*Superscript numbers correspond to publications listed under References.

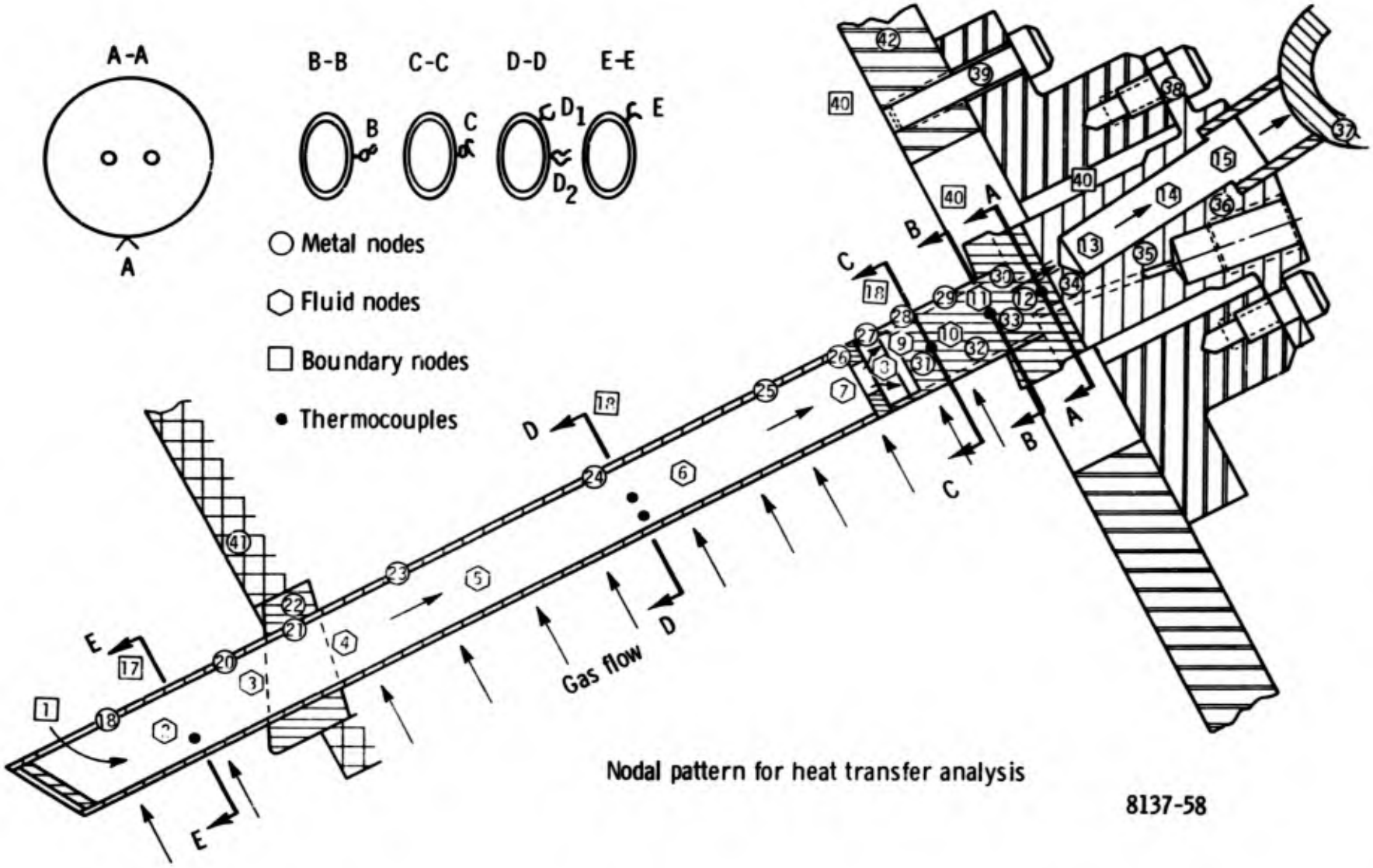

Figure C-1. Thermocouple instrumentation attached to sensor No. 2.

TABLE C-1. TEST RUNS ANALYZED AND CONDITIONS ASSUMED

Run No.	Sensor No.	Direction inlet faces	Gas flow rate
27	2	Downstream	Nominal
33	1	Downstream	Nominal
35	1	Downstream	3.35 × nominal

Conditions assumed:

$T_{gas} \approx 90°F$ at t = 0 sec and $\approx 480°F$* at t > 0 (step up)
$M_{N_{gas}} \approx 0.05$ (for nominal flow rate)
$P_{gas} \approx 30$ psia $\Rightarrow W_{sensor} \approx 5.4$ lbm/sec (from calibration data)
$\Rightarrow$ Reynolds No. ≈ 3500 (in the tube)

*This temperature is at the tube inlet. Thermocouple data show that $T_{gas} \approx 510°F$ near the center of the channel.

The test runs and conditions considered in post-test analysis are listed in Table C-1. The test data for Sensor No. 1 included the transient response of six thermocouples attached to the sensor walls as shown in Figure C-1. Data from thermocouple D_1 were used primarily in the analysis. This thermocouple measures approximately an average wall temperature (at that axial location) which is the temperature considered in the analytical model.

The procedure employed and results of adjusting the boundary conditions are described in a later subsection of this appendix, Adjustment of Boundary Control. The key finding from this work is that for the model to correctly predict the sensor response, the air temperature near the cavity exit has to be used to represent the response. A similar problem occurred in a previous analysis,[4] but was attributed to heat transfer at the outer cavity walls. Such an explanation would not resolve the predicted and measured response differences in the present data. The flow field and acoustics in the cavity are so complex that proper modeling of this region is difficult without additional data.

Response of Sensor With Liner

The response of sensor No. 2 predicted using the heat transfer model with adjusted boundary conditions and is shown as Curve B in Figure C-2. Curves C and D in this figure are measured data for Test Runs No. 33 and 27, respectively. It is apparent from Curve C versus Curve D that the liner did not improve the response as much as anticipated.[4] There were two reasons for this lack of improved response.

- A leak in the liner was detected during testing. The leak decreased the insulating effect of the liner.
- Sensor response had been previously represented by the average cavity air temperature (Curve A in Figure C-2). The average cavity air temperature is affected more by the liner than is the exit air temperature.

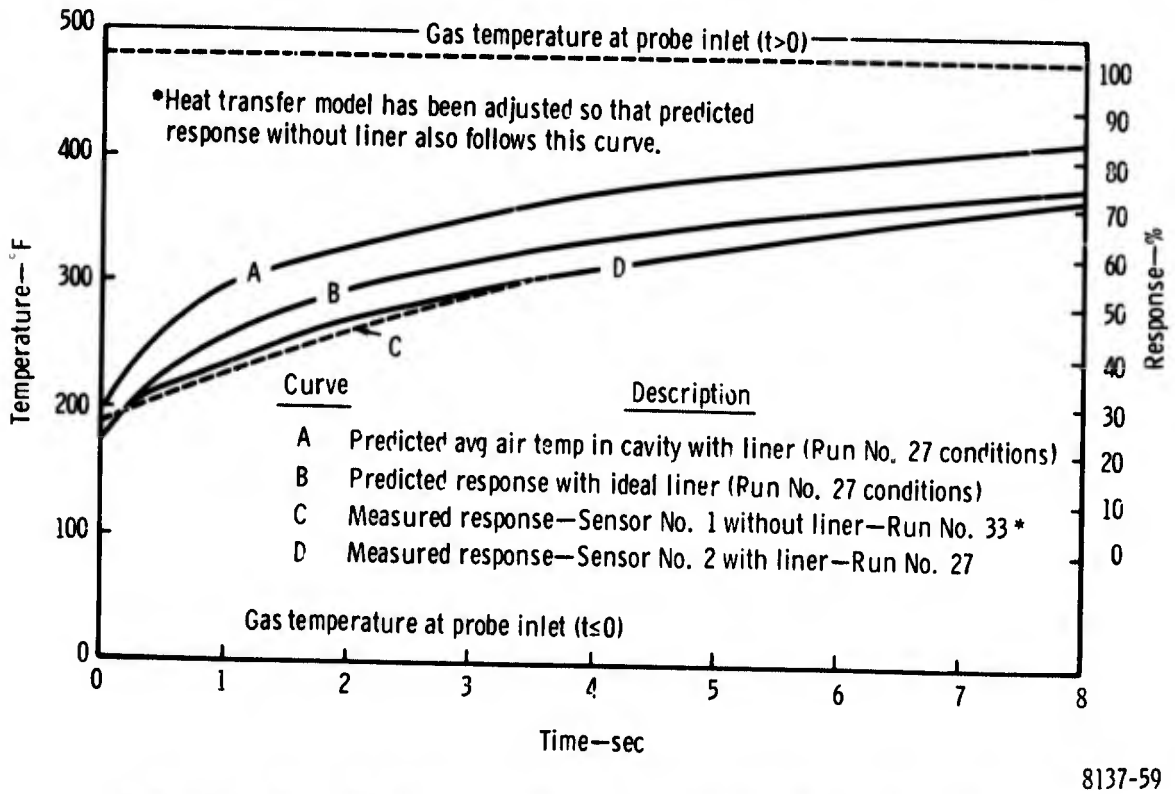

Figure C-2. Effect of liner or fluidic sensor response.

Response of an Improved Probe Design

The response of the two probes tested was much worse than originally expected.[4] This response would not be acceptable for an engine application. To determine if a fluidic sensor design could be used in the intended application, an improve probe was designed, based on the heat transfer model, and test results were obtained. This new probe is shown in Figure C-3. It has an inlet tube which is as short as possible.

Predicted response data for the new design are given in Figures C-4 and C-5 with wall thickness and flow rate as parameters. The gas flow conditions are the same as those for Test Run No. 33. Figures C-4 and C-5 also show the response of a 0.040-in. dia thermocouple[5] for reference. This is a typical thermocouple size for an engine application. The data in these two illustrations demonstrate that the new probe design responds much faster than the probes tested and also is quicker than the thermocouple in the first 1.5 to 3 sec.

To determine the feasibility of the short probe design in an engine application, both the short probe and thermocouple are being evaluated as components of the control system. This work is being carried out in the DDA Controls Department. The HP compressor inlet conditions are being considered for the

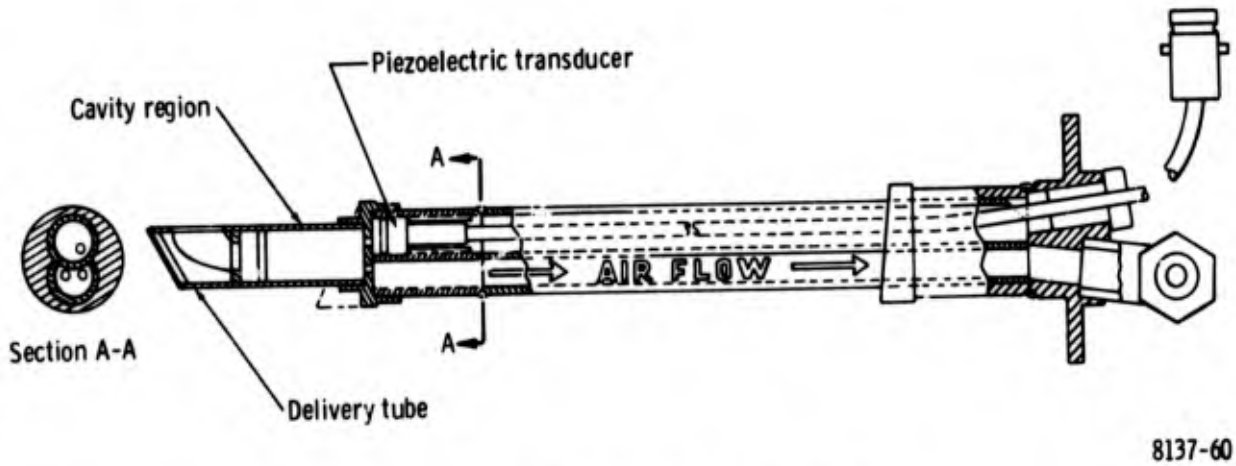

Figure C-3. Improved probe design.

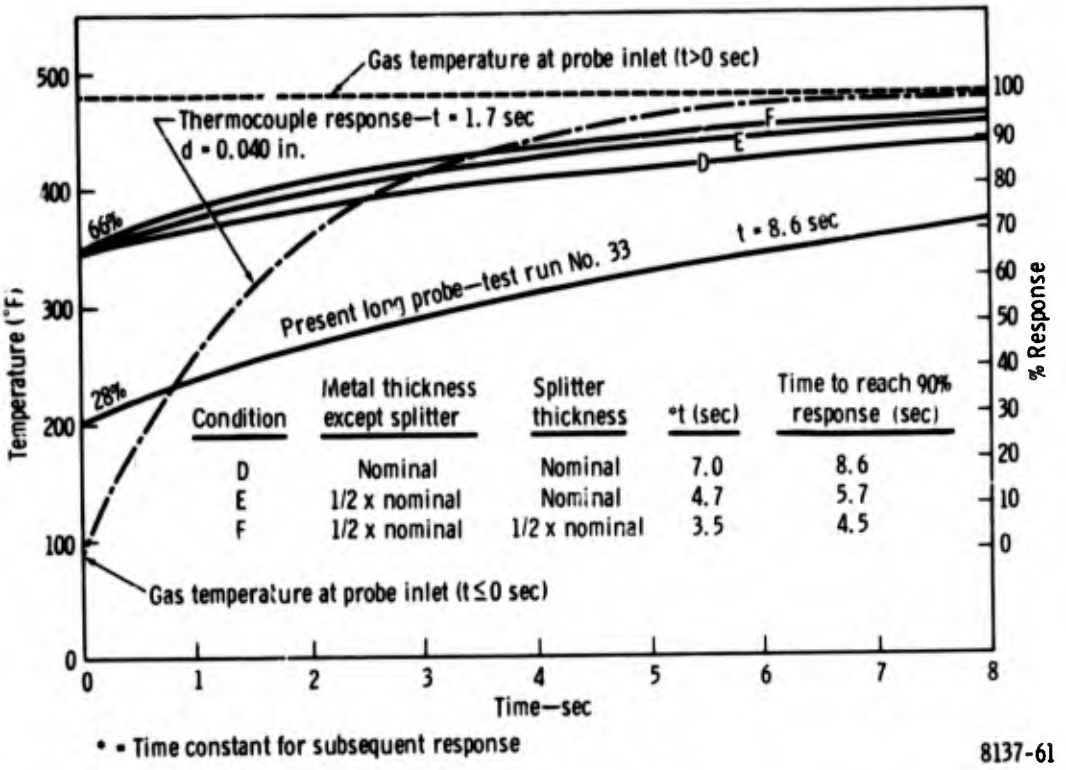

Figure C-4. Predicted response of fluidic sensor for several short probe designs with twice times nominal flow rate.

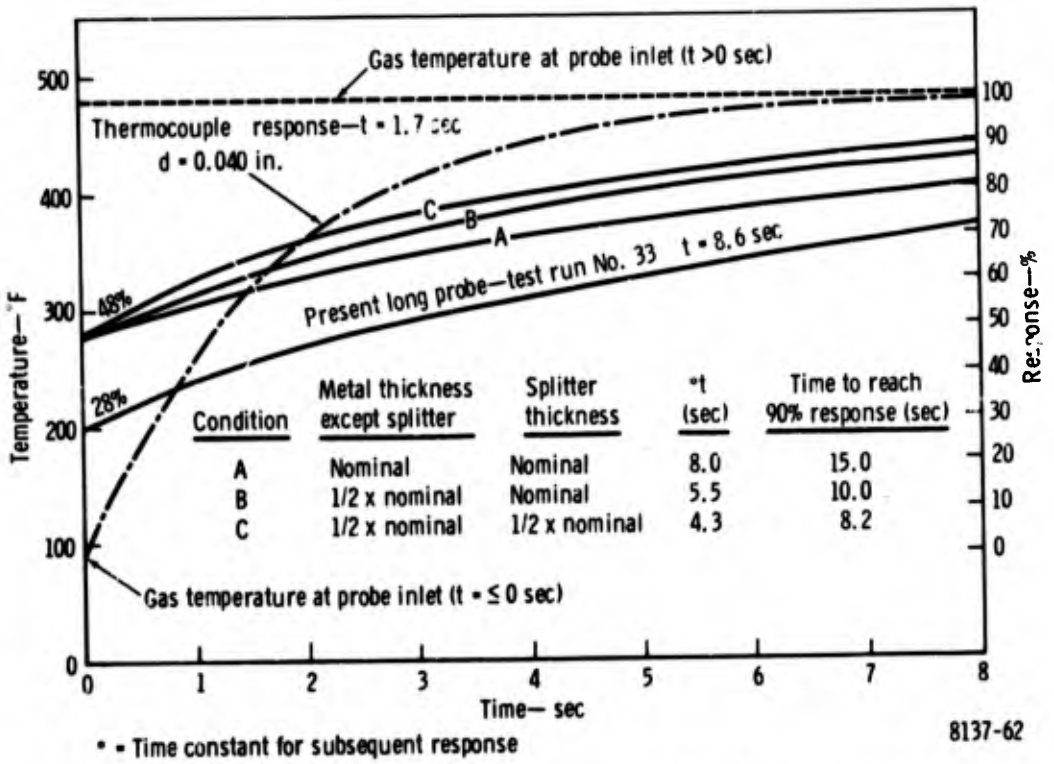

Figure C-5. Predicted response of fluidic sensor for various short probe designs with nominal flow rate.

sea level flight profile of the JTDE. The DDA Heat Transfer Section provided the response characteristics of the new short probe and thermocouple as input to this study. Table C-2 gives the gas flow conditions and predicted responses for four points on the flight profile.

TABLE C-2. FLIGHT CONDITIONS AND PREDICTED FLUIDIC SENSOR RESPONSE FOR DEMONSTRATOR HP COMPRESSOR INLET

Flight Conditions

No.	Total press. (psia)	Mach No.	Temperature (°R)	Static press. (psia)
1	17	0.285	560	16
2	29	0.315	650	26
3	40	0.383	715	36
4	44	0.510	740	36

Predicted Response of Sensor*

Flight condition No.	Wall thickness	Percent initial response	Time constant; subsequent response (sec)	T/C** time (sec)
1	Nominal	61.3	5.5	0.85
	1/2 × nominal	61.3	2.8	0.85
2	Nominal	64.1	3.7	0.61
	1/2 × nominal	64.1	1.9	0.61
3	Nominal	65.6	2.9	0.47
	1/2 × nominal	65.6	1.5	0.47
4	Nominal	66.2	2.6	0.39
	1/2 × nominal	66.2	1.4	0.39

*For sensor having twice the orifice area as the nominal design.

**Thermocouple with a 0.040-in. wire diameter.

ADJUSTMENT OF BOUNDARY CONDITIONS

Three boundary conditions were adjusted in the heat transfer model: the average heat transfer coefficient around the outside of the probe, $h_{outside}$, the heat transfer coefficient variation with axial length inside the delivery tube, h_{tube}, and the heat transfer coefficient variation with axial length along the splitter wall, $h_{splitter}$. The other boundary conditions were held constant because they have only a minor effect on the sensor response. Data from Test Runs No. 33 and 35 were used exclusively in adjusting the boundary conditions.

As a first attempt, response predictions were made for Test Run No. 33 with $h_{outside}$, h_{tube}, and $h_{splitter}$ calculated, using the procedure employed in pretest analysis.[4] The initial response step was predicted to be 42% compared to the 28% measured (Figure C-2). Thus, the boundary conditions used in a previous analysis were in error.

The correct values for the three boundary conditions were determined by trial and error. The solution criterion employed was to match the predicted and measured response data for Test Runs No. 33 and 35. The measured data for these runs are shown in Figure C-6. This illustration includes both the sensor and thermocouple D_1 response. The initial step in the sensor output is the same for the two runs since only the gas stream flow rate was different; the gas stream pressure and thus the sensor flow rate were the same. The three boundary conditions influence the predicted response as follows:

- h_{tube} and $h_{splitter}$ primarily affect the initial step with only a slight effect on the subsequent response of the sensor and thermocouple D_1.
- $h_{outside}$ has no effect on the initial step, but has a big influence on the subsequent response.

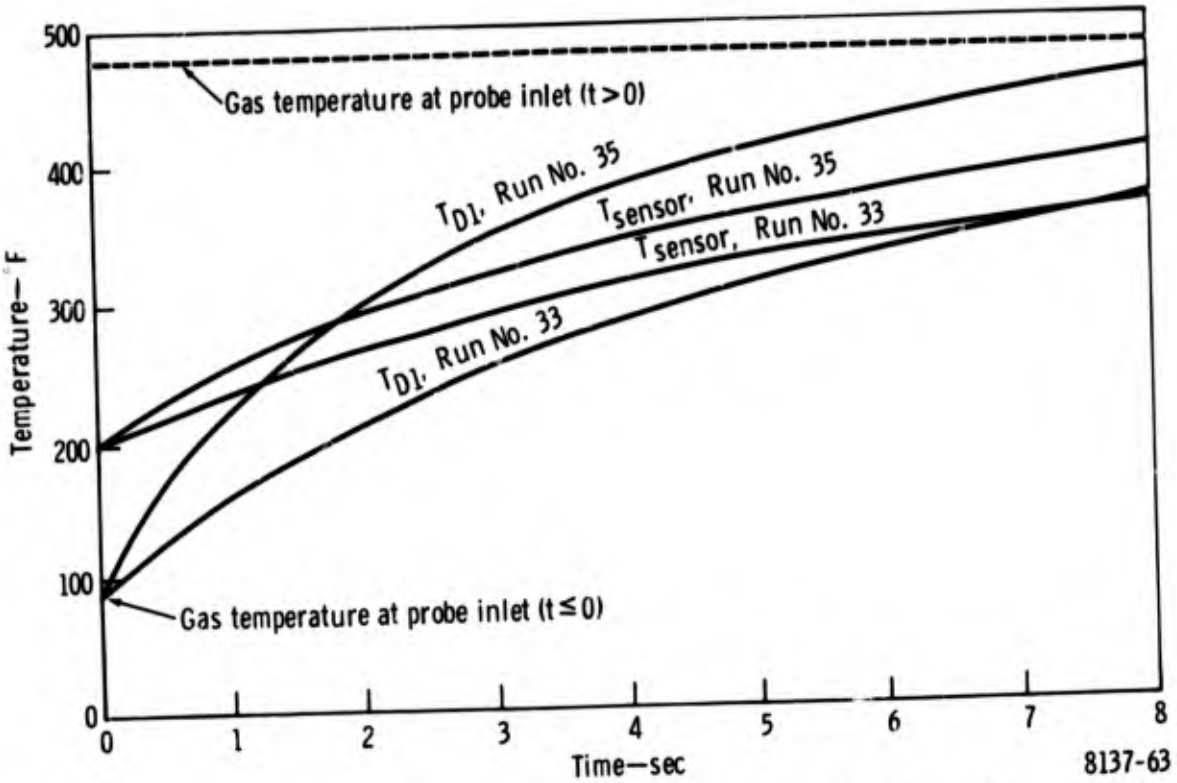

Figure C-6. Measured response data for Sensor No. 1 used to adjust model boundary conditions.

The only difference in the boundary conditions between Test Run No. 33 and 35 should be in $h_{outside}$. Thus, the independent effect of $h_{outside}$ versus h_{tube} and $h_{splitter}$ can be ascertained from the data.

The approach taken in modifying the boundary conditions was to assume a reasonable axial variation (except for $h_{outside}$ which should not vary axially) and then simply adjust the levels. In a previous analysis,[4] h_{tube} was assumed to be constant. However, applying a reasonable L/D correction[6] raised the overall level of h_{tube} by 43%. This was the major error in the boundary conditions.

In the trial and error process, a good prediction of the subsequent sensor response (for $t \geq 15$ sec) could only be obtained when an air temperature near the cavity exit was used to represent the sensor response. Otherwise, the

predicted response was faster than the measured one. The predicted response of the air temperature is slower near the exit because the thermal inertia of the sensor head starts to affect the air temperature response in this region after about 15 sec from the transient start. Both the flow field in the sensor cavity and the actual air temperature that the sensor responds to are unknown. Thus, the calculated air temperature near the cavity exit may very well be the correct one to represent the sensor response. The final adjustments made to the three boundary conditions are:

- h_{tube} had the L/D correction added.
- $h_{splitter}$ was decreased by one-third with the same L/D as used previously.[4]
- $h_{outside}$ was not changed for Test Run No. 33 conditions, but varied with W_{gas} to the 0.5 power instead of 0.8 in going to Test Run No. 35 conditions.

APPENDIX D

COMPARISON OF FLUIDIC AND THERMOCOUPLE TEMPERATURE SENSORS DURING ENGINE TRANSIENTS

(The following discussion is based on DDA Technical Data Report AX. 1260-026 by T. J. Christie, DDA Advanced Controls Systems Group, Controls Research and Development.)

TEST ANALYSIS

There were two typical engine transients used in this analysis: (1) an acceleration from idle to maximum power at sea level static conditions, and (2) hot gas ingestion during missile firing. A simplified digital computer program was developed to make the sensor comparison. Figure D-1 shows the functional block diagram of the computer program. As shown, the transient response of actual HP compressor inlet temperature and HP rotor speed are represented as functions of time. Each of those signals is lagged by their appropriate sensor dynamics and then used to calculate lagged corrected HP rotor speed. The HP compressor vane setting is then scheduled by the corrected speed value. An HP compressor vane position error is produced by comparing the scheduled vane setting minus the feedback vane setting. This vane position error determines the appropriate rate at which the vane actuator will move. This vane actuator rate is integrated to determine actual vane position and then checked against the maximum and minimum vane position. The actual vane position is also fed back through position sensor dynamics which produces the feedback vane setting. The HP rotor speed sensor dynamics and the vane actuator dynamic characteristics were common to both the fluidic and thermocouple sensors in this analysis.

The type of analysis described by the diagram in Figure D-1 is an open loop analysis, i.e., the actual vane position does not influence or affect the engine transient. If this were an actual engine, the HP compressor vane position would affect the engine transient by affecting both the engine transient time and HP compressor surge margin.

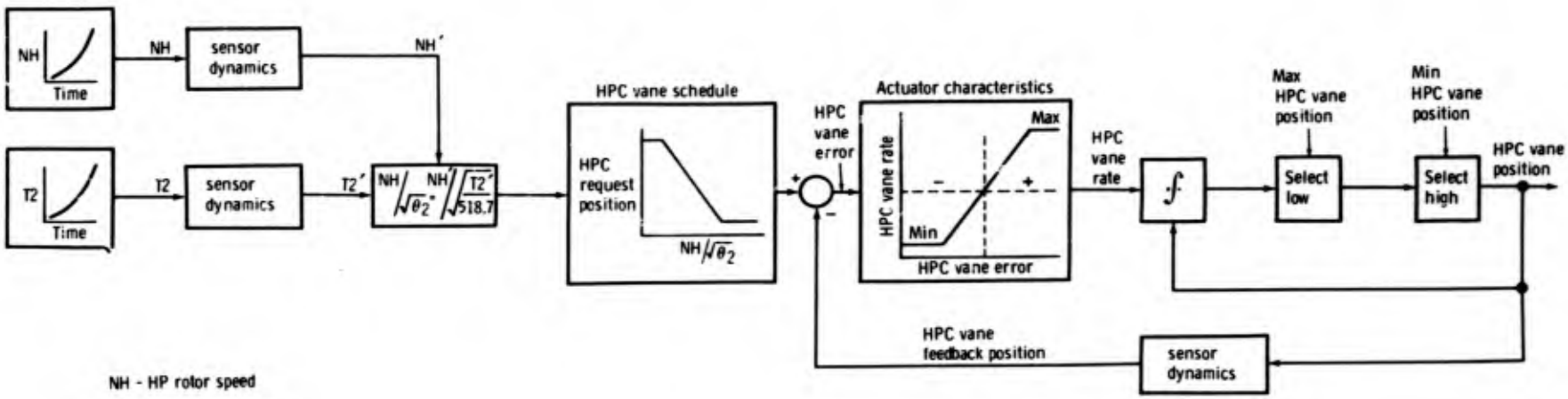

Figure D-1. Functional block diagram of digital computer program.

A typical 0.040-in. dia bare wire thermocouple probe was used in this analysis. This thermocouple has an approximate first order time constant of 0.6 sec. The three different types of fluidic sensor probes used were:

- Test probe designed under the Air Force contract
- Redesigned probe which puts the edgetone resonator near the tip of the probe and has twice the flow rate through the two orifices in the probe (shown as D probe)
- Same as the D probe design with half the metal thickness including the splitter (shown as F probe).

These fluidic probes are explained in more detail in Air Force Contract F33657-73-C-0618 report. The F probe is the optimum fluidic probe design followed by the D probe and then the test probe.

Figures D-2 through D-4 show, respectively, an HP compressor vane schedule, the typical vane actuator dynamic characteristics, and the necessary constants used in the program. Figures D-5 and D-6 show the sensor response characteristics to a step and ramp temperature change (90 to 500°F) which were used in checking the computer program against the actual test results.

Engine Acceleration Results

Figures D-7 through D-9 show, respectively, a sensor comparison of the time history for HP compressor inlet temperature, HP rotor speed, and HP compressor vane position. Figure D-10 shows a sensor comparison for HP compressor vane position versus corrected HP rotor speed. As a result of the sensor dynamic lags shown in Figures D-7 and D-8, Figures D-9 and D-10 indicate the amount of error in scheduling the HP compressor vanes using the various sensor probes. In Figure D-9 is shown the "requested HP compressor vane position." (This means that if there were no dynamic lags involved in sensing HP rotor speed or HP compressor inlet temperature and

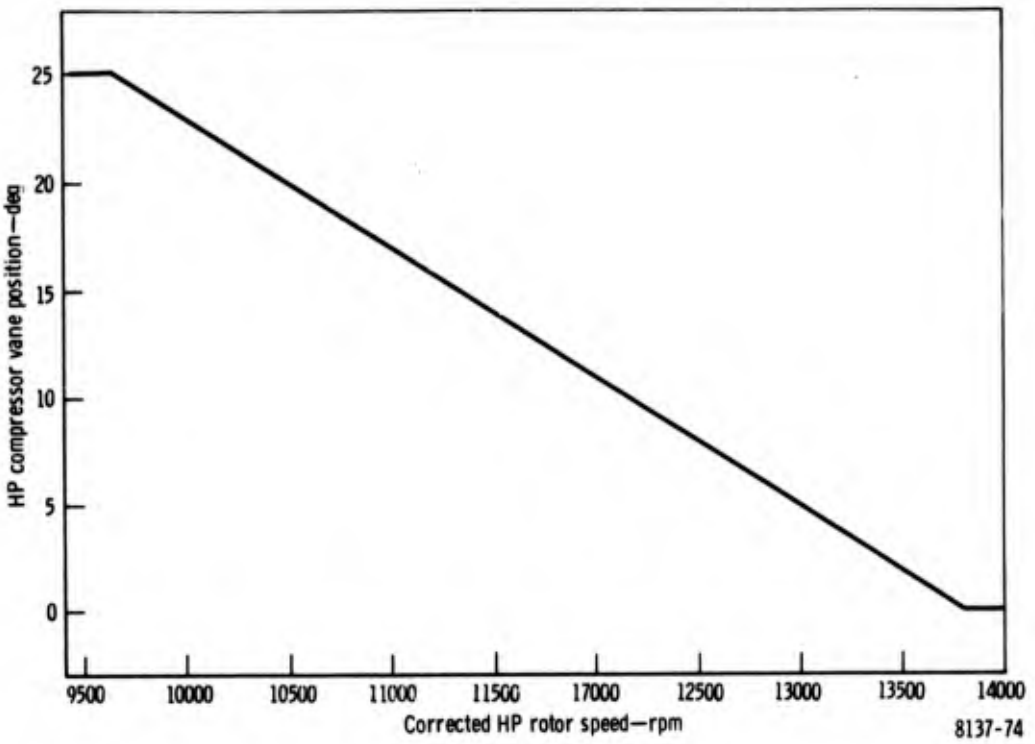

Figure D-2. Possible GMA200 HP compressor vane schedule.

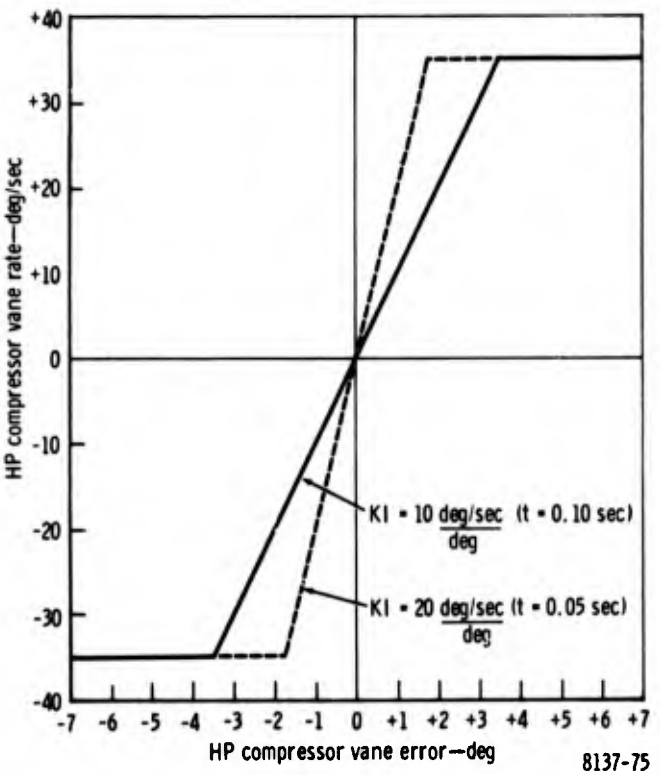

Figure D-3. HP compressor vane actuator dynamic characteristics.

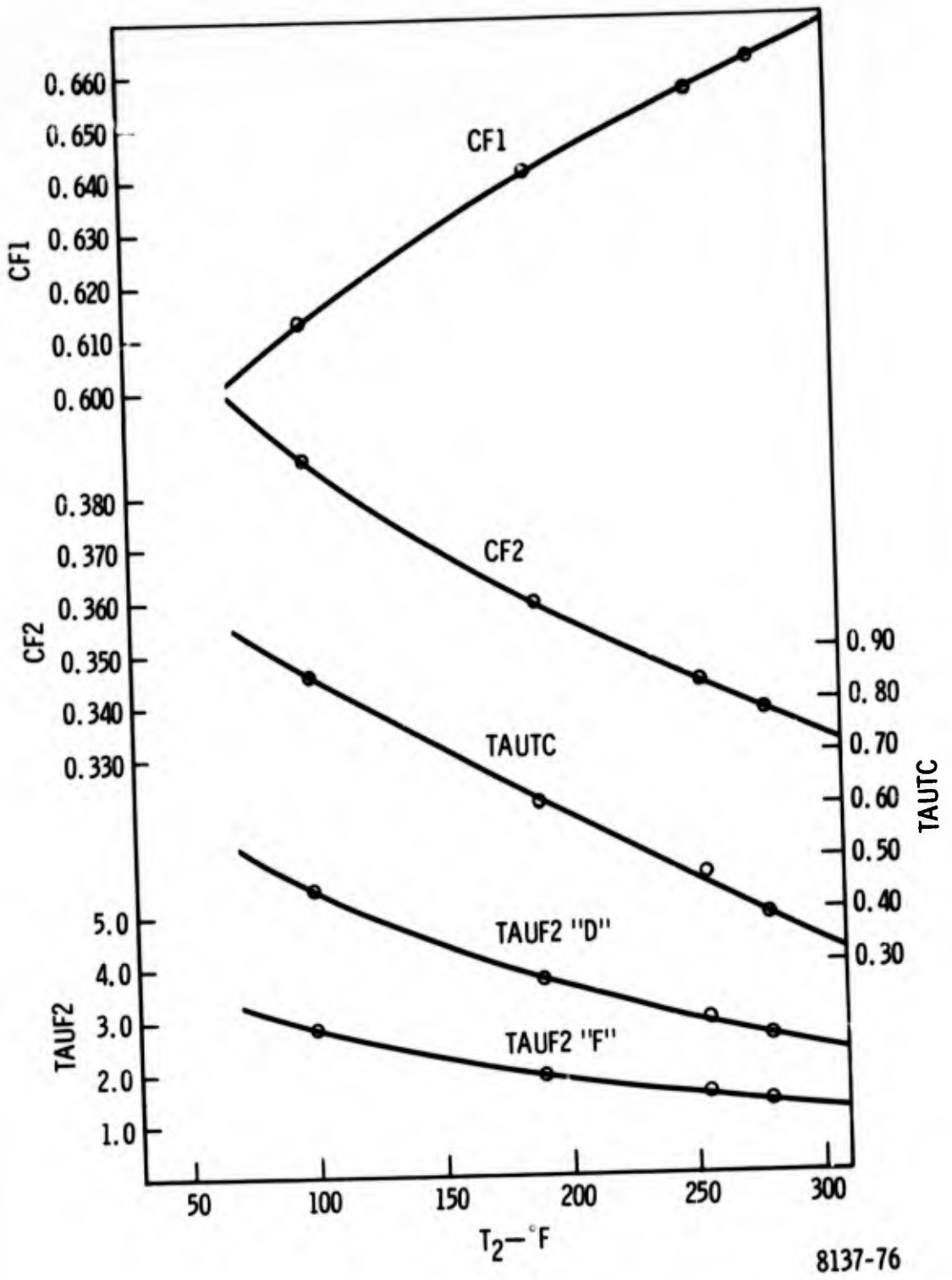

Figure D-4. Computer program constants.

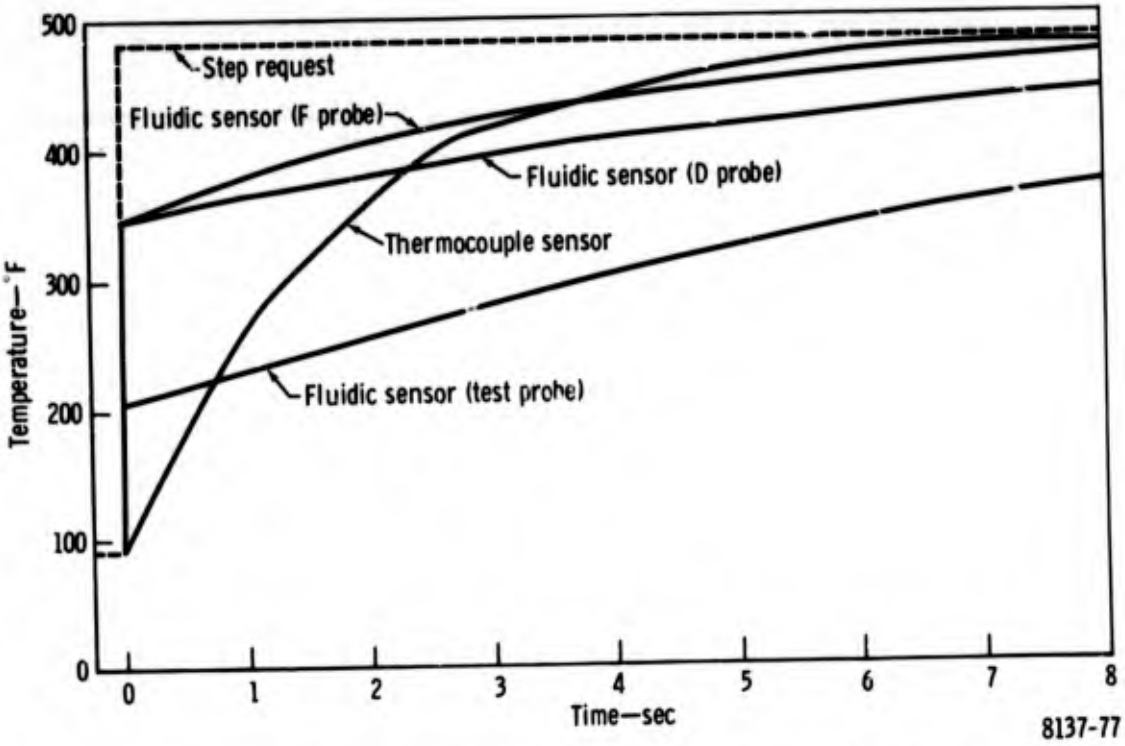

Figure D-5. Temperature response to a step change.

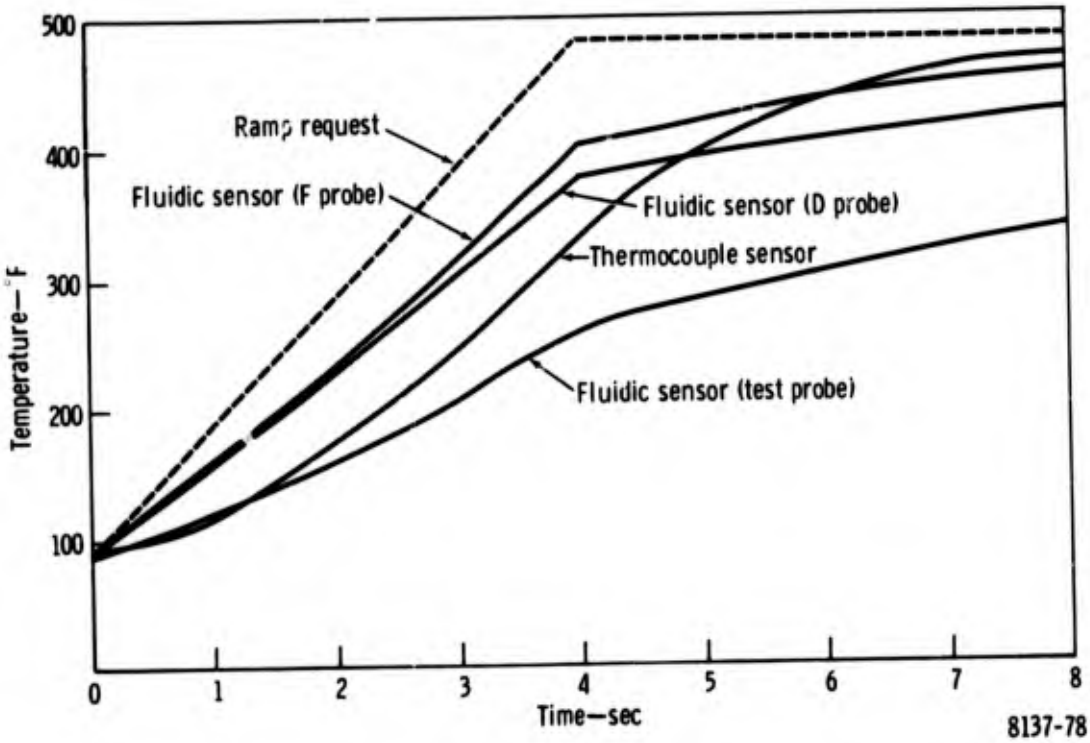

Figure D-6. Temperature response to a ramp change.

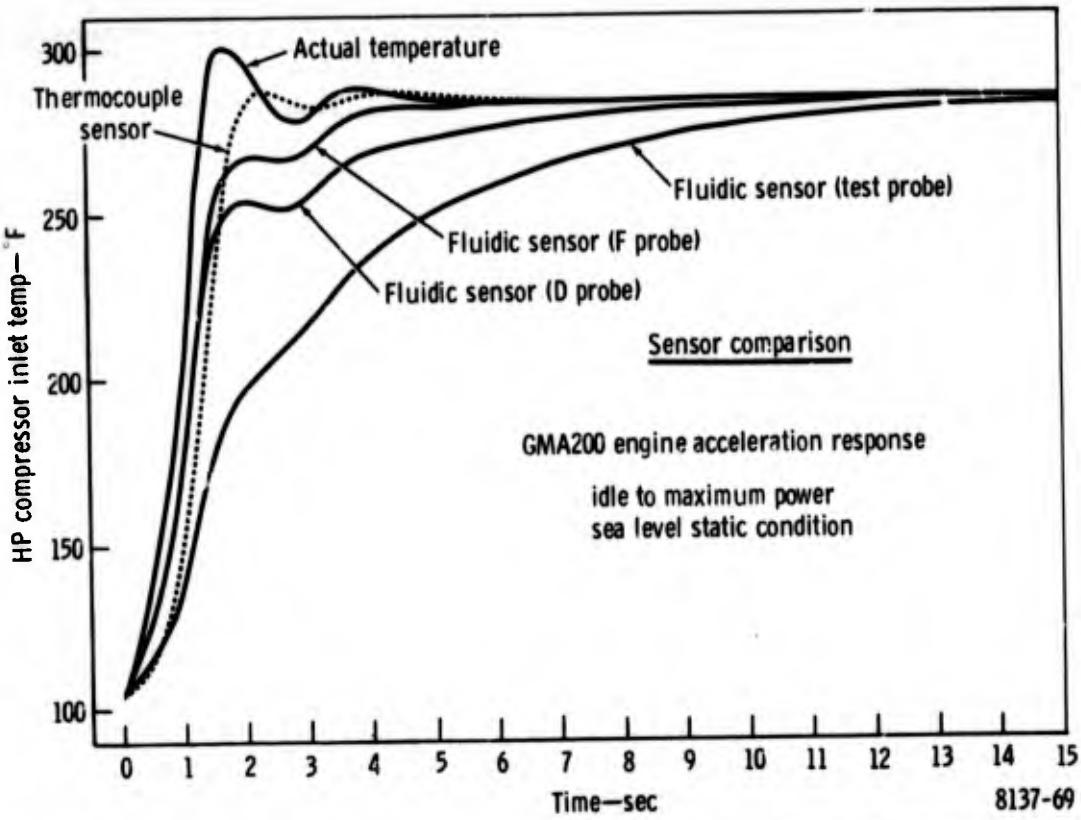

Figure D-7. HP compressor inlet temperature response.

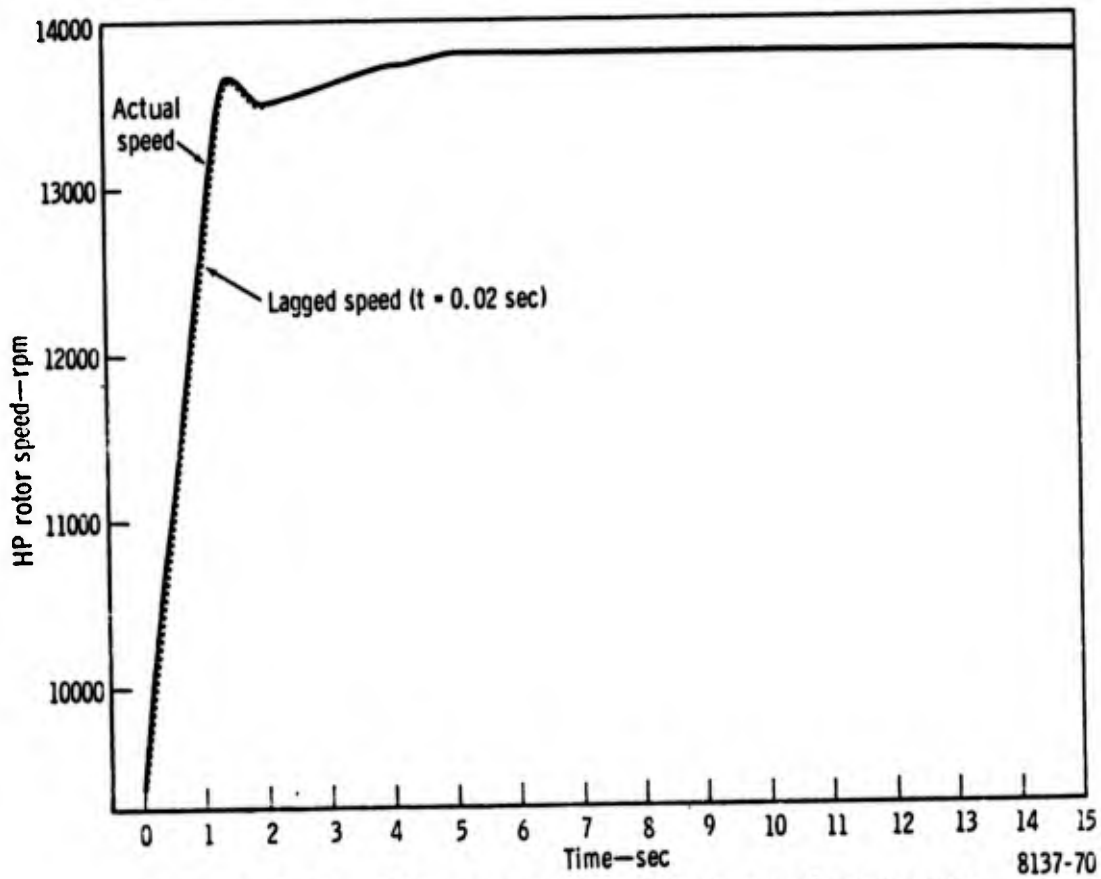

Figure D-8. HP compressor rotor speed response.

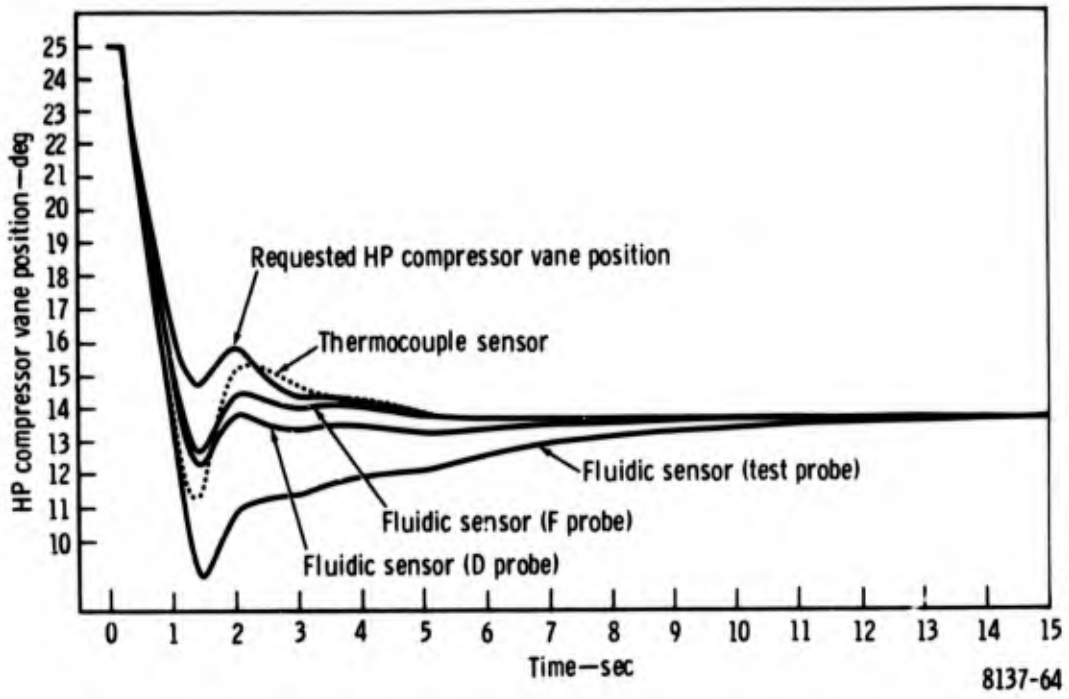

Figure D-9. HP compressor vane position response showing performance of fluidic F and D probes.

there were no vane actuator dynamic characteristics, this is the ideal position the HP compressor vanes should be in during the engine transient. Therefore, the other response curves for the various sensor probes are compared to the requested HP compressor vane position to determine the amount of error in scheduling the HP compressor vanes.

An increase in the amount of error in scheduling the HP compressor vanes during the engine transient will result in affecting the engine response time and in the possibility of less HP compressor surge margin (this can only be quantitatively assessed in closed loop analysis). Figures D-9 and D-10 show that the fluidic F probe produces less maximum error in scheduling the HP compressor vanes, followed by the fluidic D probe, the thermocouple probe, and the fluidic test probe. The fluidic test probe appears to be unacceptable in scheduling the HP compressor vanes. The fluidic F and D probes show a slight engine performance advantage over the thermocouple probe. Actual numbers are not being quoted in this comparison because "typical" engine performance data are being used and, therefore, only relative comparisons are being considered.

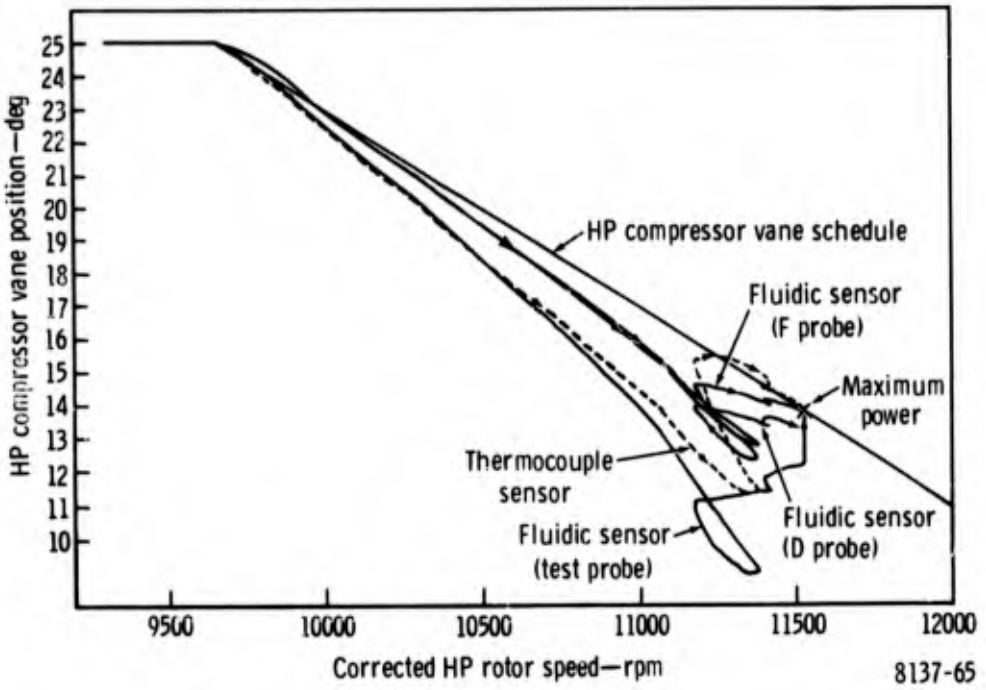

Figure D-10. HP compressor vane position response showing performance of fluidic F and D probes.

Missile Fire Results

This condition was used in this sensor comparison to show the effect of hot gas ingestion during missile firing. Figures D-11 and D-12 show a sensor comparison of the time history for HP compressor inlet temperature and HP compressor vane position, respectively.

Figure D-13 shows the sensor comparison for HP compressor vane position versus corrected HP rotor speed. This missile firing is done at maximum power and the HP rotor speed is assumed to stay at the same value during the entire transient. As a result of the sensor dynamic lags shown in Figure D-11, Figures D-12 and D-13 indicate the amount of error in scheduling the HP compressor vanes during this kind of transient, using the different sensor probes. Figures D-12 and D-13 show that the fluidic F probe produces less error in scheduling the HP compressor vanes than the thermocouple probe. Therefore, the fluidic F probe shows much more of an engine performance advantage than the thermocouple probe. As previously explained, this is a relative advantage.

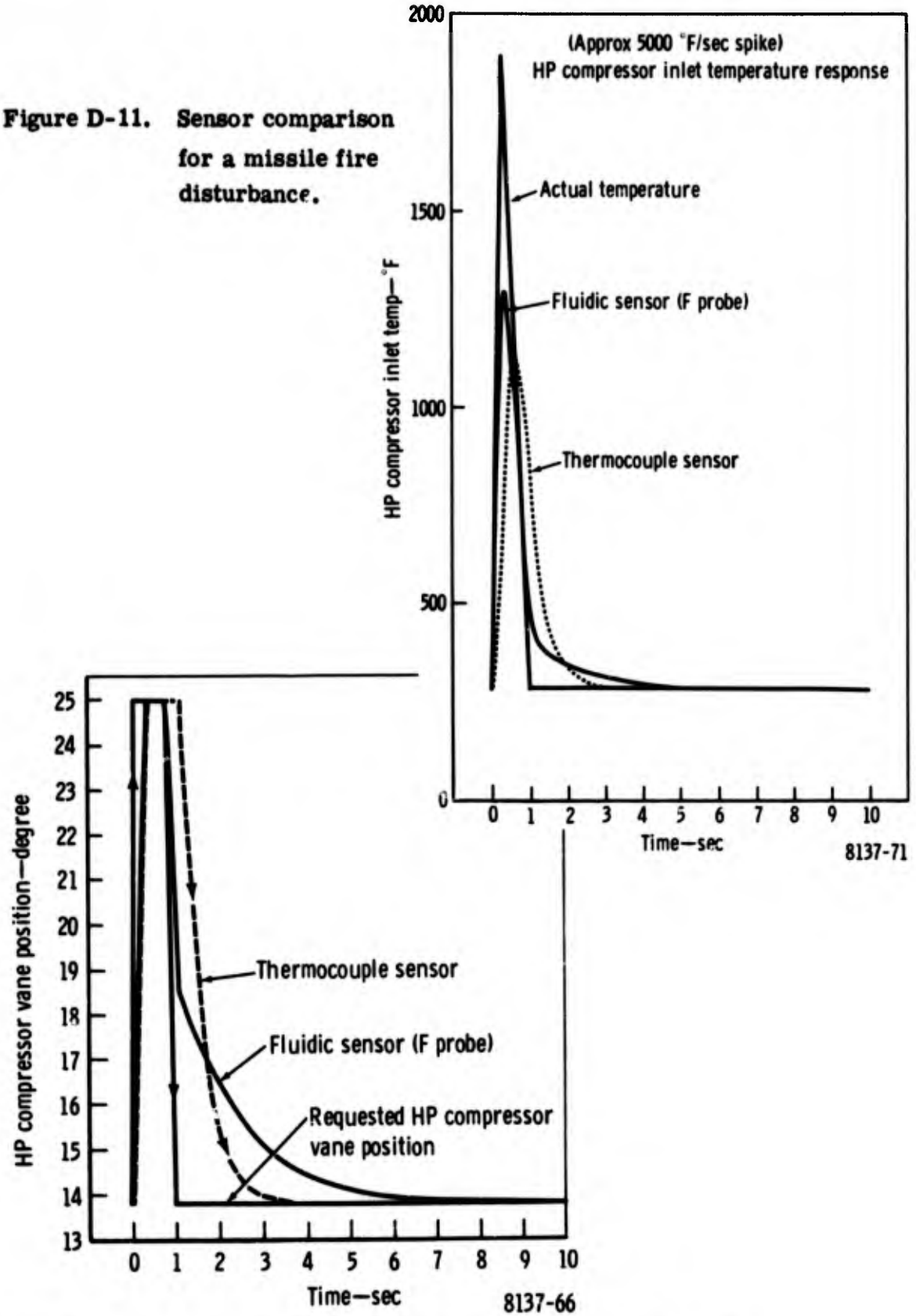

Figure D-11. Sensor comparison for a missile fire disturbance.

Figure D-12. HP compressor vane position response comparing fluidic F probe with thermocouple probe.

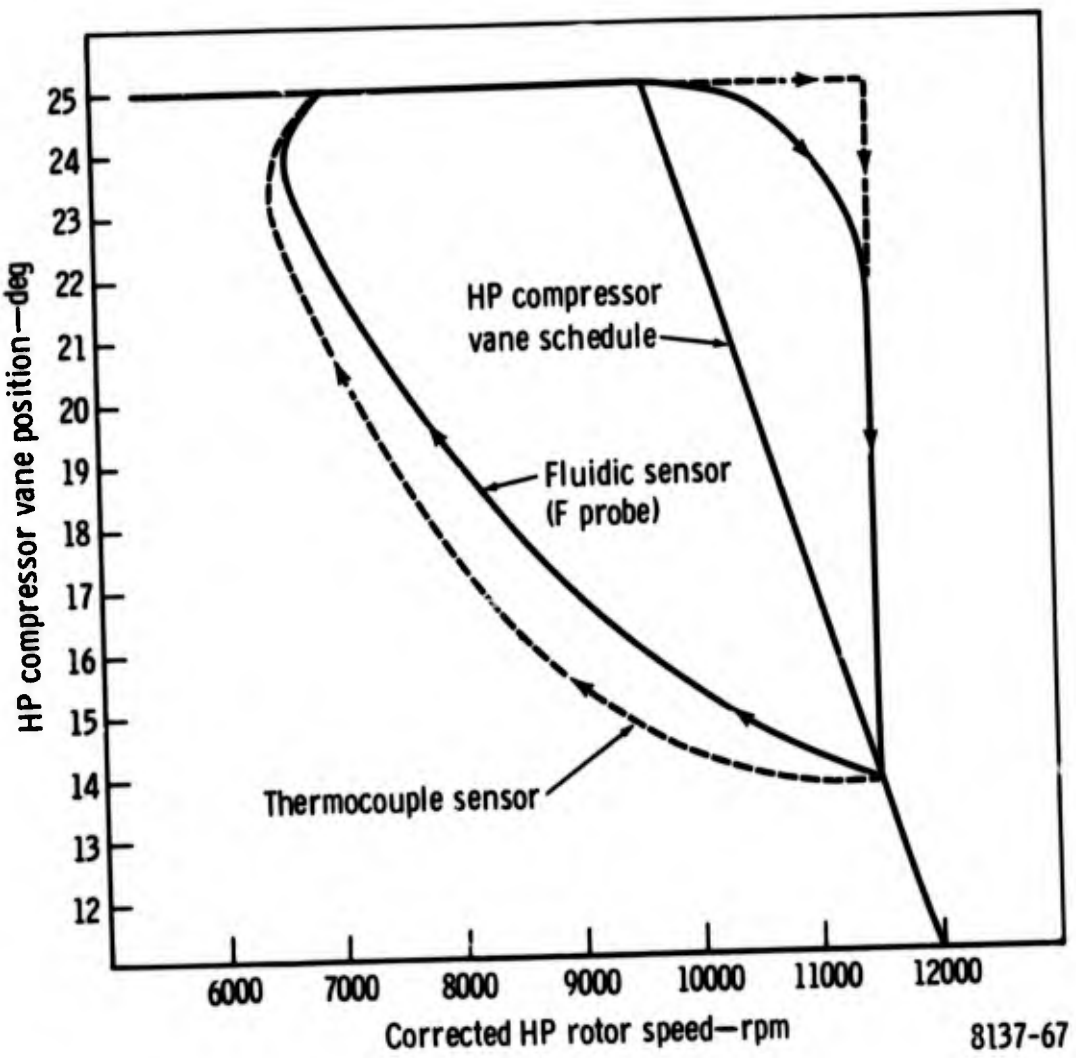

Figure D-13. HP compressor vane position response comparing fluidic F probe wit' thermocouple probe.

REFERENCES

REFERENCES

1. Mikkelson, R. A. Heat Transfer Analysis of a Fluidic Temperature Sensor. DDA TDR AX. 1260-021A. 11 May 1970.

2. Whicker, J. E. Evaluation of Iridium/Rhodium Integrated Probe/ Fluidic Sensor Concept. Air Force Aero Propulsion Laboratory AFAPL-TR-72-48. June 1972.

3. Chupp, R. E. Transient-Temperature Analysis of a General Nodal-Network System: Computer Program EJ-8. DDA TDR AX. 0013-030. 28 April 1972.

4. Chupp, R. E. Thermal Analysis of A Fluidic Sensor Probe for Measuring Compressor Inlet Temperatures. DDA TDR AX. 1260-025, 11 February 1974.

5. Moffat, R. J. "Designing Thermocouples for Response Rate." Trans ASME, 80, pp 257-262, 1959.

6. Rohsenow, W. M. and Hartnett, J. P., editors. Handbook of Heat Transfer. McGraw-Hill Book Co., New York, p 7-38. 1973.

LIST OF ABBREVIATIONS AND SYMBOLS

LIST OF ABBREVIATIONS AND SYMBOLS

A	orifice area
C_D	discharge coefficient
dev	deviation
f, freq	frequency
h	heat transfer
HP	high pressure
KI	actuator slew rate
L/D	length/diameter
M_N	Mach number
pCb	picocoulomb
P	pressure
t	time
T	Sensor No. 1 and 2 indicated temperature (°R)
t/c	thermocouple
W	flow rate
η_t	thermal effectiveness
μ	micro

Subscripts

g	gas conditions outside the tube

*U.S.Government Printing Office: 1975 — 657-019/455